DOCTORAL THESIS

"Protein kinase VRK-1 and its role in cell proliferation and differentiation"

Centro Andaluz de Biología del Desarrollo

Universidad Pablo de Olavide

Agnieszka Dobrzyńska

Director:

Dr. Peter Askjaer

Tutor:

Dr. Manuel J. Muñoz

Seville, 2014

Centro
Andaluz
de Biología
del Desarrollo

El **Dr. Peter Askjaer**, científico titular del Consejo Superior de Investigaciones Científicas (CSIC),

Y

El **Dr. Manuel J. Muñoz**, profesor titular de la Universidad Pablo de Olavide,

CERTIFICAN:

Que la **licenciada Agnieszka Dobrzynska** ha realizado bajo su dirección el trabajo titulado "Protein kinase VRK-1 and its role in cell proliferation and differentiation", el cual reúne las condiciones de originalidad y calidad científica necesarias para optar al grado de Doctor por la Universidad Pablo de Olavide.

Y para que así conste, expedimos el presente certificado en Sevilla, a 8 de Mayo de 2014.

Fdo.:

Dr. Peter Askjaer	Dr. Manuel J. Muñoz
Director de Tesis	Tutor de Tesis

Index

Index of Figures

I. INTRODUCTION

II. RESULTS

Index of Tables

Abbreviations

µg	microgram
˚C	degrees celsius
3´UTR	three prime untranslated region
aa	amino acid
AC	anchor cell
ATP	adenosine triphosphate
BAB	bacic acidic bacic motif
bp	basepairs
CPC	Chromosome Passenger Complex
DIC	differential interference contrast
DMEM	Dulbecco´s Modified Eagle Medium
DTT	Dithiothreitol
ER	endoplasmic reticulum
E.coli	*Escherichia coli*
FBS	Fetal Bovine Serum
GFP	green florescent protein
H2A	histone 2A
kDa	kilo Dalton
LB	Lysogeny broth
mg	miligram
MW	molecular weight
NE	nuclear envelope
NEBD	nuclear envelope breakdown

NGM	nematode growth medium
NLS	nuclear localization signal
ok1181	oklahoma 1181
ORF	open reading frame
π cells	pi cells
PBS	phosphate buffer salinum
PCR	polymerase chain reaction
p-value	probability value
Pvl	protruding vulva
pvrk-1	promoter of vrk-1
RNAi	RNA interference
Ser	serine
SD	standard deviation
SDS-PAGE	sodium dodecyl sulfate-poly-acrylamide gel electroforesis
sec	seconds
Thr	threonine
Tyr	tyrosine
utse	uterine seam
VPC	ventral precursor cell
vs	versus
WT	wild type
Y2H	Yeast Two Hybrid
YFP	yellow fluorescent protein

RESUMEN

RESUMEN

Caenorhabditis elegans es un nematodo pequeño que se alimenta de microorganismos, es transparente y fácil y barato para cultivar en el laboratorio. Además, su naturaleza hermafrodita, un ciclo de vida rápido, posibilidad de congelación y recuperación de los nematodos viables facilitan muchas manipulaciones genéticas. Por estas ventajas se utiliza como un sistema modelo en casi todas las áreas de la biología célullar, neurobiología y desarrollo. La elucidación de la organogénesis es importante para la comprensión del desarrollo de los organismos multicelulares. La vulva de un adulto hermafrodita sirve como un pasillo que conecta el útero con el ambiente externo y su desarrollo es un excelente modelo para estudiar los mecanismos que subyacen a la especificación del destino celular y las vías de señalización intercelular (Sternberg, 2005).

Durante el estadio larvario L3 una célula especializada de la gónada llamada célula ancla (AC), induce el desarrollo de la vulva mediante la secreción de la proteína LIN-3, un ligando del factor de crecimiento epidérmico (EGF) a los precursores celulares de la vulva (VPC) subyacentes, llamados P3.p-P8.p para adoptar los destinos vulvares (Hill and Sternberg, 1992). El nivel mas alto de LIN-3 lo recibe P6.p para adoptar 1˚ destino celular y activar el LIN-12 (Notch) en P5.p y P7.p y adoptar el 2˚ destino celular (Sternberg, 1988). Los tres restantes VPCs (P3.p , P4.p y P8.p) que no reciben el señal inductiva ni las señales laterales adoptan el 3˚ destino celular, se dividen una vez y se fusionan con la hipodermis (hyp7). Después de tres rondas de divisiones celulares durante los estadios larvarios L3 y L4 se generan 22 células de la vulva de siete tipos diferentes que se invaginan y fusionan para formar siete

anillos toroidales diferentes, se conectan al útero y emergen durante la última muda para formar la vulva madura del hermafrodita.

La AC desempeña un papel crucial no sólo durante el desarrollo de la vulva, sino también en la morfogénesis uterina. Después de la inducción de tres VPCs para adoptar sus destinos vulvares, la AC señala, a través de LAG-2 y su receptor LIN-12, a seis de los doce descendientes de las células ventrales del útero (VU) a adoptar el destino celular π. Durante el estadio larvario L4, ocho células π fusionan con la AC y forman el sinsitio llamado utse.

La fosforilación de proteínas por parte de quinasas es una modificación postraduccional que juega un papel importante en procesos biológicos numerosos. Se estima que aproximadamente el 30 % de las proteínas intracelulares se fosforila de forma reversible (Cohen, 2000), lo que hace que las proteínas quinasas sean reguladores clave de procesos biológicos incluyendo la transducción de la señal, la transcripción, la progresión del ciclo celular, el crecimiento, la diferenciación y la apoptosis.

La familia de quinasas humanas *Vaccinia Related Kinases*, VRKs, está constituida por tres miembros proteínas, VRK1 – 3, de los cuales sólo VRK1 y VRK2 son catalíticamente activos (Nichols and Traktman, 2004). En *Caenorhabditis elegans* y *Drosophila melanogaster* hay sólo un ortólogo (VRK-1 y NHK-1, respectivamente). No hay ortólogos de las VRKs identificados en la levadura.

VRK1 humana es el miembro más estudiado de la familia de VRK. Experimentos en diferentes organismos han demostrado que VRK1 fosforila varios factores de transcripción (p53, c-Jun y ATF2) y proteínas

asociadas a la cromatina (histonas H2A y H3, BAF1) (Klerkx et al., 2009b). VRK1 regula la progresión del ciclo celular y juega un papel importante en la dinámica de la envoltura nuclear (Gorjanacz et al., 2007; Nichols et al., 2006). En los mamíferos, la pérdida de VRK1 conduce a la esterilidad y puede causar trastornos neurológicos (Renbaum et al., 2009; Wiebe et al., 2010). Además, la expresión de VRK1 se correlaciona con la progresión de ciertos tipos de cáncer (Santos et al., 2006). Los estudios realizados en nuestro laboratorio utilizando los nematodos *C. elegans* como organismo modelo han demostrado que VRK1 juega un papel crítico en el desarrollo de órganos, así como en la proliferación de células germinales y divisiones mitóticas durante la embriogénesis temprana (Gorjanacz et al., 2007; Klerkx et al., 2009a). Sin embargo, poco se sabe acerca de la dinámica de VRK1, su regulación y sus sustratos durante el desarrollo.

Los objetivos de mi tesis doctoral han sido situar a VRK-1 dentro del contexto del desarrollo de órganos de *C. elegans*, caracterizar la dinámica de la localización de VRK-1 tanto en *C. elegans* como en las células humanas e identificar nuevos sustratos de esta quinasa.

La primera parte de mi tesis se concentra en la caracterización de la localización y la movilidad de VRK1 tanto en *C. elegans* como en las células humanas. Con el fin de caracterizar la dinámica de VRK1 y garantizar los niveles de expresión uniformes hemos utilizado los sistemas MosSCI y Flp-In para generar nuevas cepas transgénicas de *C. elegans* y líneas celulares humanas, que expresan solo una copia de los transgenes. Hemos observado que las nuevas cepas muestran la expresión de VRK-1 no sólo en las células previamente reportadas

(neuronas, células hipodérmica y células precursoras de la vulva), sino también en las celulas del utero y la célula ancla. Ademas, hemos observado que VRK1 humano es nuclear durante la interfase y en mitosis se asocia con los cromosomas condensados, igual a lo descrito para los embriones de *C. elegans* (Gorjanacz et al., 2007*).* Por otra parte, una mutagénesis dirigida a tres argininas conservadas en la región carboxyl terminal identificó un nuevo motivo conservado, responsable de la localización de VRK1 en cromatina durante la mitosis. La recuperación de *fluorescencia* posterior al foto-blanqueamiento (FRAP) sugiere una asociación transitoria de VRK1 con la cromatina. Se observaron cinéticas idénticas en interfase y en la mitosis, lo que sugiere que VRK1 puede interactuar con las mismas proteínas de la cromatina durante todo el ciclo celular.

La segunda parte de mi tesis se concentra en la relación entre VRK1 y las vías de señalización implicadas en el desarrollo de *C. elegans*. Durante el desarrollo de la vulva la AC se fusiona con células uterinas para formar el utse. Los defectos en la formación de utse producen un fenotipo conocido como vulva protuberante (Pvl). Hemos demostrado que la AC no se fusiona en los mutantes de *vrk-1*, muy probablemente debido a la pérdida de VRK-1 en el tejido uterino, lo cúal, esta perdida se caracteriza por defectos en la proliferación y la diferenciación en las células uterinas.

La tercera parte de esta tesis se centra en la identificación de las proteínas que interaccionan con VRK1. Hemos expresado y purificado VRK1 de células humanas asincrónicas y mitóticas, seguido por espectrometría de masas de alta resolución. Algunos de los principales candidatos identificados fueron miembros del complejo de pasajeros

cromosómica (CPC) - Aurora B, Borealin y survivin. Experimentos en curso servirán para confirmar la interacción de VRK1 con el CPC.

En conclusión, en esta tesis hemos destapado nuevos dominios reguladores de la proteína quinasa VRK1 y proteínas que interaccionan con VRK1. Estos resultados son importantes para comprender las actividades moleculares de esta quinasa, que está vinculada a la organogénesis, así como a los cánceres humanos y a trastornos neurológicos.

I. INTRODUCTION

I. INTRODUCTION

1. 1 *Caenorhabditis elegans* as a Model System

"Part of the success of molecular genetics was due to the use of extremely simple organisms which could be handled in large numbers...We should like to attack the problem of cellular development in a similar fashion, choosing the simplest possible differentiated organism and subjecting it to the analytical methods of microbial genetics...We think we have a good candidate in the form of a small nematode worm, *Caenorhabditis briggsae*..."

Sydney Brenner, 1963

The popularity of *Caenorhabditis elegans* derives from 1963 when Sydney Brenner, South African biologist, observed that this worm offers a great potential for scientific analysis. Although initially he was thinking about another closely related species, his final choice was *C. elegans*.

C. elegans is a small, 1mm long, free-living soil nematode that feeds on microorganisms and is used as a model system in almost every area of cell, developmental, behavioural and neurobiology. It is transparent, easy and inexpensive to cultivate in large numbers in the laboratory on a simple Petri dishes seeded with *Escherichia coli* bacteria as food source. Its self-fertilizing hermaphroditic nature and a fast life cycle facilitate many genetic manipulations. An enormous tactical advantage that enables stock maintenance of that model system is, discovered by John Sulston, the possibility of freezing and recovery of viable worms. The adult hermaphrodite contains exactly 959 somatic cells and the fate of each of them is known, which makes it an excellent model for developmental biology. Even though being a very simple organism, it

already has complex nervous, digestive and germline systems. Gene knockdown is easily and efficiently achieved through the usage of RNA interference (RNAi) by feeding. Finally, it was the first multicellular organism to have its genome fully sequenced. It comprises over 20000 protein coding genes, organized in five pairs of autosomes (I-V) and one pair of sex chromosomes (X).

In the following part of my thesis, I will give a short introduction to the *C. elegans* development and anatomy, which is mostly based on the WormBook (http://www.wormbook.org) and WormAtlas (http://www.wormatlas.org) open resources with particular emphasis on development of the egg laying organs(Gupta et al., 2012; Sternberg, 2005) (Gupta et al., 2012; Sternberg, 2005).

1.1.1 Life-cycle

A great advantage of working with *C. elegans* is that it has a short life cycle. Under standard laboratory conditions, the development from an egg to an adult takes only 3.5 days at 20˚C. During adulthood, a self-fertilizing hermaphrodite generates approximately 300 eggs (Figure 1).

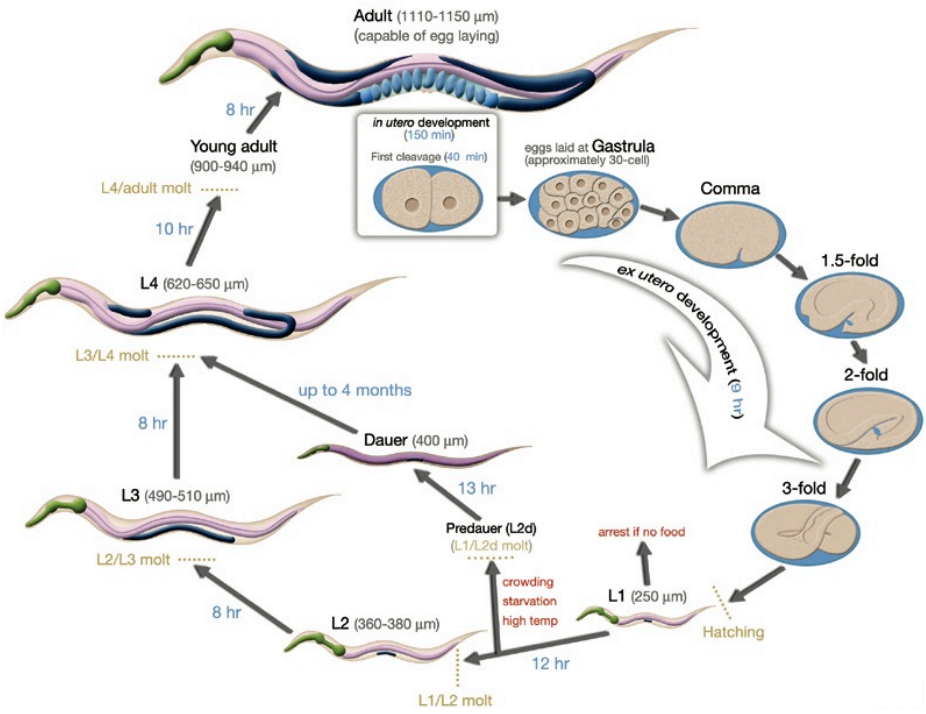

Figure 1. Life cycle of *C. elegans* at 22˚C. The time between each larval molt is shown in blue. The length of the worm at each larval stage is shown next to the stage name. Adapted from WormAtlas.

The embryonic stage lasts 14 hours and during the first few hours occurs within the uterus of the hermathrodite. Shortly after fertilization a tough chitinous shell is secreted. Embryogenesis is divided into two stages. During proliferation are generated founder cells (AB, E, MS, C, D and germline P_4) which give raise to a specific subset of cell types and at the end of that stage ectoderm, mesoderm and endoderm are specified. The second phase of embryogenesis includes terminal differentiation of cells and final morphogenesis establishes the main body plan of the worm with fully differentiated tissues and organs.

Post-embryonic development comprises, in the presence of food, growth through four larval stages (L1-L4) each separated by a molt, to generate the adult worm (Figure 1). In the absence of food or in the crowded conditions, at the end of L2 stage, *C. elegans* develops an alternative larval stage called dauer.

The dauer larva is very thin, has a thicker cuticle and altered metabolism which allows the larva to survive for several months. When conditions become favourable again, animals exit the dauer stage and develop into normal L4 larval stage.

1.1.2 Anatomy

There are two *C. elegans* sexes, male and hermaphrodite and they both have the same cylindrical, un-segmented body shape that consists of two concentric tubes separated by fluid filled space (pseudocoelom). The cuticle, hypodermis, and excretory system form the outer tube while the inner tube is formed by the pharynx, intestine and gonad (Figures 2 and 3).

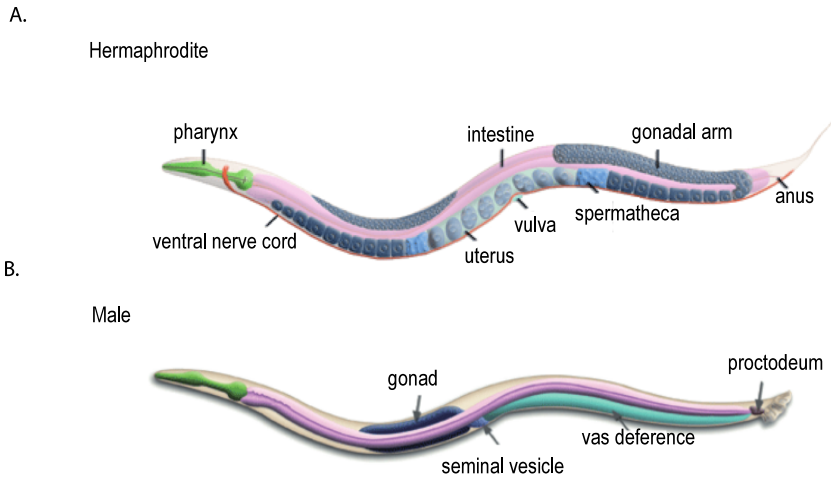

Figure 2. Anatomy of an adult heraphrodite (A.) and male (B.) *C. elegans*. Schematic drawing of basic anatomical structures. Adapted from WormAtlas.

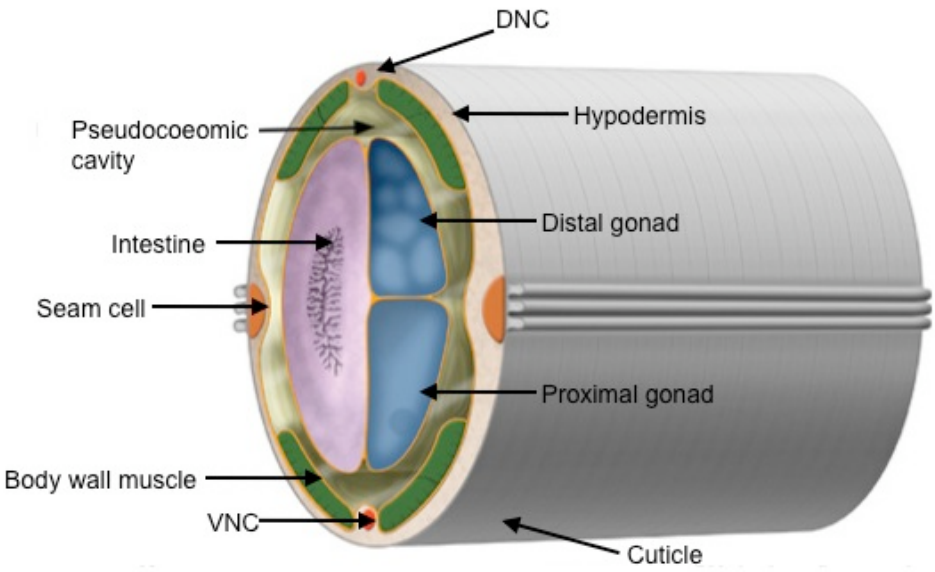

Figure 3. Cross section of the posterior body region indicating basic anatomical structures of *C. elegans* hermaphrodite. Schematic drawing of basic anatomical structures. Adapted from WormAtlas.

1.1.2.1 Cuticle

The body of *C. elegans* is covered by a tough but flexible cuticle, which forms the barrier between the worm and its environment, maintains body shape and allows the locomotion (Figure 3). It is secreted by the underlying epithelium and its most abundant components are collagens and additional insoluble proteins called cuticulins associated with glycoproteins and lipids. A new cuticle is synthetized at each molt. It has different composition, surface proteins, thickness and number of layers. The variability of the cuticle at each larval stage allows better adaptation to the environment and development during the animal's life-cycle.

1.1.2.2 Epithelial System

The cuticle together with epithelial cells form the basic body form of the worm. The epithelial system is formed by two categories of cells – hypodermal and specialized epithelial cells (Figure 3). Hypodermal cells form the external layer of the worm, serve as a storage of nutrients, secrete cuticle and create a barrier function for the pseudocoelomic cavity. The hypodermis is formed by cells that fuse to form the main body syncytium (hyp7) that extends over most of the body and smaller hypodermal cells in the head and tail of the worm.

Specialized epithelial cells consist of seam cells, interfacial epithelial cells and atypical epithelial cells. Seam cells are required for the production of stage specific cuticle and formation of alae (protruding ridges that run along the body of the worm, present in L1 larval stage, dauer and an adult; probably having role in maintenance of cuticle strength, worm movement and storage of the fat) (Figure 3). Interfacial and atypical cells are present in the junctions between the organs and the hypodermis.

1.1.2.3 Muscular System

The *C. elegans* muscular system is formed by two types of muscles - striated, multisarcomeric, somatic muscles, which are organized in four longitudinal bands located in four quadrants, two dorsal and two ventral, and run along the body of the worm (Figure 3), and smaller, nonstriated muscles, which are found in the pharynx, vulva, intestine and rectum.

1.1.2.4 Excretory System

The excretory system in nematodes mediates osmotic and ionic regulation, excretion of metabolic waste and secretion of molting exsheathment fluid and

hormones. It is formed by four cells, located in the region of the head - the H-shaped excretory cell which forms a bridge between the right and left excretory canals, a pair of fused gland cells, the duct cell which connects the excretory system to outside and finally, a pore cell which encloses the cuticle-linked excretory duct.

1.1.2.5 Coelomocyte System

The coelomocytes are scavenger cells that are highly active in endocytosis of fluid from the psedocoelom (body cavity) (Figure 3). In *C. elegans* exist three pairs of coelomocytes, right, left and dorsal, situated in the pseudocoelomic cavity and adjoining somatic musculature. Since *C. elegans* lacks an adaptive immune system and coelomocytes were reported to be able to act similarly to the macrophages of vertebrates, this system is suggested to play a role in immune, scavenging and hepatic functions.

1.1.2.6 Alimentary System

The *C. elegans* digestive system is composed of the pharynx, which is responsible for ingestion, concentration and crushing the bacteria, followed by the 20-cell intestine tube, where food is digested, absorbed and macromolecules are synthesized and stored. The intestinal contents are excreted via opening of the anus at the posterior end (Figures 2 and 3).

1.1.2.7 Reproductive System

C. elegans exists either as a hermaphrodite (XX) or a male (X0). The predominant sexual form is the self-fertilizing hermaphrodite, which produces

both sperm and oocytes. Males are found at low frequency (~0.1%) as a result of spontaneous meiotic non-disjunction, or up to 50%, through mating. Adult males can be distinguished from hermaphrodites by their smaller and slimmer body and distinctive tail with a copulatory apparatus (Figure 2).

The reproductive system of hermaphrodites consists of the somatic gonad, the germ line and the egg-laying apparatus. The gonad of both sexes has the same simple tubular structure. Hermaphrodites have two symmetrically arranged U-shaped gonad arms that are connected to a central uterus through the spermatheca. Self-fertility is achieved by a switch from production of sperm that are generated during L3 and stored in spermatheca, to oogenesis in the L4 larval stage.

When worm hatches from the egg, the gonad primordium is composed of four founder cells Z1-Z4. Z1 and Z4 are precursors of the somatic gonad, while Z2 and Z3 give raise to the germ cells. The somatic gonad of hermaphrodites consists of distal tip cells (DTCs), sheath cells, spermatheca, spermatheca-uterine valve and uterus. DTCs are situated at the tip of each gonad arm and are important for germ cells proliferation and gonadal arm elongation. The gonadal sheath consists of five pairs of cells forming a single layer covering the germ line. Composed of 24 cells, the spermatheca contains sperm and is the site of oocyte fertilization. Embryos pass from the spermatheca to the uterus via the spermatheca-uterine valve.

The adult germ line shows distal–proximal polarity. Germ cells at the distal tip of the gonad are proliferative (mitotic) and organized in a syncytium. As the gonad elongate they pass through different stages of meiotic prophase and diakinesis towards proximal part of the gonad and gradually grow. Gametogenesis occurs in the proximal part of the gonad (Figure 4).

In contrast to the hermaphrodites, males have a single-armed somatic gonad of only 55 cells that opens at the cloaca via proctodeum (modified rectum) and is able to produce up to 3000 spermatides.

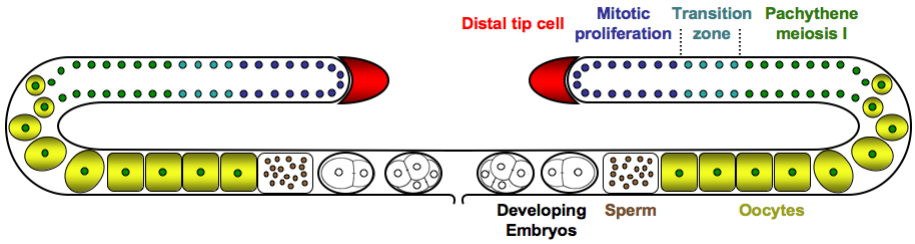

Figure 4. Schematic representation of an adult hermaphrodite germline. The gonad of the hermaphrodite has two arms and germs cells are derived from a proliferating stem cell population located at the distal tip cell (red). Each arm produces first sperm (brown), then oocytes (yellow). As cells migrate towards the proximal part they pass through different stages of meiotic prophase and diakinesis. The mature oocytes pass through the spermatheca where they are fertilized. In the uterus they complete two meiotic divisions and undergo several cycles of mitotic divisions before they are released to the outside. Adapted from (Minasaki et al., 2009).

1.1.3 Development of the Reproductive Organs

The elucidation of organogenesis is important to the understanding of development of multicellular organisms. The egg-laying apparatus of the *C. elegans* hermaphrodite consists of the uterus, the uterine muscles, the vulva, the vulval muscles, and the egg-laying neurons. Fertilized embryos pass from the spermatheca to the uterus, where they undergo approximately one third of embryogenesis before being expelled into the environment through the vulva.

1.1.3.1 Vulva

The vulva of an adult hermaphrodite serves as a passageway that connects the uterus to the external environment and its development provides an excellent

model to study mechanisms underlying cell fate specification and intercellular signalling pathways (Sternberg, 2005).

During *C. elegans* development, in late L2 larval stage, two developmentally equivalent cells of the somatic gonad primordium, called Z1.ppp and Z4.aaa, undergo anchor cell/ventral uterine ("AC/VU") precursor cell decision. The AC/VU decision is mediated by the interaction between receptor LIN-12 (Notch) and its ligand LAG-2, so only one of the cells becomes AC and the other a VU (Greenwald et al., 1983; Wilkinson et al., 1994)(Figure 5).

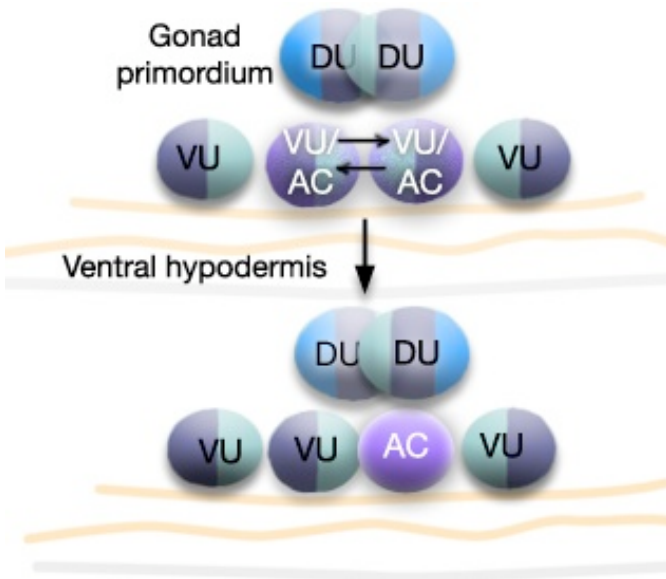

Figure 5. Schematic representation of "AC/VU" decision. During the "AC/VU" decision, one of the two equivalent cells of somatic gonad primodium becomes anchor cell (AC) and the other ventral uterine cell (VU). Adapted from WormAtlas.

When AC fate is determined, six of the eleven ventrally located epidermal Pn.p cells (P3.p – P8.p) are specified as vulva precursor cells (VPCs) by LET-60 (Ras) and Wnt signalling pathways acting on the Hox gene *lin-39*, which maintains six VPCs as competent cells to acquire vulval fates (Figure 6). During L3 larval

stage the AC induces development of the vulva by secreting the epidermal growth factor (EGF-like) ligand LIN-3 to the underlying VPCs so they adopt specific vulval fates (Hill and Sternberg, 1992). Each of the VPCs expresses the EGF-receptor LET-23 (Aroian et al., 1990). P6.p receives the highest level of LIN-3, adopts 1˚ cell fate and activates the LIN-12 (Notch) signalling pathway in P5.p and P7.p to take on 2˚ cell fate (Sternberg, 1988). The remaining three VPCs (P3.p, P4.p and P8.p) that receive neither inductive nor lateral signals adopt 3˚ cell fate, divide once and fuse with the hypodermis (hyp7). After three rounds of cell divisions during L3 and L4 larval stages 22 vulval cells of seven different types (vulA, vulB1, vulB2, vulC, vulD, vulE, and vulF) are generated. The seven different types of vulval cells invaginate, fuse with each other (except vulB1 and vulB2 that remain unfused) to form seven different toroidal rings, connect to the uterus and evert during the last molt to finally form the mature vulva of the hermaphrodite.

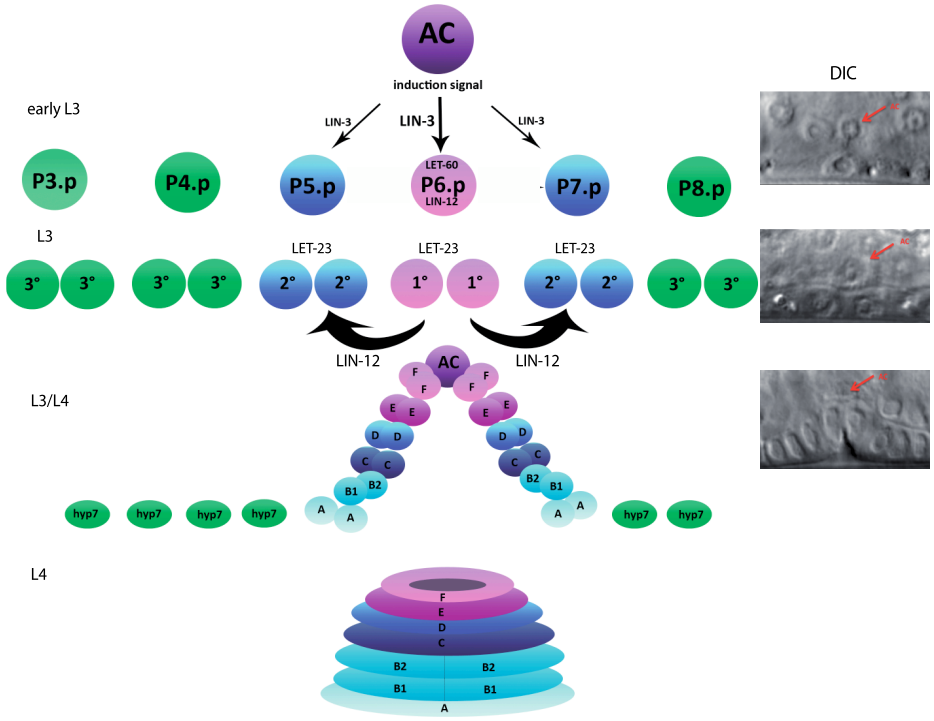

Figure 6. Development of the *C. elegans* vulva. During L3 stage six of the epidermal Pn.p cells (P3.p – P8.p) become specified as vulva precursor cells. The gonadal anchor cell (AC) produces and secretes LIN-3 epidermal growth factor that activates its receptor LET-23 in the closest VPCs. P6.p receives the highest amount of the inductive signal, thus adopts the 1° cell fate. P6.p generates a later signal that activates the LIN-12 signalling pathway in P5.p and P7.p to take on 2° cell fate. The P3.p, P4.p and P8.p adopt 3° cell fate, divide once and fuse with the hypodermis (hyp7). During the L3 and L4 larval stages P5.p, P6.p and P7.p undergo three rounds of division to generate 22 vulval cells of seven different cell types (A, B1, B2, C, D, E, F). The vulval cells invaginate and undergo homotypic fusion to form seven distinct toroids. Right panel shows DIC images of the developing vulva. Red arrows indicate the AC.

1.1.3.2 Uterus

The *C. elegans* uterus consists of 60 cells, descendants of two dorsal uterine precursors (DU) and three ventral uterine precursors (VU). Out of 48 cells produced by DU cells, 28 build uterine tissue, while the rest contribute to the

spermatheca and uterine-spermathecal junction. Three VU cells undergo four rounds of cell divisions during L3 and L4 larval stages and produce 36 descendants, from which 32 make the uterus and four the uterine-spermathecal junction (Newman et al., 1996). The AC plays a crucial role not only during development of the vulva, but also in uterine morphogenesis. After induction of three VPCs to adopt vulval fates, it signals via LAG-2 and its receptor LIN-12 to six of twelve VU descendants to adopt π cell fate (Figure 6). The π cells divide and differentiate into two classes – four cells will connect to the dorsal side of the vulva, and eight cells will fuse with the AC during L4 larval stage and form the H-shaped uterine seam syncytium (utse). Utse forms the ventral surface of the uterus. Its two longer sides of the H shape attach to the lateral seams and hold the uterus in place, while the central part forms a membrane between uterus and vulva, which is broken by the first egg leaving the uterus (Figure 7).

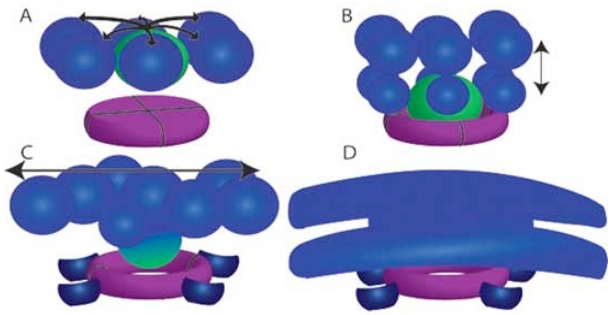

Figure 7. Uterus development. A. AC (green) induces six nearest ventral uterine (VU) cells (blue) situated above the vulval cells (purple) to adopt a π fate via LIN-12 signal (arrows) **B.** π cells divide once producing twelve π cells **C.** Eight π cell progeny fuse with each other and with AC to form uterine seam cell (utse) **D.** The mature utse cell. Adapted from (Gupta et al., 2012).

1.1.3.3 Anchor Cell invasion

After induction of the P6.p VPC to adopt 1° cell fate at the beginning of the L3 larval stage, the AC invades the basement membrane separating the uterine tissue from the underlying developing vulva and attaches to two of the descendants of

the central VPC, P6.pap and P6.ppa (Sherwood and Sternberg, 2003) to mediate the uterine-vulval connection in L4 larval stage. AC invasion is controlled by the netrin and integrin pathways. INA-1/PAT-3 integrin promotes membrane association of the components of the invasive cell membrane, such as the netrin receptor UNC-40, actin regulators phospholipid PI(4,5)P2, Rac GTPase MIG-2 and F-actin (Hagedorn et al., 2009), while secretion of UNC-6 (Netrin) from the ventral nerve cord (VNC) orients these components towards the invasive membrane. The invasive protrusions are generated in response to the 1° vulval cell cue (Sherwood and Sternberg, 2003). Recently has been described that the invasion is initiated by the formation of F-actin-based invadopodia that breach the basement membrane. UNC-40 specifically enriches the penetrating invadopodia at the side of the basement membrane, what initiates the invasive process (Hagedorn et al., 2013). Cell autonomous signalling of AC, via transcription factor FOS-1A activity, is also necessary for basement membrane removal and AC invasion (Sherwood et al., 2005).

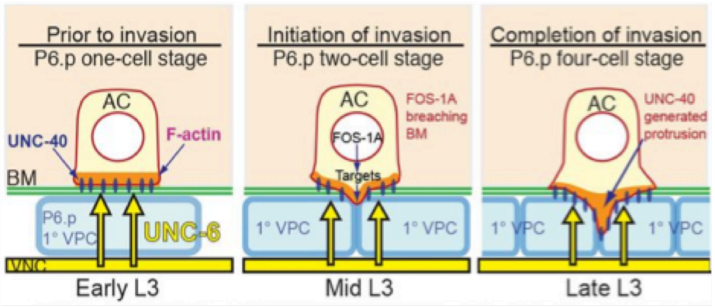

Figure 8. Schematic diagram of the AC invasion regulation. During early L3 larval stage UNC-6 (netrin) (yellow arrows) secreted from the ventral nerve cord (VNC) polarizes its receptor UNC-40 and F-actin towards invasive membrane in contact with the basement membrane (green). During mid L3 larval stage transcription factor FOS-1A promotes AC to breach the basement membrane and UNC-40 mediates the formation of the invasive protrusions. Adapted from (Wang et al., 2014).

The fact that *C. elegans* vulval and uterine development is controlled by highly conserved signalling pathways has established *C. elegans* as a popular model system to understand organogenesis. Several components of these signalling

pathways were indeed first identified in *C. elegans* and later shown to act similarly in other species. Moreover, the process of AC invasion shares several characteristics with invasive cell behaviour in vertebrate and has been proposed as a relevant system to study aspects of metastasis. For these reasons, we propose that the observations on the role of the Vaccinia-Related Kinase 1 during vulval and uterine development reported below may have broad relevance to biology and biomedicine.

1. 2. The family of Vaccinia-Related Kinases

1. 2.1 Protein kinases

Phosphorylation of proteins is an important regulatory mechanism that controls numerous biological processes. It is estimated that approximately 30% of intracellular proteins are reversibly phosphorylated (Cohen, 2000), which makes protein kinases key regulators of biological processes including signal transduction, transcription, cell cycle progression, growth, differentiation and apoptosis. The human kinome consists of 518 protein kinases, what constitutes ~2% of protein encoding genes in human genome (Manning et al., 2002b) and makes kinases one of the largest gene families. There are 130 protein kinases identified in *Saccharomyces cerevisiae*, 239 in *Drosophila melanogaster* and almost twice as much, 454, in *C. elegans* (Manning et al., 2002a). There are several protein kinase classifications described in the literature. Hanks and Hunter's classification into 5 major groups and 55 families was based on conservation and phylogeny analysis of the catalytic domains (Hanks and Hunter, 1995) and has been later extended into 10 groups containing 8 super families and 256 families by Manning and coworkers (Figure 9), who organized proteins kinases based on sequence comparison of catalytic domains aided by sequence similarity and domain structure outside of the catalytic domains,

known biological functions, and a similar classification of the yeast, worm, and fly kinomes (Manning et al., 2002b).

Phylogenetic comparison of human and model organisms' kinomes shows that most protein kinase families are conserved throughout metazoans and only 13 kinase families present in humans are absent either in fly or worm (Manning et al., 2002a).

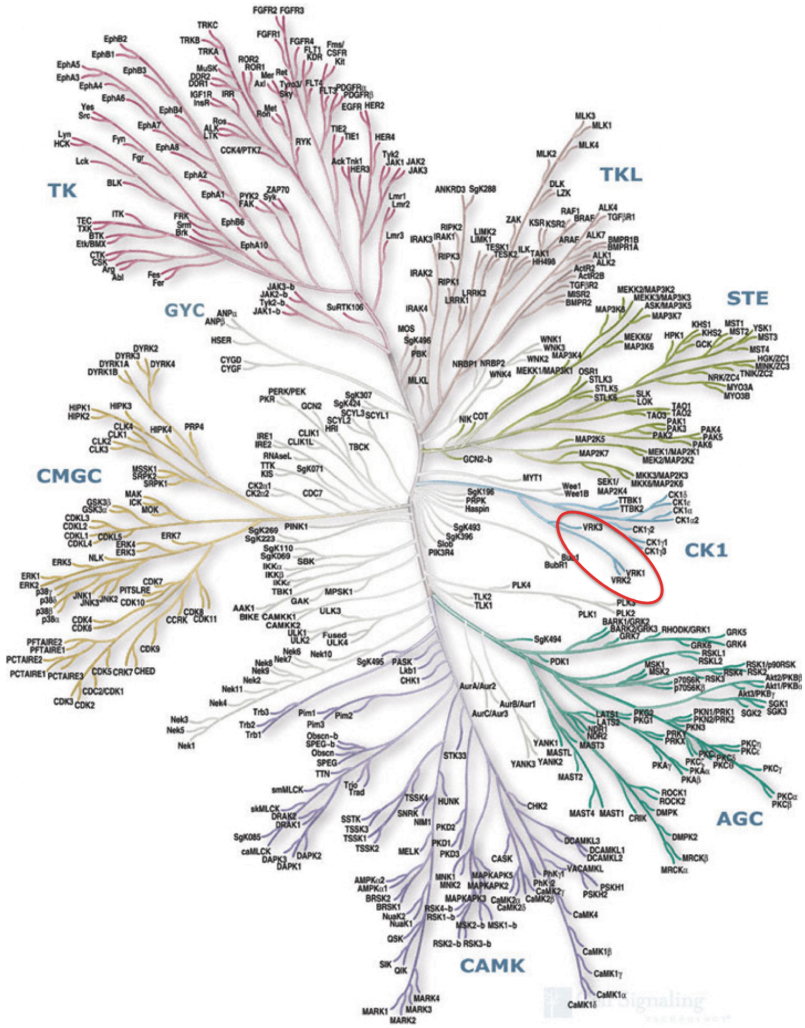

Figure 9. Phylogenetic tree of human kinases. The family of Vaccinia-Related Kinases is marked by a red ellipse. Adapted from Cell Signaling Inc. (http://www.cellsignal.com/).

1.2.2 The Vaccinia-Related Kinases

The human vaccinia-related kinase 1 (VRK1) is a member of a small branch of the casein kinase 1 (CK1) super family (Figure). It was initially discovered by its homology to a serine-threonine vaccinia virus B1R kinase in a screen for genes involved in the regulation of cell division (Nezu et al., 1997). B1R is an early viral gene essential for successful DNA synthesis and replication (Nezu et al., 1997; Rempel and Traktman, 1992).

The VRK kinase family in humans is composed of three proteins – VRK1-3 of which only VRK1 and VRK2 are catalytically active kinases with autophosphorylation activity (Nichols and Traktman, 2004). In worms and flies there is only one ortholog (VRK-1 and nuclosomal-histone kinase 1, NHK-1, respectively). There is no identified VRK ortholog in yeast.

According to standard genetic nomenclature, the proper name of the kinase in humans and *C. elegans* is VRK1 and VRK-1, respectively. However, we adopt the following definition in this thesis: VRK-1 for the *C. elegans* protein, hVRK1 for the human protein and VRK1 as the general denominator across species.

The VRK kinases are highly conserved proteins (Figure 10). Human VRK1 has 40% sequence similarity to the B1R kinase (Nezu et al., 1997). Between orthologs there is a high overall identity – human and mouse VRK1 show 87% identity, VRK2 – 68% and VRK3 – 74%. The identity is lower between paralogs– hVRK1 and hVRK2 show an overall similarity of 44%, hVRK2 and hVRK3 of 23% and hVRK1 and hVRK3 of 33% (Nichols and Traktman, 2004). Human VRKs show highest degree of identity in their catalytic domains, whereas their carboxyl terminus domains are quite variable and show low homology, what suggest that the C-terminal parts of these proteins may play a regulative role (Lopez-Borges and Lazo, 2000).

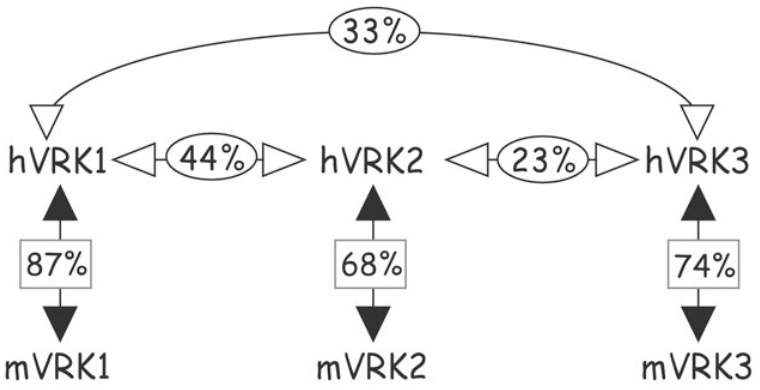

Figure 10. Schematic comparison of the sequence identities between members of human mouse orthologs. Adapted from (Nichols and Traktman, 2004).

VRKs have diverged early from the family of CK1 (Manning et al., 2002b) and they share several sequence variations within their catalytic domains that distinguish them from the majority of protein kinases (Nichols and Traktman, 2004). Protein kinases are grouped mostly because of their catalytic domains, which are divided into 12 motifs (I-XII). While most protein kinases contain an APE tripeptide motif within subdomain VIII, this is substituted by a SIN motif in the CK1 super family, and is further diverged by a (P/S)XD motif in the VRK family. The DFG motif usually present in subdomain VII, is replaced by a DYG motif in all VRKs, except in the fly and worm orthologs (Klerkx et al., 2009b; Nichols and Traktman, 2004).

Human VRK1 is the most studied member of the family. Its open reading frame encodes a 396 amino acid protein, which contains an N-terminal serine-threonine protein kinase domain. Its C-terminal region has a putative nuclear localization signal and a loosely defined basic-acidic-basic motif (BAB motif) of unknown function, which is also present in VRKs in other species (Figure 11). In the region 304–320 it has an endosomal-lysosomal targeting sequence (ELTS) (Valbuena et al., 2008).

INTRODUCTION

VRK2, which was identified by EST database searches (Nezu et al., 1997), has two isoforms (VRK2A and VRK2B) generated by an alternative splicing. VRK2A and VRK2B consist of 508 and 397 amino acids, respectively, and have different C-terminal regions (Blanco et al., 2006). VRK2A contains a C-terminal transmembrane domain as well as two overlapping BAB motifs, which are absent in the shorter isoform (Figure 11).

The last member of the human VRK family, VRK3, which consists of 474 amino acids, is the most divergent kinase. It is the only VRK that lack enzymatic activity due to substitutions at several key residues essential for the catalytic activity (Nichols and Traktman, 2004). However, the VKR3 structure is very similar to VRK2 and their catalytic domain structures show that the overall fold is intact, which demonstrates that the lack of activity of VRK3 is not because of any major structural changes (Scheeff et al., 2009). VRK3 contains a bipartite NLS in the N-terminal region (Figure 11).

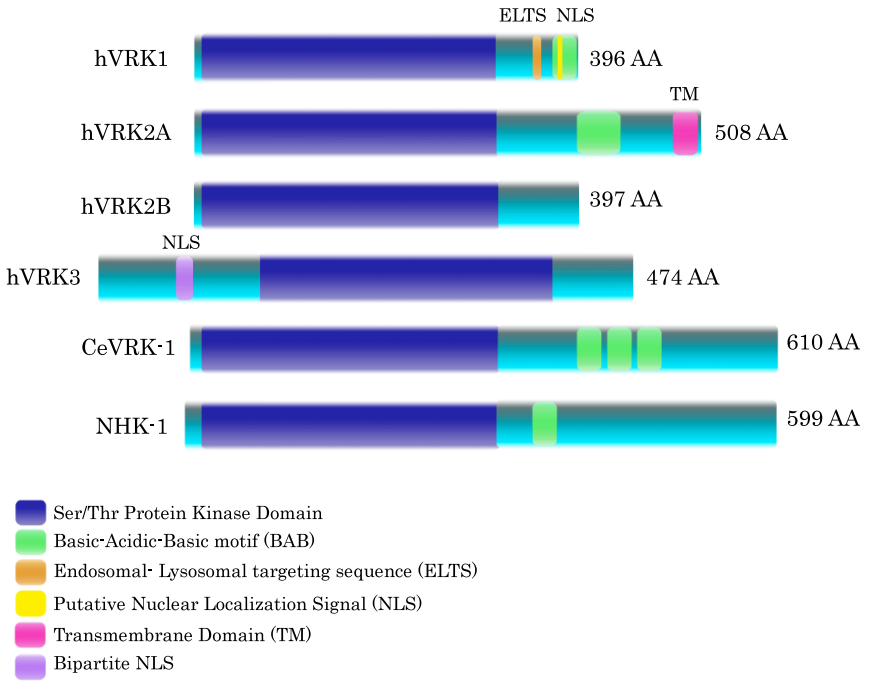

Figure 11. Schematic comparison of the members of VRK family.

Human VRKs are ubiquitously expressed. VRK1 is a nuclear kinase enriched in highly proliferative tissues, like fetal liver, testis and thymus (Nezu et al., 1997), however it is also highly expressed in tissues with lower proliferation rates, like adult liver. Moreover, VRK1 has been related with the development of different human cancers, like lung carcinomas and breast cancer where its expression is highly elevated (Finetti et al., 2008; Valbuena et al., 2007b). What is more, VRK1 expression level positively correlates with several proliferation markers in head and neck squamous cell carcinomas (Santos et al., 2006).

VRK2A is anchored to endoplasmic reticulum (ER) membranes and mitochondria via its C-terminal transmembrane domain, whereas VRK2B, despite the fact that it lacks NLS, is expressed in both cytoplasm and nucleus (Blanco et al., 2006; Nichols and Traktman, 2004). VRK3 localizes exclusively to the nucleus (Nichols and Traktman, 2004).

C. elegans VRK-1 contains 610 amino acids including a N-terminal kinase domain and three C-terminal BAB motifs (Aihara et al., 2004; Klerkx et al., 2009b)(Figure 11).

Identified in a biochemical purification of histone kinases, the *D. melanogaster* ortholog of VRK, nhk-1, encodes a 599 amino acids protein with a conserved N-terminal kinase domain and a BAB motif in its C-terminus (Aihara et al., 2004) (Figure 11).

1.2.3 Role of VRK1

1.2.3.1 Regulation of Transcription Factors

VRK1 phosphorylates several transcription factors including the tumor suppressor p53. p53 (aka TP53) is one of the most studied proteins and its regulation plays a critical role in the control of cell cycle progression, DNA

replication and apoptosis. p53 is regulated by reversible phosphorylation in many threonine and serine residues and VRK1 phosphorylates p53 in vitro at Thr18 located in the N-terminal transactivation domain (Barcia et al., 2002; Lopez-Borges and Lazo, 2000; Vega et al., 2004). Phosphorylation at Thr18 disrupts p53's interaction with Mdm2, which is the main p53 negative regulator, and promotes the recruitment of the p300 co-activator, which stabilizes p53 by acetylating its carboxy terminus (Vega et al., 2004). VRK1 activation of p53 promotes the degradation of VRK1 and creates an autoregulatory loop between p53 and VRK1 and their levels are inversely correlated in different cultured cell lines (Valbuena et al., 2006). Damage-Regulated Autophagy Modulator (DRAM) has been proposed to be implicated in the p53-induced degradation of VRK1 in response to DNA damage (Valbuena et al., 2011a). What is more, p53 co-activators, p300 and CBP, have been demonstrated to prevent p53 downregulation of VRK1 in an acetylation independent manner (Valbuena et al., 2008). However, the p53-VRK1 autoregulatory loop is altered in human cancers with inactivating p53 mutations, which results in elevated levels of VRK1 (Valbuena et al., 2007b), because the targeting of VRK1 to enter the endosome-lysosome degradation pathway requires the transcriptional induction by p53 (Valbuena et al., 2006). Recent publications demonstrate that VRK1 forms a stable complex with p53 in non-damaged cells and that the C-terminus of VRK1 and the DNA binding domain of p53 are involved in the binding (Lopez-Sanchez et al., 2014). The existence of a basal intracellular p53-VRK1 complex ensures immediate p53 phosphorylation in response to UV-induced DNA damage and suggests a role of VRK1 in detection of DNA damage.

Besides p53, VRK1 is reported to phosphorylate other transcription factors, like c-Jun, ATF2 and CREB (Kang et al., 2008; Sevilla et al., 2004a; Sevilla et al., 2004b). c-Jun is a critical component of AP-1 transcription factors that are dimeric proteins composed of basic region-leucine zipper proteins and belong to the FOS, JUN, ATF, and MAF protein subfamilies (Shaulian and Karin, 2002). c-

Jun has been linked to tumor cell survival, proliferation and apoptosis. It is phosphorylated by several mitogen-activated protein kinases (MAPK) that include extracellular signal regulated kinase (ERK) and c-Jun N-terminal kinase (JNK). VRK1 phosphorylates c-Jun on the same residues that JNK (Ser63 and Ser73), independently from JNK, resulting in intracellular accumulation and stabilization of c-Jun and there is an additive effect on c-Jun phosphorylation by these two kinases (Sevilla et al., 2004a).

Sevilla and coworkers have described that VRK1 phosphorylates the cAMP-dependent transcription factor ATF2 (Sevilla et al., 2004b), a member of the family of ATF/CREB transcription factors that are implicated in the regulation of cellular growth, metabolism, proliferation and apoptosis (Persengiev and Green, 2003). VRK1 phosphorylates ATF2 in its amino-terminal region on Thr73 and Ser62, which stabilizes ATF2 protein and increases its transcriptional activity (Sevilla et al., 2004b).

VRK1 phosphorylation of the CREB (cAMP response element-binding protein) transcription factor at Ser133 (Kang et al., 2008) links VRK1 with the regulation of the cell cycle. Phosphorylation of CREB promotes its binding to the cAMP response element (CRE) of the cyclin D1 promoter, activating its transcription and accumulation, which promotes the G1 to S phase progression in the cell cycle. Moreover, Myc stimulates VRK1 expression by direct binding to its promoter.

1.2.3.2 VRK1 and Nuclear Envelope Dynamics

The Nuclear Envelope (NE), a specialized cisterna of the endoplasmic reticulum (ER), is made of two distinct membrane domains. The inner nuclear membrane (INM) and outer nuclear membrane (ONM) are connected by nuclear pore complexes (NPC), which ensure transport between nucleus and cytoplasm.

While the ONM is continuous with the ER, the INM harbors different transmembrane proteins and contacts to the filamentous nuclear lamina. During cell division the NE is disassembled when cells enter mitosis (nuclear envelope breakdown, NEBD) and reassembles after chromosomes segregation. Barrier-to autointegration factor (BAF) is a small protein that is essential for the maintenance of the chromatin structure and chromosome segregation, binds DNA, histones, various transcription factors and components of the INM (Lee et al., 2001; Margalit et al., 2007). The localization of BAF is cell cycle dependent. BAF concentrates at the nuclear periphery and interacts with LEM domain proteins of the INM during interphase, but is soluble during mitosis (Gorjanacz et al., 2007; Haraguchi et al., 2001). Phosphorylation of BAF is critical for its function in NE disassembly and reassembly and VRK1 phosphorylates the N-terminus of mammalian BAF (Nichols et al., 2006). This activity is conserved among species, since *C. elegans* VRK-1, *D. melanogaster* NHK-1 and viral B1 kinases also phosphorylate BAF (Gorjanacz et al., 2007; Lancaster et al., 2007; Wiebe and Traktman, 2007). Phosphorylation of BAF upon entry into mitosis releases BAF from chromatin and reduces its affinity for LEM domain proteins (Nichols et al., 2006), which allows the NEBD and mitosis progression. During mitotic exit, Lem4 in *C. elegans* and human cells directly interacts with and inhibits VRK1, and recruits protein phosphatase 2 (PP2A) complex to BAF, which results in BAF dephosphorylation and NE reassembly (Asencio et al., 2012)(Figure 12).

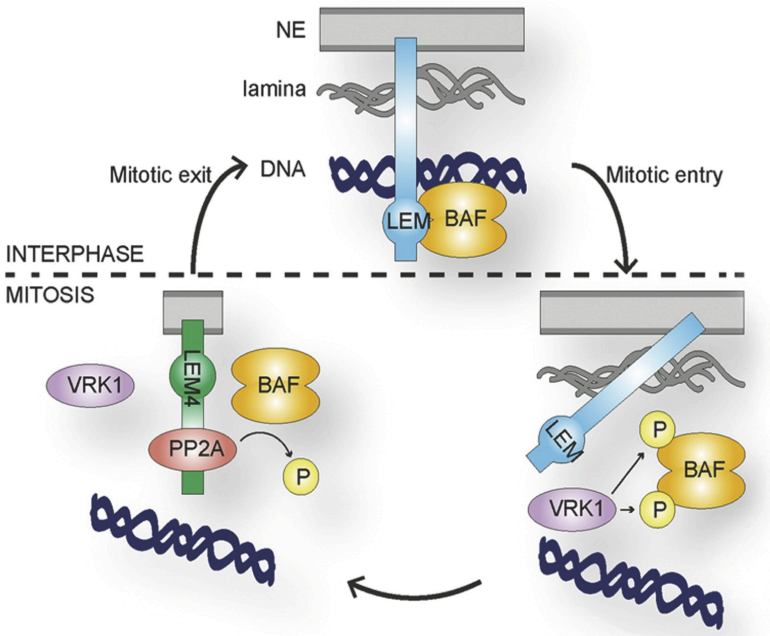

Figure 12. Schematic model of the coordination of VRK1 and BAF activity during mitosis. See Adapted from (Asencio et al., 2012)

Depletion of VRK-1 in *C. elegans* embryos results in an abnormal NE completely devoid of NPCs (Gorjanacz et al., 2007) and a similar phenotype was observed in VRK1 depleted human cells (Molitor and Traktman, 2014). In the absence of VRK1 in *C. elegans* embryos and human cells BAF remains chromosome-bound upon mitotic entry and defects in chromosome segregation are observed (Gorjanacz et al., 2007; Molitor and Traktman, 2014)(Figure 13 A and B).

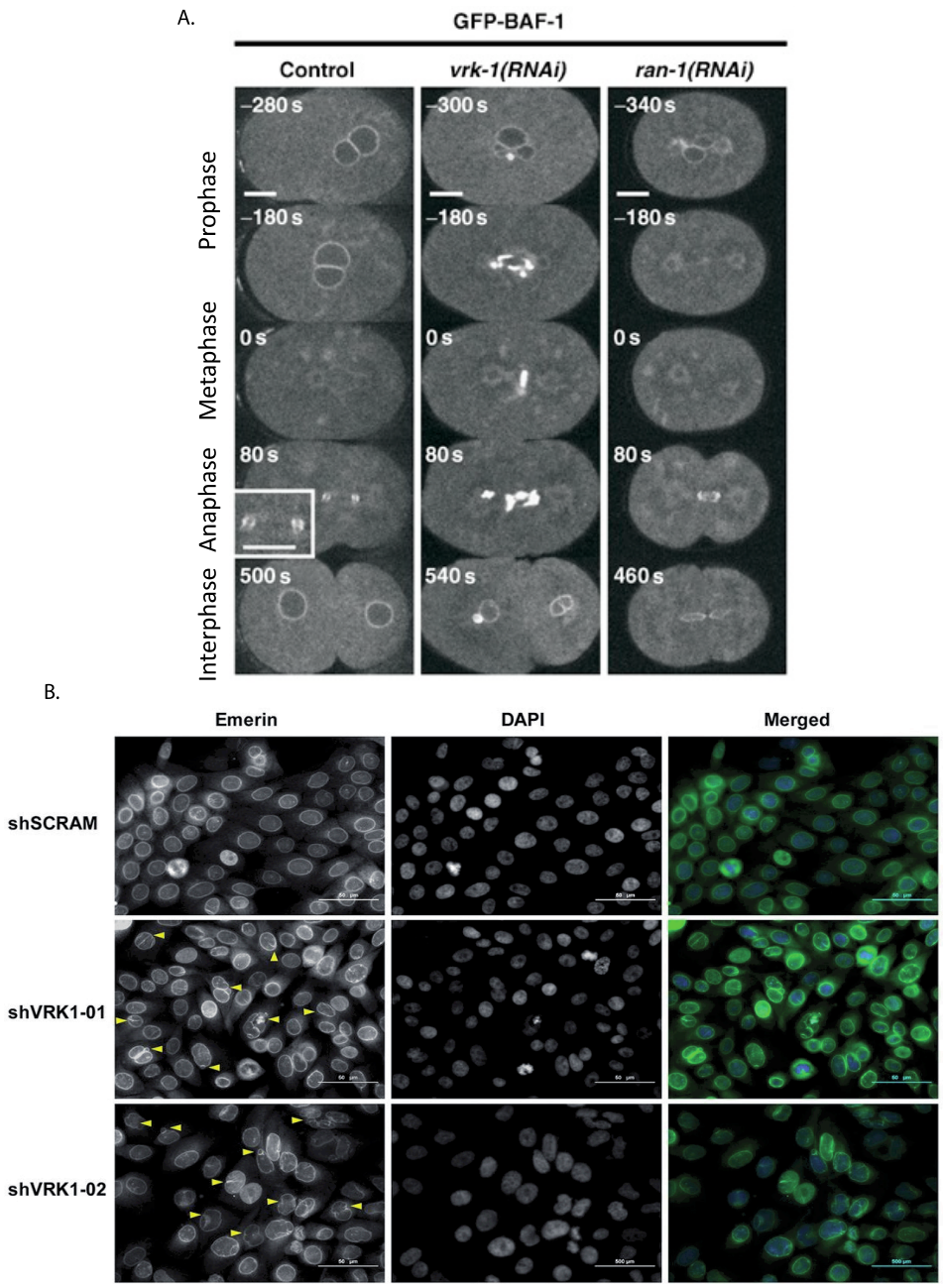

Figure 13. Defects upon loss of VRK1 in *C. elegans* embryos and human cells A. Depletion of VRK-1 by RNAi in *C. elegans* embryos causes BAF-1 association with chromatin during mitosis. Scale bars, 10µm. Adapted from (Gorjanacz et al., 2007) **B.** Depletion of VRK1 in human cells by RNAi causes an increase in the aberrant nuclear envelope morphology. Adapted from (Molitor and Traktman, 2014).

1.2.3.3 VRK1, Histone Phosphorylation and Chromatin Condensation

The variety of posttranslational modifications of histones includes reversible acetylation, phosphorylation, ubiquitination and sumolyation, and plays fundamental roles in the regulation of transcription, DNA repair, replication and recombination (Bannister and Kouzarides, 2011). Moreover, histone modifications are thought to pattern epigenetic codes, which regulate chromatin organization and transcription. VRK1's capacity to phosphorylate histones introduced above is likely to reflect a role in chromatin modification.

D. melanogaster NHK-1 phosphorylates the conserved Thr119 of histone H2A in vitro (Aihara et al., 2004; Ivanovska et al., 2005), which is required for the acetylation of lysine residues on histone H3 and H4 in *Drosophila* oocytes (Ivanovska et al., 2005). Mutation in NHK-1 causes sterility due to defects in the formation of the karyosome and the metaphase I arrest (Ivanovska et al., 2005; Lancaster et al., 2007). Moreover, NHK-1 is essential for mitotic progression and its depletion causes overcondensation of chromosomes and defects in mitotic spindle formation (Cullen et al., 2005). H2A Thr119 phosphorylation is found throughout chromatin during interphase, while it is specific to centromers in mitosis (Brittle et al., 2007) and it has been shown that Polo kinase suppresses H2A phosphorylation by NHK-1 on chromosome arms, which is independent from Aurora B kinase that also phosphorylates histone H2A on Thr119.

VRK1 in mammalian cells phosphorylates histone H3 on Thr3 and Ser10 both in vitro and in vivo (Kang et al., 2007). Thr3 and Ser10 are also phosphorylated by haspin and AuroraB, respectively, and the contribution of VRK1 to the Ser10 phosphorylation is similar to Aurora B. Similarly to the depletion of NHK-1 in flies and RNAi against VRK-1 in worms which causes dramatic nuclear condensation (Cullen et al., 2005; Gorjanacz et al., 2007), overexpression of VRK1 in mammalian cells leads to hypercondensed chromatin (Kang et al., 2007).

In addition to Lem4 mentioned above, few other inhibitors of VRK1 have been described. The nuclear Ran GTPase, a member of the small GTPase family of signaling proteins, was identified in biochemical co-purifications as a negative regulator of VRK1 activity (Sanz-Garcia et al., 2008). When Ran is in its inactive form, bound to GDP, but not active, bound to GTP, it reduces VRK1 autophosphorylation and phosphorylation of histone H3 on Thr 3 and Ser10. Also RCC1, which is the nucleotide exchange factor for Ran, facilitates the interaction of VRK1 with Ran.

More recently, MKP2, a member of mitogen-activated protein kinase phosphatases (MKPs), which inactivate MAPKs, was identified as a VRK1 suppressor (Jeong et al., 2013). MKP2 negatively regulates histone H3 phosphorylation by VRK1 independently from MKP2 phosphatase activity. Moreover, MKP2 and VRK1 interact in the chromatin fraction, with a peak at the M phase.

VRK1 phosphorylation of histone H3, in order to ensure chromosome compaction and precise progression of the cell cycle should be restricted to mitosis and macrohistone H2A1.2 (MacroH2A1) has been reported as a VRK1 suppressor during interphase (Kim et al., 2012). MacroH2A1 is a core histone variant associated with X chromosome inactivation and repression of transcription (Angelov et al., 2003; Costanzi and Pehrson, 1998). It interacts with VRK1 via its macrodomain and affects the phosphorylation of VRK1 substrates, however during mitosis, when the expression level of MacroH2A1 decreases VRK1 is liberated and can phosphorylate histone H3 together with Aurora B and haspin kinases (Kim et al., 2012) (Figure 14).

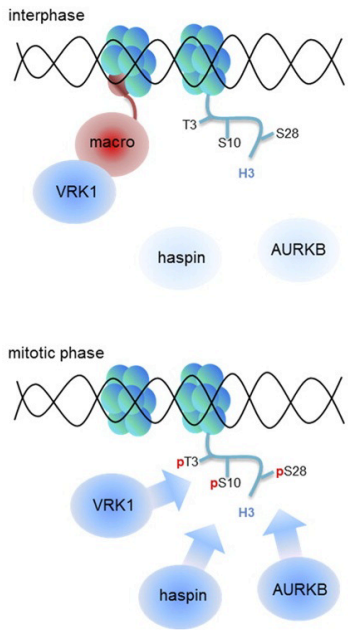

Figure 14. Schematic model proposing cell-cycle dependent inhibition of VRK1 by a histone variant MacroH2A1. During interphase VRK1 phosphorylation activity, which is suppressed by MacroH2A1, as well as low levels of haspin and Aurora B maintain histone H3 dephosphorylated, however during mitosis, when expression of MacroH2A1 decreases and of Aurora B and haspin increases, histone H3 is phosphorylated by VRK1, Aurora B and haspin. Adapted from (Kim et al., 2012).

1.2.3.4 VRK1 and Cell Cycle Progression

It has been proposed that VRK1 participates in the control of cell cycle progression. VRK1 is highly expressed in the proliferative tissues (Vega et al., 2003) and its expression correlates with proliferation markers in human normal tissues (Ki67 proliferation marker), and cancers (CDK2, CDK6, cyclin A and B1, topoisomarese II and survivin) (Santos et al., 2006). Moreover, the loss of VRK1 causes a block in progression from G1 to S phase and its expression parallels that of c-*myc* and c-*fos,* which are early response genes (Valbuena et al., 2008). VRK1 regulates cell cycle progression by phosphorylation of the cAMP-

response element-binding protein and increasing cyclin D1 expression (Kang et al., 2008). Additionally, its crucial role in chromatin and nuclear envelope dynamics by phosphorylation of BAF (Nichols et al., 2006) and histone H3 during mitosis (Kang et al., 2007) may impinge on cell cycle progression. VRK1 has been demonstrated to be essential for the maintenance of mouse spermatogonial stem cell (Choi et al., 2010) and in meiotic progression during oogenesis (Schober et al., 2011). Also in *C. elegans and D. melanogaster* VRK1 has been implicated in the germ cell development and mitotic and meiotic progression (Walters et al. 2010).

1.2.3.5 VRK1 Localization During Cell Cycle

Human VRK1 is expressed in the nucleus of most cell types with variable localization also in the cytosol and Golgi apparatus, depending on cell type and study (Lopez-Sanchez et al., 2009; Nichols and Traktman, 2004; Valbuena et al., 2007a). Kang and coworkers have shown that in mammalian cells VRK1 expression is variable during cell cycle, being hardly detectable during G1 phase and with a gradual increase in its expression from G1 to M phase (Kang et al., 2007). VRK1 is found soluble in the nucleoplasm, but can also be isolated in heterochromatin and euchromatin fractions. According to one study, VRK1 is associated with chromatin both, during interphase and mitosis and colocalizes with chromatin associated gamma heterochromatin protein 1 (HP1γ) during interphase (Kang et al., 2007). However, another publication claims that VRK1 does not bind chromatin during mitosis, but is dispersed throughout the nucleus (Valbuena et al., 2011b), so more detailed analysis is required to describe VRK1 dynamics during cell cycle. In *C. elegans*, VRK-1 is nuclear and is expressed in neurons in the head and tail, hypodermal cells and vulva precursor cells (VPCs)(Klerkx et al., 2009a). During interphase it is nuclear, however, just before NEBD it goes to the nuclear rim, presumably to phosphorylate BAF and

ensure its release form chromatin (Gorjanacz et al., 2007). During mitosis VRK-1 remains associated with condensed chromatin. NHK-1 in *Drospohila* embryos is cytoplasmic during early S phase, but as cells enter into mitosis it localizes to condensed chromatin (Aihara et al., 2004).

1.2.3.6 VRK and cytoplasmic organelles

VRK1 is degraded by an endocytic-lysosomal pathway, which is p53 dependent, and it has been proposed that a subpopulation of VRK1 is localized in the Golgi apparatus (Valbuena et al., 2007). The Golgi apparatus is composed of flattened membrane-enclosed sacs (cisternae) and associated vesicles and functions in the final processing of proteins and lipids within the cell. During mitosis the Golgi, like other cellular organelles, is redistributed into the two daughter cells. Polo kinase (Plk3) mediates MEK1 function in Golgi fragmentation during cell division and VRK1 has been linked to that pathway as a downstream target of Plk3, which phosphorylates C-terminus of VRK1 on Ser342 (Lopez-Sanchez et al., 2008). VRK1 interacts with Plk3 and has been postulated to be required for the induction of Golgi fragmentation during mitosis.

1.2.4 Role of VRK2

The catalytic domains of human VRK1 and VRK2 are closely related as they show 92% identity (Nichols and Traktman, 2004) and they share some substrates. VRK2, like VRK1, can phosphorylate p53 at Thr18 (Blanco et al., 2006), the extreme N-terminus of BAF in vitro (Nichols et al., 2006) and both interact with the Ran GTPase (Sanz-Garcia et al., 2008). However, the role of VRK2A in vivo is related mostly with its interactions with scaffold proteins. It has been associated with the regulation of the stress response induced by hypoxia or interleukin-*1*β by its interaction with the JNK interacting proteins

(JIPs) (Blanco et al., 2007; Blanco et al., 2008). Moreover, VRK2A is able to downregulate the MAPK signaling pathway by directly interacting with a KSR1 scaffold protein (Fernandez et al., 2010; Fernandez et al., 2012). VRK2 is also reported to have role in protection from apoptosis. It increases cell survival upon interaction with BHRF1, an Epstein-Barr virus gene product homologous to the cellular anti-apoptotic protein Bcl-2 (Li et al., 2006). Other studies have associated VRK2 expression with a better prognosis in malignant astrocytomas (Rodriguez-Hernandez et al., 2013) and recent publications have linked VRK2 with schizophrenia (Li et al., 2012; Steinberg et al., 2011), epilepsy (Steffens et al., 2012) and Huntington´s disease (Kim et al., 2014).

1.2.5 Role of VRK3

VRK3 is the least characterized member of VRK family. Although it lacks enzymatic activity, it is reported to inhibit extracellular signal-regulated kinase (ERK) signaling, implicated in controlling proliferation and differentiation, by directly activating vaccinia H1-related (VHR) phosphatase (Kang and Kim, 2006, 2008). Combined transcriptomic and proteomic studies revealed VRK3 as a putative VHR substrate (Hennig et al., 2012).

1.3. *vrk-1* mutant phenotypes in *C. elegans* post-embryonic development

C. elegans VRK-1 was first identified in a large scale RNAi functional analysis of genes enriched in ovaries as potentially regulating nuclear appearance (Piano et al., 2002).

The *vrk-1* mutant allele *ok1181* lacks almost 30% of the open reading frame (Figure 15A) and the truncated protein is not detectable by Western blot analysis (Klerkx et al., 2009). Loss of *vrk-1* in *C. elegans* hermaphrodite causes

severe defects in post-embryonic development, in particular abnormalities in the development of the egg-laying apparatus and sterility. Depletion of *vrk-1* affects anchor cell polarity and invasion, formation of the vulva, uterus lumen and uterus seam syncytium (utse), which leads to a severe protruding vulva phenotype (Pvl) (Klerkx et al., 2009 and Figure 15B). VRK-1 was also implicated in proper specification and proliferation of uterine cells and regulation of EGL-17, a fibroblast growth factor (FGF)-like protein (Klerkx et al., 2009), which activity is necessary for proper migration of sex myoblasts (Burdine et al., 1997). Expression of both EGL-17 and its receptor EGL-15 in *vrk-1* mutants was significantly reduced, which suggests that VRK-1 regulates, at least partially FGF signaling. Loss of *vrk-1* from the gonad causes severe proliferation defects that result in a reduction in the number of nuclei and DNA morphology, which was both condensed and fragmented (Waters et al., 2010; Figure 15C).

Depletion of VRK-1 by RNAi leads to early embryonic lethality (Gorjanacz et al., 2007; Piano et al., 2002), however homozygous *vrk-1(ok1181)* animals produced by heterozygous *vrk-1(ok1181)* hermaphrodites are viable, and do not show any evident defects until early L3 larval stage, which can be explained by the maternal contribution.

For the purpose of this thesis we will refer to homozygous *vrk-1(ok1181)* worms coming from heterozygous *vrk-1(ok1181)* hermaphrodites as “mutant” animals and heterozygous vrk-1(ok1181) as “control” animals, unless otherwise indicated.

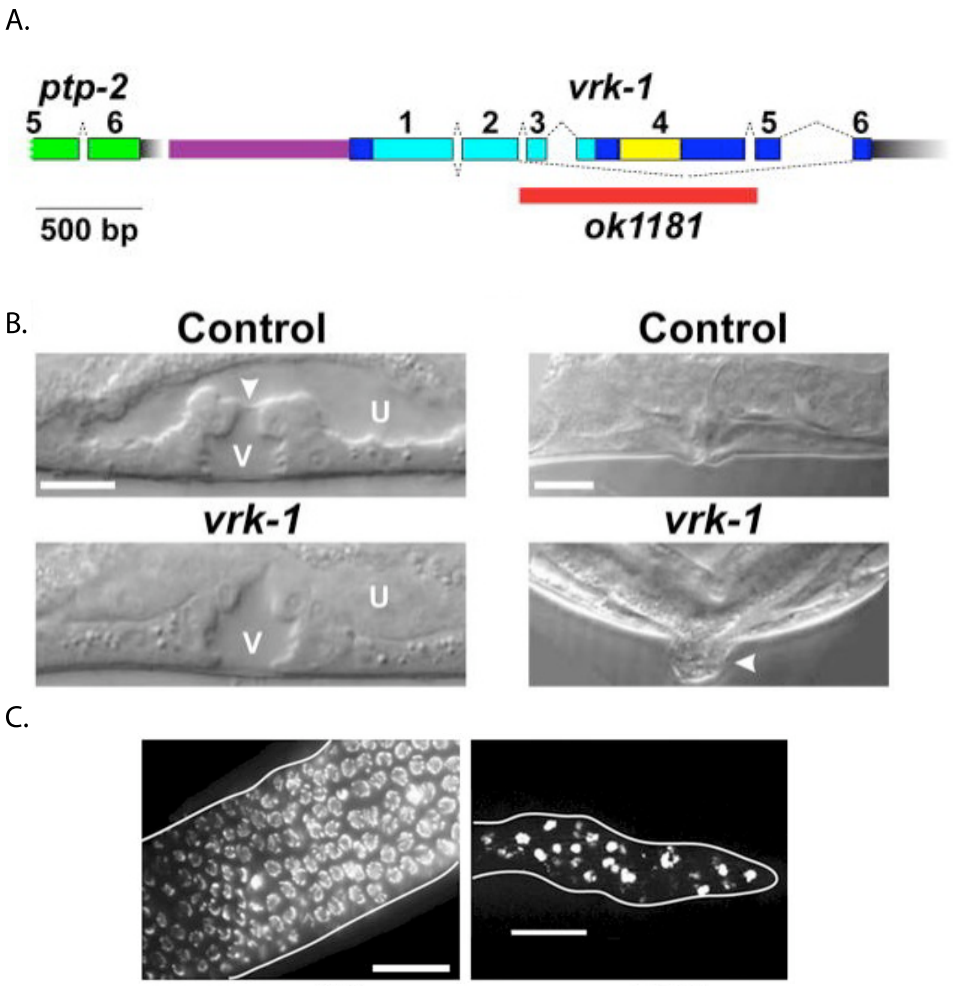

Figure 15. A. Schematic representation of the *vrk-1* gene. Purple- *vrk-1* promoter; blue boxes – *vrk-1* exons; light blue boxes – *vrk-1* kinase domain; yellow box – BAB domain, grey – 3ÚTRs, red bar- region deletaed in *ok1181*; dashed lines – mRNA splicing pattern. Adapted from (Klerkx et al., 2009a) **B. VRK-1 depletion phenotypes.** *C. elegans vrk-1(ok1181)* mutants show defects in the development of the vulva (V) and uterus (U), and they lack uterine seam syncytium (utse, arrow head in top left panel) which results in the Pvl phenotype (arrow head in bottom right panel). Scale bar 10µm. Adapted from (Klerx et al., 2009) **C.** *vrk-1(ok1181)* mutants (left) show defects in the proliferation of the germ line. Scale bars, 20µm. Adapted from (Waters et al., 2010).

II. OBJECTIVES

1. Characterize the dynamics of VRK1 localization both in *C. elegans* and human cells.
2. Relate VRK-1 with signalling pathways involved in development of *C. elegans* reproductive organs and organ development in general.
3. Identify interacting partners of VRK1.

III. RESULTS

RESULTS

III. RESULTS

OBJECTIVE 1

3.1. VRK-1 is a ubiquitously expressed protein

3.1.1 Single copy transgenic strains show more ubiquitous expression than strains carrying multiple copies of the transgene

Initially described postembryonic nuclear expression of VRK-1 in *C. elegans* included neurons in the head and tail, ventral nerve cord (VNC), hypodermal cells and vulva precursor cells (VPCs). These results were based on the usage of the YL255 and YL262 transgenic strains, obtained by microparticle bombardment, expressing VRK-1::GFP under control of the putative *vrk-1* promoter (Klerkx et al., 2009a). Microparticle bombardment is a method to generate transgenic *C. elegans* strains that has been designed to create low copy chromosomal insertions and thereby offering an alternative to injection of multicopy extrachromosomal arrays, which are less stable and can contain hundreds of copies of the transforming DNA. Multiple copies of the transgene can cause overexpression, underexpression and silencing of the transgene (Praitis, 2006). However, the microparticle bombardment method also has similar, although not so dramatic, limitations. It is based on the integration of an unknown copy number of the transgene and random positioning of the integration, which can affect the expression (Praitis, 2006).

It was reported that inserted by microparticle bombardment, the VRK-1::GFP transgene reduced the Pvl phenotype of *vrk-1* deficient mutants from 75% to 24%. However, adult animals remained sterile, presumably because of the lack of expression in the germ line (Klerkx et al., 2009).

RESULTS

In order to better characterize the expression pattern of VRK-1 in *C. elegans* and rescue more efficiently the *vrk-1* mutant phenotype, we decided to use the *Mos1* mediated Single Copy Insertion (MosSCI) method that inserts a single copy of a transgene into a defined site and allows expression at endogenous level (Frokjaer-Jensen et al., 2008).

We created three new constructs to be inserted in a intergenic region on chromosome IV, using GFP, mCherry and Dendra2 (strains BN156, BN171 and BN193, respectively) as fluorescent tag inserted in frame at the carboxyl terminus of VRK-1 followed by the *vrk-1* 3´UTR. Transgenes were expressed under control of the previously described endogenous promoter (Klerkx et al., 2009).

The efficiency of MosSCI for three different insertions was quite variable and is shown in Table 1.

Transgene	Insert size [kb]	Injected worms	F1 lines	F2 lines	Functional lines	Efficiency
Pvrk-1::vrk-1::GFP 3´UTR	7.9	28	5	5	1	20.0%
Pvrk-1::vrk-1::mCh 3´UTR	7.9	65	13	11	1	7.7%
Pvrk-1::vrk-1::Dendra2 3´UTR	7.9	40	≥1	≥1	1	NA

Table 1. Efficiency of MosSCI insertion. "Injected worms" is the total number of injected worms. "F1 lines" is the number of lines coming from injected worms carrying extrachromosomal array marker. "Functional lines" is the number of lines that come from animals that produced progeny carrying single copy integrated transgenes and lacking extrachromosomal array markers.

Members of the VRK family in humans show ubiquitous tissue distribution (Nezu et al., 1997; Nichols and Traktman, 2004). We examined the expression pattern of integrated *vrk-1*::GFP fusion gene in *C. elegans* (strain BN156) and compared it with the strain YL255 in order to describe more thoroughly the

distribution of VRK-1 in worms. The single copy transgene in the strain BN156 was expressed at much lower levels than the same construct in the strain YL255 (Figure 16). However, we could see more ubiquitous expression pattern of single copy transgenes when compared with previous observations for the strain YL255. Nuclear expression of VRK-1::GFP, VRK-1::mCherry and VRK-1::Dendra2 was observed not only in previously reported cells, but also in the AC, uterine tissue and germ line (Figure 17). Expression in the germ line however, was quite variable between the three strains: we observed expression in 5% of BN156 (GFP) 55% of BN171 (Cherry) and 95% of BN193 (Dendra2; n=20 adults/strain). Multi-copy transgenes are frequently silenced in the *C. elegans* germ line (Kelly et al., 2007) what could explain lack of expression of VRK-1::GFP in the germ line in YL255 strain and the fact that in our new strains single-copy transgenes are not suppressed in that tissue. However, we cannot explain the variability in germ line expression of single copy transgenes but we note that this has been reported (Shirayama et al., 2012). VRK-1 expression in the germ line is consistent with previous immunofluorescence results analyzing endogenous VRK-1 (Gorjanacz et al., 2007).

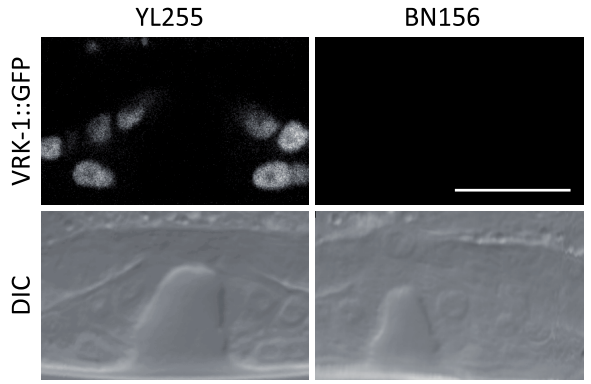

Figure 16. Expression of VRK-1 in YL255 and BN156 strains analyzed by live microscopy. Strain YL255 generated by microparticle bombardment shows much higher expression of VRK-1::GFP then single copy VRK-1::GFP in the BN156 strain generated by MosSCI. Still images taken using identical microscope settings. Scale bar, 10μm.

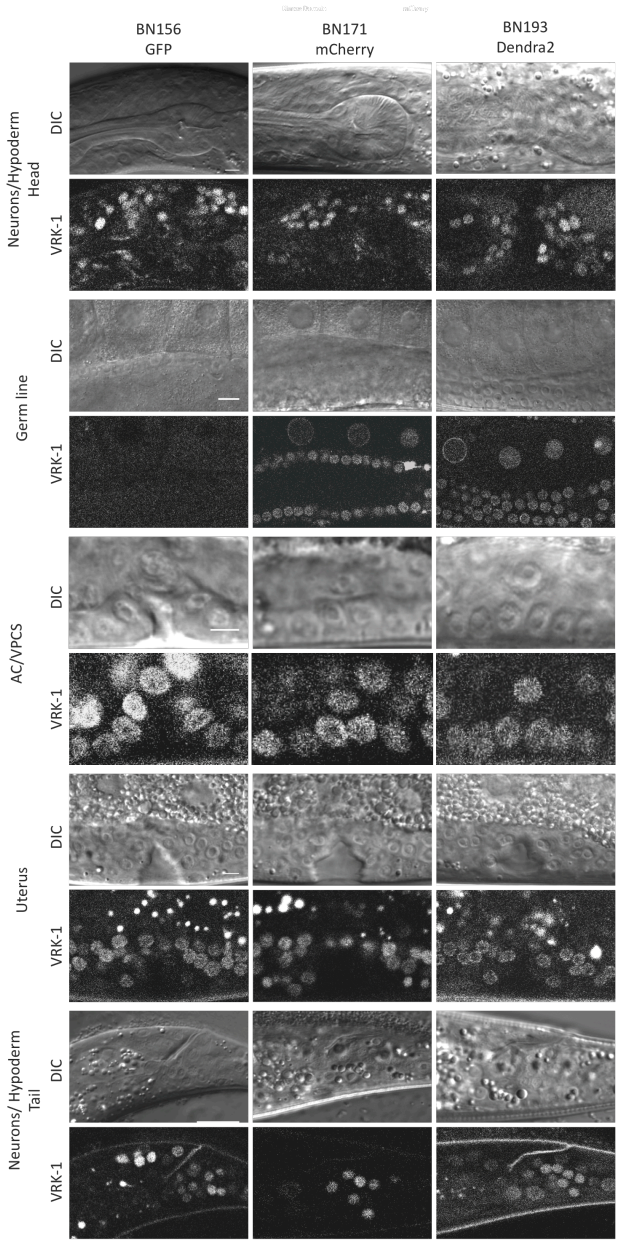

Figure 17. Expression of VRK-1 in different strains analyzed by live microscopy. Single-copy transgenic strains generated by MosSCI show ubiquitous nuclear expression of VRK-1. VRK-1 is expressed in the hypodermal cells and neurons in the head and tail of the worm, as well as in the VNC, VPCs, AC, uterine tissue and germ line. VRK-1 shows variable germ line expression in different single-copy transgenic strains. Still images taken using different microscopes and different microscope settings. Scale bars, 10 μm.

Dendra2 is a monomeric, photoconvertible fluorescent protein that can be converted from green to red when induced by intense blue or UV light (Chudakov et al., 2007). It is commonly used to monitor protein turn-over and mobility. We decided to use Dendra2 as a fusion protein in order to measure the VRK-1 turn-over in *C. elegans*, however, the signal intensity before and after photoconversion was too low to perform valid quantifications.

3.1.2 Single copy transgenic strains rescue mutant phenotypes

In order to test if our new single-copy transgenes are functional and to compare their rescue capability with strain YL255, we assayed the degree of rescue by counting worms with the protruding vulva (Pvl) phenotype and sterile adults (Figure 18). When reaching adulthood, ~100% of wild type N2 hermaphrodites are fertile and do not show the Pvl phenotype. In contrast, close to 80% of *vrk-1* mutants have a protruding vulva and 100% are sterile. As mentioned above, previous rescue experiments have shown a partial reduction of the Pvl phenotype (Klerkx et al., 2009a). When we rescued *vrk-1* mutants with single copy transgenes, we could see not only a complete rescue of the Pvl phenotype, but also recovery of the fertility. In agreement with the variability in germ line expression we observed large variation in sterility rescue efficiencies. While only 22% of adults in the strain BN171 (mCherry) and 58% in the BN193 (Dendra2) were sterile, we did not see any reduction of that phenotype in the strain BN156 (GFP) (Figure 18). The sizes of the fusion proteins were similar (Table 1), so they should not affect the rescue capability. The lowest rescue efficiency of the VRK-1::GFP could be explained by the fact that the frequency of its expression in the germline was also the lowest.

Highest rescue efficiency was obtained with mCherry as a fusion tag so we decided to use this fluorescent protein when designing additional constructs.

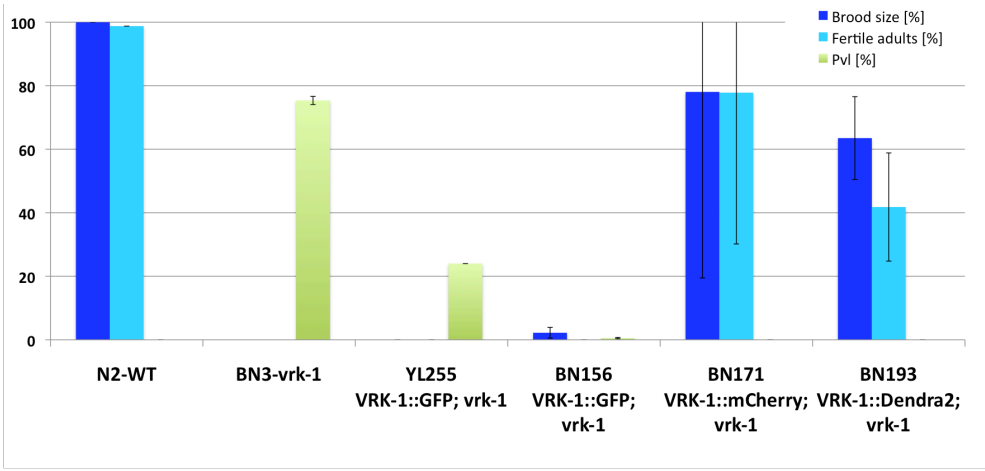

Figure 18. Single-copy transgenes rescue *vrk-1 (ok1181)* phenotypes. The percentage of fertile adults (light blue), brood size (dark blue) and adults with Pvl (green) is shown. Brood size is relative to the value of the wild type animals; fertile adults are relative to the brood size. Error bars report the standard error of the mean.; n>200.

3.2. Proper nuclear localization of VRK-1 depends on its C-terminus and is independent from kinase activity

In *C. elegans*, VRK-1 localizes mainly to the cell nucleus with a slight cytoplasmic fraction (Gorjanacz et al., 2007; Klerkx et al., 2009a). Proper localization in different cell types or tissues is a prerequisite for adequate accessibility to substrates thus proper function of protein kinases. In order to characterize the dynamics of VRK-1 localization in nematodes, we generated single copy transgenic strains expressing three different mutated proteins.

3.2.1 Kinase-dead mutant

To decipher if proper nuclear localization of VRK1 depends on its kinase activity, we generated a ´kinase dead´ mutant. Substitution of the conserved lysine residue (K179E) within the catalytic loop (VI) of the kinase domain in human VRK1 causes loss of autophosphorylation and kinase activity (Vega et al., 2004). We substituted the equivalent lysine in *C. elegans* VRK-1 (K169E; Figure

19A) and we observed that VRK-1 K169E::mCherry localizes properly to the nucleus (Figure 19B) meaning that VRK-1 kinase activity is not essential for proper nuclear localization.

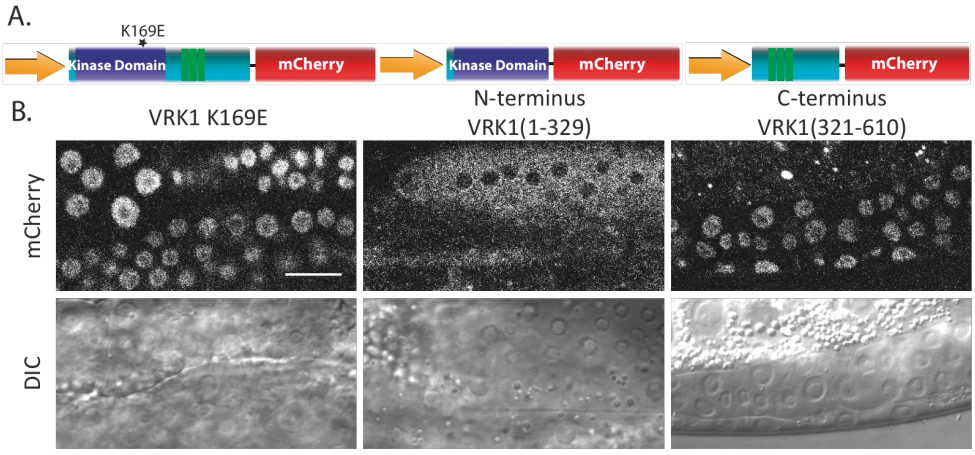

Figure 19. Expression and localization of truncated VRK-1 and ´kinase dead´ mutant A. Schematic representation of *C. elegans* mutant proteins fused to mCherry – ´kinase dead´ mutant, N-terminal and C-terminal half **B.** Inactive VRK-1 K169E::mCherry as well as C-terminal half of VRK-1::mCherry localize properly to the nucleus (left and right panels), however N-terminal half of VRK-1::mCherry containing the highly conserved protein kinase domain fails to localize to the nucleus and shows cytoplasmic expression (middle panels). Still images taken using different microscope settings. Scale bar, 10µm.

3.2.2 N-terminus and C-terminus

Next step in the characterization of the dynamics of VRK-1 localization was splitting the protein into two fragments; one containing the highly conserved N-terminal protein kinase domain and the other one the carboxyl terminus. Based on the PredictProtein tool (https://www.predictprotein.org), we decided to construct two VRK-1 fragments with a short overlap. We truncated VRK-1 at threonine 329 to create a construct containing the N-terminal half of the VRK-1 (residues 1-329), whereas the C-terminal half initiates at serine 321 (residues 321-610). The two constructs have nine amino acids overlap and are predicted

to not affect any of the putative protein motifs or secondary structures (Figure 19A).

We observed that conserved N-terminal VRK-1::mCherry fails to localize properly to the nucleus and is expressed in the cytoplasm (Figure 19B), however C-terminal VRK-1::mCherry was expressed properly in the nucleus (Figure 19B). These results suggest that that the C-terminal half of the VRK-1 contains a sequence that is responsible for the nuclear localization of the protein.

3.2.3 Truncated proteins do not rescue mutant phenotypes

We next investigated if the mutant proteins are able to rescue *vrk-1* deficiency phenotypes. As shown in Figure 20, neither the truncated VRK-1 proteins nor VRK-1 K169E are able to rescue vrk-1 mutant phenotypes. We conclude from these experiments that kinase activity and proper nuclear localization of VRK-1 are essential for its role in *C. elegans* development.

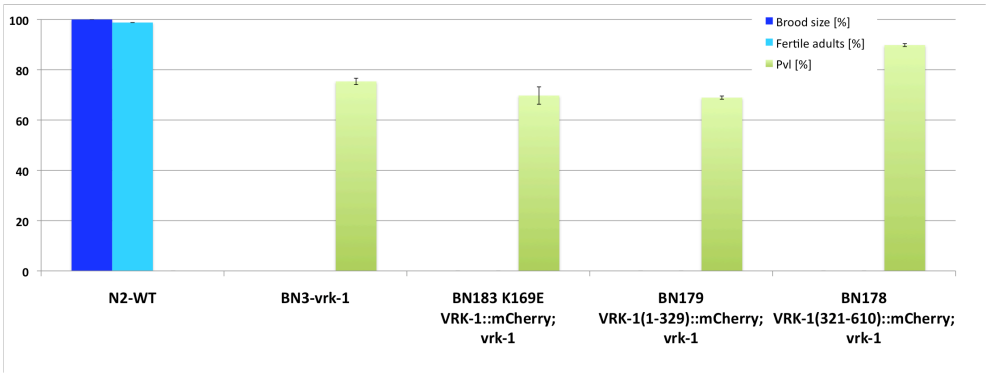

Figure 20. Neither truncated VRK-1 proteins nor a ´kinase dead´ mutant rescue mutant phenotypes. The percentage of fertile adults (light blue), brood size (dark blue) and adults with Pvl (green) is shown. Brood size is relative to the value of the wild type animals; fertile adults are relative to the brood size. Error bars report the standard error of the mean.; n>200.

3.3. Human VRK1 is a nuclear protein in interphase and associates with condensed chromosomes during mitosis

In *C. elegans* VRK-1 is nuclear during interphase, just before nuclear envelope breakdown (NEBD) it accumulates at the nuclear rim and then localizes to chromatin through mitosis (Gorjanacz et al., 2007; Klerkx et al., 2009a) (Figure 21). Previous studies have shown that similarly to *C. elegans* VRK-1, human VRK1 is a nuclear kinase, but it has also been suggested to localize to the Golgi and cytosolic vesicles (Lopez-Sanchez et al., 2009; Valbuena et al. 2007). VRK1 in HeLa cells has been described to colocalize with heterochromatin during interphase by binding gamma heterochromatin protein 1 (HP1γ) (Kang et al., 2007). However, there is controversy on whether VRK1 is associated with condensed chromosomes in mitosis (Kang et al., 2007; Valbuena et al., 2011b).

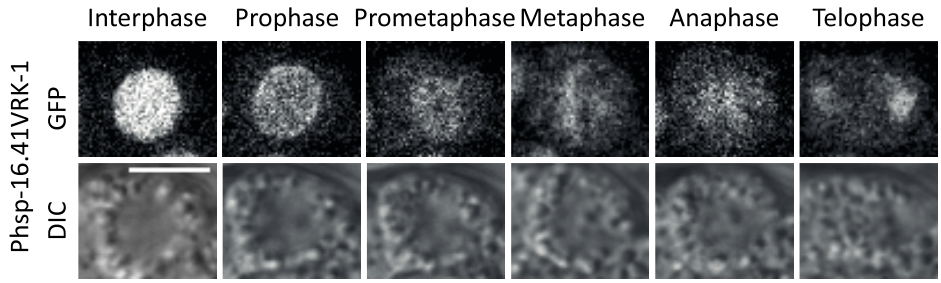

Figure 21. VRK-1 dynamics during mitosis in *C. elegans* embryos. VRK-1::GFP expressed under control of the heat shock promoter ($P_{hsp\text{-}16.41}$) in *C. elegans* embryos is nuclear during interphase, accumulates at the nuclear rim just before NEBD and associates to condensed chromatin during cell divisions. Still images from time-lapse confocal microscopy. Scale bar, 5 μm.

Having in mind the differences in expression pattern of transgenes inserted by MosSCI system and microparticle bombardment, we decided to use the Flp-In™ System to generate mammalian cell lines expressing human VRK1-mCherry from integrated single-copy transgenes to better characterize hVRK1 dynamics

during the cell cycle. The Flp-In System allows insertion of the gene of interest at a specific genomic location in mammalian cells, thus generation of isogenic stable cell lines and avoidance of overexpression artifacts. Indeed, western blot analysis confirmed that our single copy VRK1-mCherry fusion protein is expressed at the equivalent level as that the endogenous protein (Figure 22). Generation of cell lines carrying single-copy transgenes inserted into a fixed position in the genome is also advantageous when comparing several derivatives of the same transgene because of reduced experimental variability.

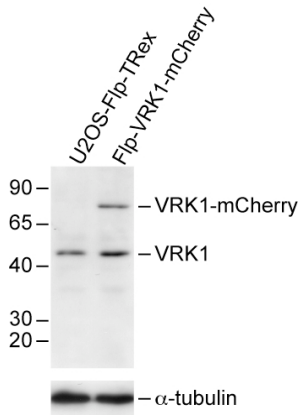

Figure 22. Western blot analysis of U2OS/FRT/TO cells and stable U2OS/FRT/TO cell line expressing VRK1-mCherry. Immunoblot analysis demonstrates that the single copy hVRK1-mCherry U2OS cell line expresses the fusion protein at similar concentration as endogenous VRK1. Upper and lower panels show probing with monoclonal α-VRK1 and α-alpha-tubulin antibodies, respectively.

First, we tried to generate a stable human embryonic kidney HEK293T cell line expressing hVRK1-mCherry. We cloned hVRK1-mCherry into the pHY12 plasmid which contains the cytomegalovirus (CMV) promoter and a hygromycin resistance gene lacking both promoter and a start codon. Once integrated into the genome the hygomycin resistance gene is fuse to the SV40 promoter and a start codon, which are already integrated in the genome of the host cell, thus

integrated cells are hygromycin resistant. We used different FuGENE 6 Transfection Reagent (µl):DNA (µg) ratios of 3:1, 3:2 and 6:1. We managed to obtain transiently expressing cell, where VRK1-mCherry localized properly to the nucleus. However, after several weeks of selection with a medium containing hygromycin, we did not obtain any stable cell line. Further increases of the amount of DNA to 2.5 and 5.0µg (FuGENE 6:DNA ratios of 3:1, 3:2, 6:1) did not improve the integration efficiency. After several unsuccessful attempts to generate a stable HEK293T cell line expressing VRK1-mCherry we decided to use a human osteosarcoma U2OS-derived cell line instead. We used FuGENE 6:DNA proportion of 3:2, using 2 and 6.7µg of DNA and we managed to generate four stable cell lines expressing our transgene (2 cell lines for each DNA concentration). To visualize chromatin, we transiently transfected one of the stable hVRK1-mCherry lines with a plasmid encoding histone H2B fused to GFP. We observed that like in *C. elegans* embryos, hVRK1 is nuclear during interphase and binds condensed chromosomes in mitosis (Figure 23). Interestingly, we did not observe nuclear envelope association in prophase, meaning that human and *C. elegans* proteins do not have completely the same behaviour during mitosis. Rather, hVRK1 shows an almost complete overlap with chromatin at all steps of the cell cycle.

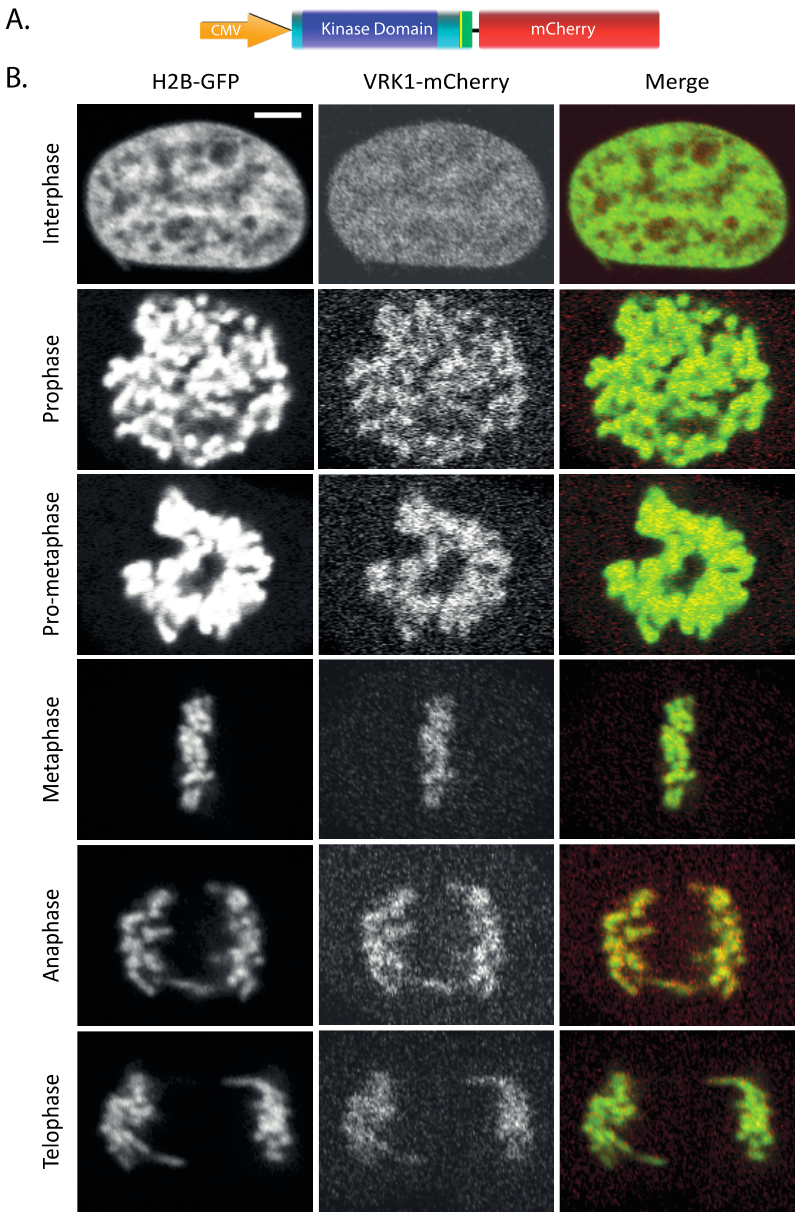

Figure 23. Human VRK1-mCherry expression and dynamics during cell cycle A. Schematic representation of human VRK-1-mCherry expressed under control of CMV promoter **B.** Stable human U2OS/Flp/TRex cell line expressing hVRK1-mCherry was transiently cotransfected with H2B-GFP. hVRK1-mCherry (red in merge) is nuclear during interphase and colocalizes with H2B-GFP (green) during mitosis. Still images from time-lapse confocal microscopy taken using different settings. Scale bar, 5µm.

In order to confirm these live imaging results, we performed immunofluorescence analysis using a α-VRK1 mouse monoclonal antibody and, as expected, we could see that endogenous hVRK1 binds the chromatin during cell division (Figure 24). Like for the exogenous protein, we did not observe nuclear envelope staining in prophase.

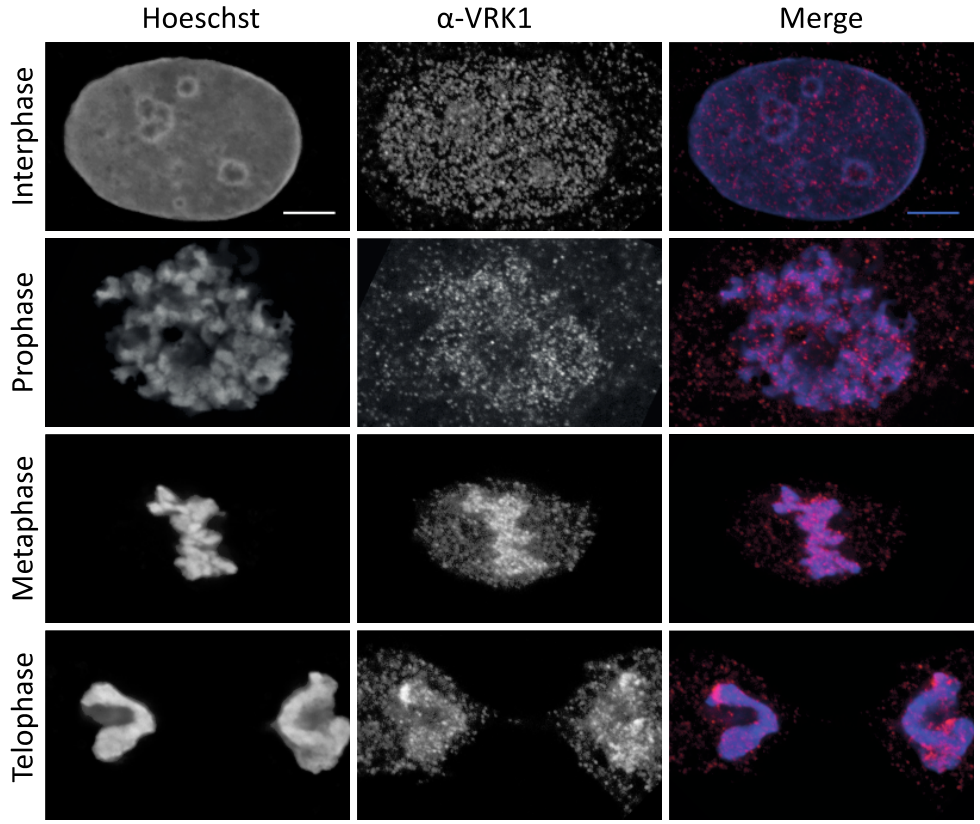

Figure 24. Endogenous VRK1 binds chromatin during mitosis. U2OS cells were fixed and stained with monoclonal α-VRK1 antibody (red in merge). Chromatin was detected using Hoechst 33258 (blue). Endogenous VRK1 is nuclear during interphase and associates with condensed chromatin during mitosis. Scale bar, 5μm.

3.4. Identification of minimal localization domain of CeVRK-1 and hVRK1

3.4.1 C-terminal domain of *C. elegans* and human VRK1 is able to bind chromatin during mitosis

Having observed that in *C. elegans*, the C-terminal half of VRK-1 localizes properly to the nucleus, we wanted to know if that fragment, without the conserved kinase domain, is sufficient to bind chromatin during mitosis. We performed live recordings of *C. elegans* embryos expressing GFP fusion with the C-terminal half of VRK-1 (residues 321-610) under control of the promoter of the heat-shock inducible gene *hsp-16.41* (Figure 25A). We decided to use the heat-shock promoter, because, as described above, our single copy transgenic strains using the *vrk-1* promoter showed variable expression of VRK-1 in the germ line and in embryos. By performing time-lapse live recordings, we could observe that the C-terminal half of VRK-1 is sufficient to localize properly to condensed chromatin during cell division in *C. elegans* embryos (Figure 25A; compare with Figure 21).

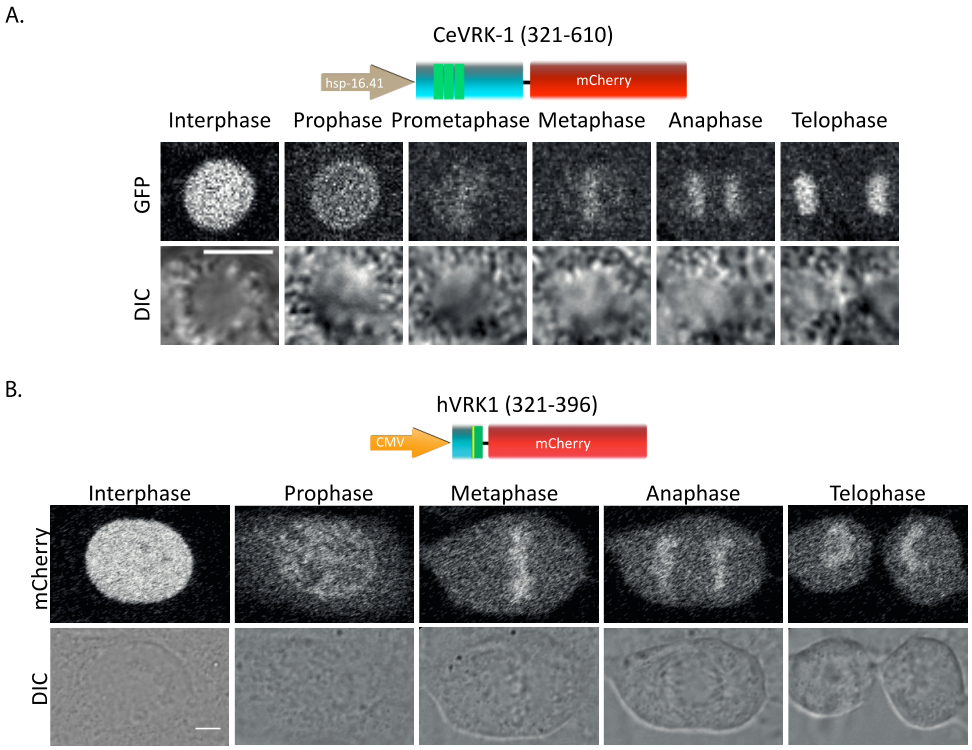

Figure 25. C-terminal domains of *C. elegans* and human VRK1 binds chromatin during mitosis A. Schematic representation of *C. elegans* C-terminal half of VRK-1::GFP expressed under control of $P_{hsp\text{-}16.41}$ (top panel). In *C. elegans* embryos C-terminal domain is nuclear during interphase, goes to nuclear rim just before NEBD and associates with condensed chromatin during cell divisions. Scale bar, 5 µm. **B)** Schematic representation of human C-terminal domain of VRK-1::mCherry expressed under control of CMV promoter (top panel). 65 aa C-terminal domain of VRK1 in U2OS cells is able to bind chromatin during cell division. Still images from time-lapse confocal microscopy. Scale bar, 5 µm.

Members of VRK protein kinase family, including CeVRK-1 and hVRK1, share a similar, highly conserved serine/threonine protein kinase domain of approximately 280 aa, but have variable carboxyl termini (Klerkx et al., 2009b; Nichols and Traktman, 2004). The C-terminus of hVRK1 does not have homology to any known protein but a 129 aa C-terminal fragment (residues 268-396; includes the last ~60 aa of the kinase domain) was described to

localize to the nucleus (Lopez-Borges et al., 2000). Although the C-terminus of human VRK1 is much smaller then the worm ortholog (contains only 65 amino acids C-terminally to the kinase domain), we wanted to investigate if it is enough to bind chromatin during mitosis. We generated a stable U2OS cell line expressing the last 65 amino acids (residues 332-396) fused to mCherry and as shown in Figure 25B, we observed that like in *C. elegans*, this small C-terminal domain is associated to condensed chromatin during mitosis.

3.4.2 Identification of minimal localization domain of CeVRK-1 and hVRK1

The VRK1 carboxyl terminus contains a putative nuclear localization signal (NLS) at positions 356-360 (a stretch of five basic amino acids – KKRKK) (Lopez-Borges et al., 2000) and a point mutation (R358X) within this sequence is associated to a complex neurological disease with pontocerebellar degeneration and muscular atrophy in humans (Renbaum et al., 2009). This disease-associated point mutation creates a premature stop codon, thus, translated VRK1 lacks the last 38 amino acids in C-terminus and fails to localize properly to the nucleus in HEK293T cells (Sanz-Garcia et al., 2011).

In order to determine a minimal localization domain of human VRK1, we decided to dissect the 65 aa C-terminus into even smaller fragments (residues 332-361 and 355-396), both of them containing the putative NLS (Figure 26A). We managed to generate a stable cell line expressing truncated proteins containing residues 332-361 fused to mCherry and we observed that chromatin association during mitosis was abolished and nuclear accumulation in interphase was reduced (Figure 26B). On the other hand, the fragment composed by the last amino acids (residues 355-396) localized properly to the nuclei of transiently transfected cells and to mitotic chromatin (preliminary data not shown). However, after integration, transgene was repressed and we could not detect any expression performing time-lapse live recordings. We are

currently repeating the experiments with the residue 355-396 fragment to acquire more images.

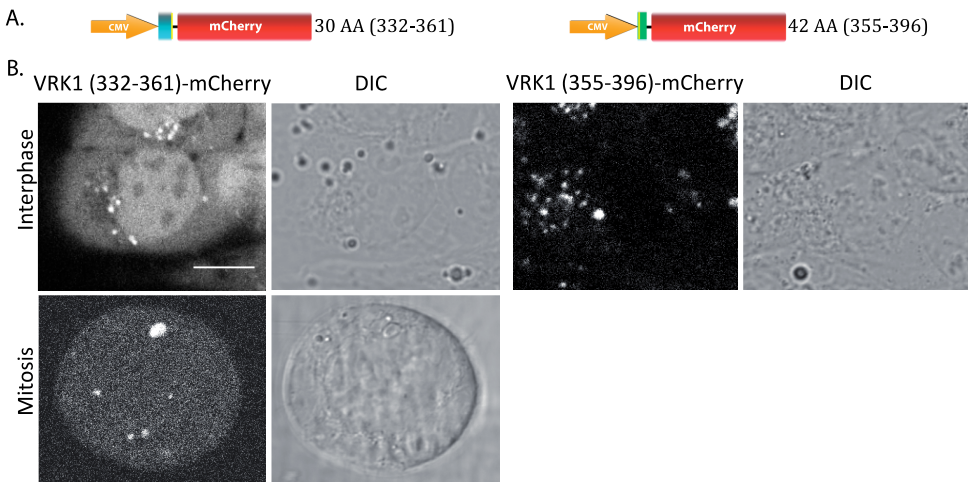

Figure 26. C-terminal domain of VRK-1 binds chromatin during mitosis A. Schematic representation of the 42 and 30 aa C-terminal fragments of human VRK-1::mCherry containing a putative NLS expressed under control of the CMV promoter **B.** Small 30 aa C-terminal fragment of human VRK1 lacking last 35 amino acids fails to bind chromatin during mitosis. Last 42 aa of VRK1 bind chromatin during mitosis in transiently transfected cells (not shown), however we did not observe any expression of that transgene in the integrated cell line. Still images from time-lapse confocal microscopy. Scale bar, 10μm.

We next aligned the C-terminal 65 aa fragment of hVRK1 with VRK1 orthologs of other species (Figure 27A). From this sequence comparison we decided to mutate several highly conserved amino acids in order to reveal their possible role in chromatin binding. We mutated at the extreme carboxyl end arginines to glycines at positions 389, 391 and 393 (RG mutant), serine and threonine to alanines at positions 388 and 390 (STA mutant), and aspartic acids to alanines at positions 340, 335 and 336 (DA mutant). We performed live recordings of stable U2OS cell lines expressing the different mutated C-terminal fragments and found that the STA (Figure 27B) and DA (data not shown) mutants localized

normally. In contrast, the RG mutation caused abrogation of chromatin localization during mitosis. The same results were obtained when we mutated these three conserved arginines in the full length hVRK1 (Figure 27B), thus arguing that they are also responsible for chromatin interaction in the context of the native protein.

Arginine, a positively charged amino acid, is one of the basic amino acids typically involved in protein-nucleic acid interactions. The protein surface in contact with DNA is often rich in positively charged groups, which allows the formation of electrostatic interactions and hydrogen bond with the negatively charged DNA (Nadassy et al., 1999; Rohs et al., 2009). Unfortunately, the published Nuclear Magnetic Resonance (NMR) solution structure of hVRK1 does not include the last 35 aa (Shin et al., 2011). The position of arginines 389, 391 and 393 in the three-dimensional VRK1 structure remains therefore unknown. However, the NMR structure shows that the putative NLS residues are localized on the protein surface, thus it is possible that also the conserved arginines at the extreme C-terminus of VRK1 are surface-exposed, enabling them to interact with DNA.

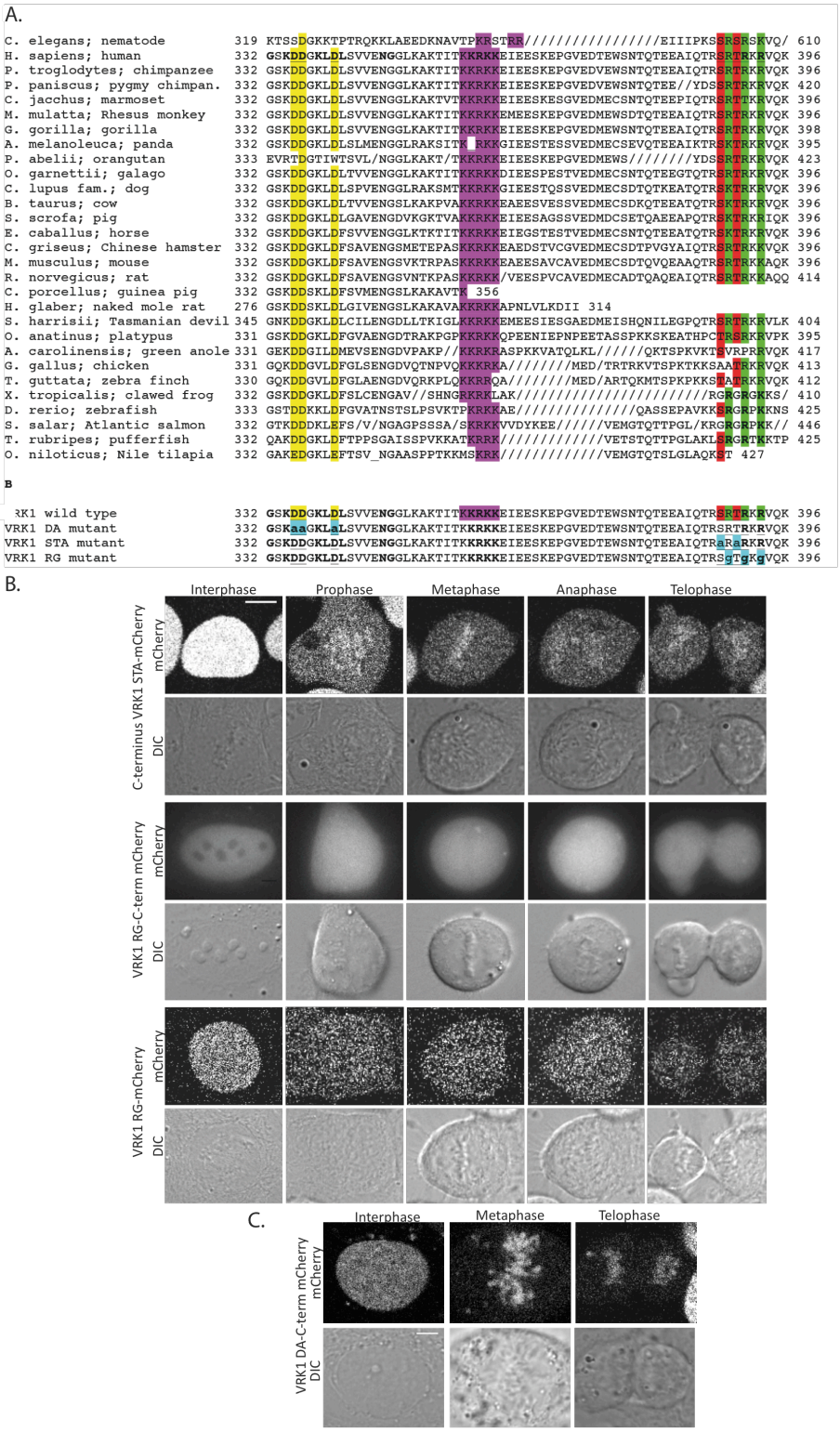
A.
C. elegans; nematode 319 KTSSDGKKTPTRQKKLAEEDKNAVTPKKSTRR////////////////EIIIPKSSRSRSKVQ/ 610
H. sapiens; human 332 GSKDDGKLDLSVVENGGLKAKTITKKRKKKEIEESKEPGVEDTEWSNTQTEEAIQTRSRTRKRVQK 396
P. troglodytes; chimpanzee 332 GSKDDGKLDLSVVENGGLKAKTITKKRKKEIEESKEPGVEDVEWSNTQTEEAIQTRSRTRKRVQK 396
P. paniscus; pygmy chimpan. 332 GSKDDGKLDLSVVENGGLKAKTITKKRKKEIEESKEPGVEDVEWSNTQTEE//YDSSRTRKRVQK 420
C. jacchus; marmoset 332 GSKDDGKLDLSVVENGGLKAKTVTKKRKKEIEESKESGVEDMECSNTQTEEPIQTRSRTTKRVQK 396
M. mulatta; Rhesus monkey 332 GSKDDGKLDLSVVENGGLKAKTITKKRKKEMEESKEPGVEDMEWSDTQTEEAIQTRSRTRKRVQK 396
G. gorilla; gorilla 332 GSKDDGKLDLSVVENGGLKAKTITKKRKKEIEESKEPGVEDMEWSNTQTEEAIQTRSRTRKRVQK 398
A. melanoleuca; panda 332 GSKDDGKLDLSLMENGGLRAKSITK RKKGIEESTESSVEDMECSEVQTEEAIKTRSKTRKRVQK 395
P. abelii; orangutan 333 EVRTDGTIWTSVL/NGGLKAKT/TKKRKKEIEESKEPGVEDMEWS////////YDSSRTRKRVQK 423
O. garnettii; galago 332 GSKDDGKLDLTVVENGGLKAKTITKKRKKDIEESPESTVEDMECSNTQTEEGTQTRSRTRKRVQK 396
C. lupus fam.; dog 332 GSKDDGKLDLSPVENGGLRAKSMTKKRKKGIEESTQSSVEDMECSDTQTKEATQTRSKTRKRVQK 396
B. taurus; cow 332 GSKDDGKLDLTVVENGSLKAKPVAKKRKKEAEESVESSVEDMECSDKQTEEATQTRSKTRKRVQK 396
S. scrofa; pig 332 GSKDDGKLDLGAVENGDVKGKTVAKKRKKEIEESAGSSVEDMDCSETQAEEAPQTRSKTRKRIQK 396
E. caballus; horse 332 GSKDDGKLDFSVVENGGLKTKTITKKRKKEIEGSTESTVEDMECSNTQTEEATQTRSKTRKRVQK 396
C. griseus; Chinese hamster 332 GSKDDGKLDFSAVENGSMETEPASKKRKKEAEDSTVCGVEDMECSDTPVGYAIQTRSRTRKRVQK 396
M. musculus; mouse 332 GSKDDGKLDFSAVENGSVKTRPASKKRKKEAEESAVCAVEDMECSDTQVQEAAQTRSRTRKKAQK 396
R. norvegicus; rat 332 GSKDDGKLDFSAVENGSVNTKPASKKRKK/VEESPVCAVEDMECADTQAQEAIQTRSRTRKKAQQ 414
C. porcellus; guinea pig 332 GSKDDSKLDFSVMENGSLKAKAVTK 356
H. glaber; naked mole rat 276 GSKDDSKLDLGIVENGSLKAKAVAKKRKKAPNLVLKDII 314
S. harrisii; Tasmanian devil 345 GNKDDGKLDLCILENGDLLTKIGLKKRKKEMEESIESGAEDMEISHQNILEGPQTRSRTRKRVLK 404
O. anatinus; platypus 331 GSKDDGKLDFGVAENGDTRAKPGPKKRKKQPEENIEPNPEETASSPKKSKEATHPCTRSRKRVPK 395
A. carolinensis; green anole 331 GEKDDGILDMEVSENGDVPAKP//KKRKRASPKKVATQLKL//////QKTSPKVKTSVRPRRVQK 417
G. gallus; chicken 331 GQKDDGVLDFGLSENGDVQTNPVQKKRKKA////////MED/TRTRKVTSPKTKKSAATRKRVQK 413
T. guttata; zebra finch 330 GQKDDGVLDFGLAENGDVQRKPLQKKRRQA////////MED/ARTQKMTSPKPKKSTATRKRVQK 412
X. tropicalis; clawed frog 332 GSKDDGKLDFSLCENGAV//SHNGRKRKLAK//////////////////////RGRGRGKKS/ 410
D. rerio; zebrafish 333 GSTDDKKLDFGVATNSTSLPSVKTPKRKKAE//////////////QASSEPAVKKSRGRPKKNS 425
S. salar; Atlantic salmon 332 GTKDDDKLEFS/V/NGAGPSSSA/SKRKKVVDYKEE//////VEMGTQTTPGL/KRGRGRPKK// 446
T. rubripes; pufferfish 332 QAKDDGKLDFTPPSGAISSPVKKATKRRK//////////////VETSTQTTPGLAKLSRGRTKKTP 425
O. niloticus; Nile tilapia 332 GAKEDGKLEFTSV_NGAASPPTKKMSKRK//////////////VEMGTQTSLGLAQKST 427
B
VRK1 wild type 332 GSKDDGKLDLSVVENGGLKAKTITKKRKKEIEESKEPGVEDTEWSNTQTEEAIQTRSRTRKRVQK 396
VRK1 DA mutant 332 GSKaaGKLaLSVVENGGLKAKTITKKRKKEIEESKEPGVEDTEWSNTQTEEAIQTRSRTRKRVQK 396
VRK1 STA mutant 332 GSKDDGKLDLSVVENGGLKAKTITKKRKKEIEESKEPGVEDTEWSNTQTEEAIQTRaRaRKRVQK 396
VRK1 RG mutant 332 GSKDDGKLDLSVVENGGLKAKTITKKRKKEIEESKEPGVEDTEWSNTQTEEAIQTRSgTgKgVQK 396
B.
Interphase
Prophase
Metaphase
Anaphase
Telophase
C-terminus VRK1 STA-mCherry
mCherry
DIC
VRK1 RG-C-term mCherry
mCherry
DIC
VRK1 RG-mCherry
mCherry
DIC
C.
Interphase
Metaphase
Telophase
VRK1 DA-C-term mCherry
mCherry
DIC

Figure 27. Site-directed mutagenesis of several conserved residues in the human VRK1 A. Sequence analysis of the hVRK1 C-terminus. Upper panel – alignment of hVRK1 C-terminal 65 aa fragment with VRK1 orthologs of 27 other vertebrates (mammals, birds, reptile, amphibian fish) species and with *C. elegans*. Bold indicates residues conserved (identical or similar) in >90% of vertebrate VRK1 sequences. Underlined residues were analyzed in three groups (yellow, red and green) by site-directed mutagenesis. Magenta residues indicate a proposed nuclear localization signal in hVRK1 and alignment to other species. We speculate that *C. porcellus* and *H. glaber* sequences may be incomplete, hence the C-terminal truncations. In addition, the *P. abelii* sequence is annotated as "low quality" in the NCBI database, which may explain the poor alignment in the N-terminal part. Lower panel – based on the homology of VRK1 residues between species, we designed three mutants, designated DA, STA and RG mutant, respectively. Light blue case letters indicate amino acid substitutions **B.** Still images from time-lapse confocal microscopy show that STA mutant binds chromatin during mitosis (upper panel). RG mutation affects chromatin association of C-terminal fragment (middle panel) as well as of full length protein (bottom panel) **C.** Still images from time-lapse confocal microscopy show that DA mutant binds chromatin during mitosis. Scale bar, 5 μm.

Alignment of hVRK1 with CeVRK-1 suggests that the critical arginines at the extreme C-terminus of hVRK1 may correspond to R432, R434 and K436 of CeVRK-1, although these residues are located ~175 aa from the C-terminus. We therefore investigated if mutation of these three residues in *C. elegans* affects VRK-1 localization by substituting them with glycines. Interestingly, contrary to hVRK1, substitution of these conserved amino acids in the context of the C-terminal half of CeVRK-1 did not affect binding to chromatin during mitosis (Figure 28). The observed differences between species agree with the fact that carboxyl terminus of VRK1 is variable between species and suggest that CeVRK-1 has different or additional residues critical for chromatin binding.

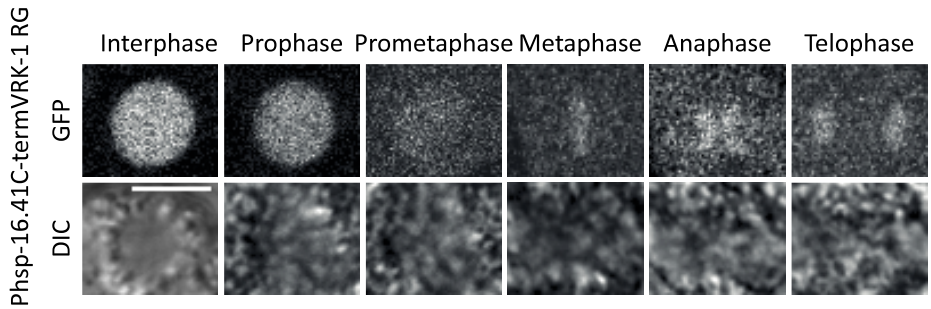

Figure 28. Mutagenesis of conserved arginines in *C. elegans* C-terminal half of VRK-1 does not affect the ability to bind chromatin during mitosis. C-terminal half of VRK-1 RG::GFP shows the same localization and dynamics as wild type protein. Still images from time-lapse confocal microscopy. Scale bar, 5μm.

The above experiments show that VRK1 is nuclear in interphase and associated with chromatin during mitosis. To estimate if the total population of VRK1 that during interphase is localized in the nucleus, binds chromatin, we measured the average fluorescence intensity of hVRK1-mCherry and CeVRK-1-mCherry during interphase (both inside the nucleus and cytoplasm) and during mitosis (at the metaphase plate and dispersed in the cell). We observed, that during interphase, close to 100% of hVRK1-mCherry localizes to the nucleus (Figure 29A). During mitosis, 87% is associated with chromatin, while 12% is cytoplasmic. The same measurements of CeVRK-1-mCherry demonstrate that 76% is nuclear during interphase and during mitosis 63% localizes on the metaphase plate (Figure 29B). For the C-terminal domain of human kinase we observed a significant reduction, while for worm protein, an increase in the nuclear vs cytoplasmic fraction during interphase. The ratio between chromatin-associated and dispersed during mitosis was significantly affected for the hVRK1-mCherry. Mutation of conserved Ser and Thr significantly reduced the chromatin-associated fraction of human C-terminal VRK1 during mitosis. In agreement with the live microscopy recordings, mutation of conserved arginines at the extreme C-terminus of human kinase abrogated its association with chromatin during mitosis, however it did not affect chromatin binding of *C. elegans* ortholog.

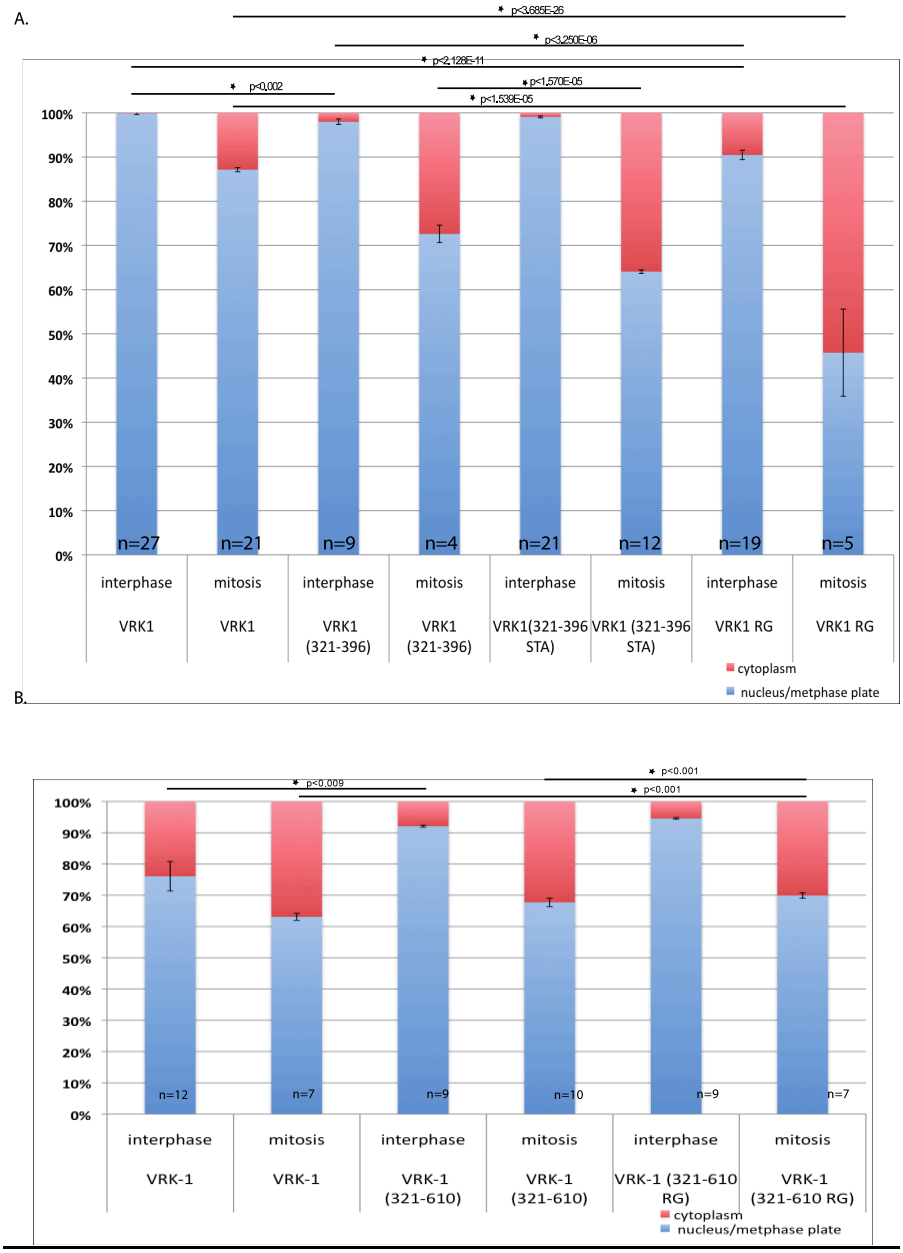

Figure 29. Relative fuorescence intensity in the nuclear and cytoplasmic or metaphase plate regions of hVRK1 (A.) and CeVRK-1 (B) wild type and mutatnt proteins. The average fluorescence intensity of cytoplasmic and nuclear or metaphase plate fractions during interphase and mitosis was measured. Error bars report the standard error of the mean. Measurements of the *C. elegans* RG mutant come from 9 and 7 (interphase and mitosis respectively) cells of one embryo. Work to obtain more embryos is in progress.

3.5. VRK1 associates transiently with chromatin during interphase and mitosis

To characterize VRK1 mobility, we performed FRAP analysis in U2OS cells stably expressing hVRK1-mCherry. We photobleached nuclei of a total of 7 cells during interphase and 8 cells during metaphase, and measured the kinetics of hVRK-1-mCherry recovery (Figure 30A). As shown in Figure 30B and C, there was an immediate fluorescence recovery for nuclear as well as for mitotic chromosome associated VRK1-mCherry ($t^1/_2$=3.19sec and $t^1/_2$= 3.36sec, respectively). Thus, we conclude that VRK1 is a highly mobile protein and its fast recovery suggests that it associates transiently with chromatin during interphase and mitosis. Moreover, the fact that similar kinetics were observed in interphase and mitosis may imply that VRK1 binds to the same protein(s) throughout the cell cycle.

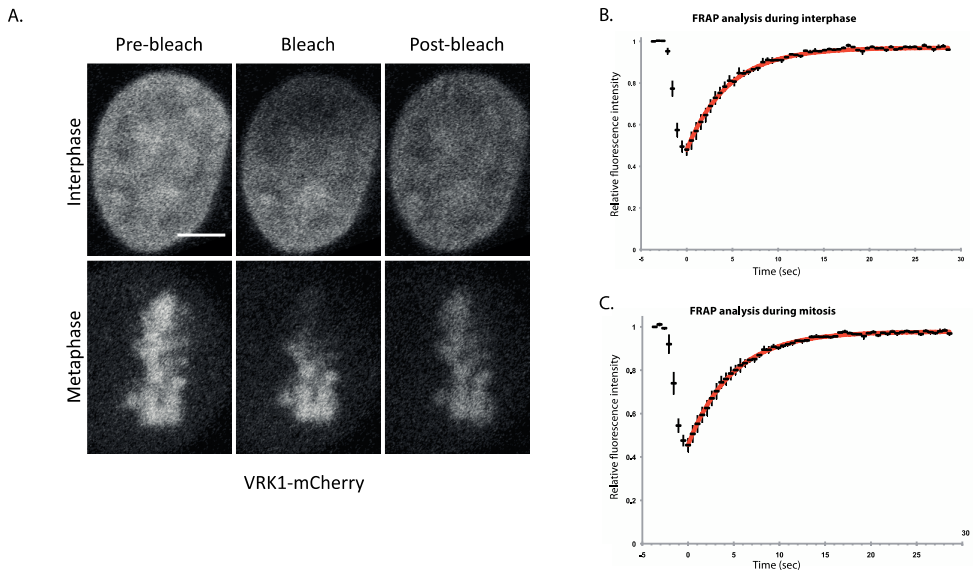

Figure 30. FRAP analysis demonstrates fast recovery of VRK1-mCherry in U2OS cells. A) Still images from time-lapse confocal microscopy. Scale bar, 5µm. **B and C)** Measurements of the fluorescence recovery of bleached area in U2OS cells expressing hVRK1-mCherry during interphase (B) and mitosis (C) show fast dynamics of hVRK1.

RESULTS

OBJECTIVE 2

3.6. Role of VRK-1 in C. elegans postembryonic development

In the second part of my thesis, I will concentrate on the role of VRK-1 in *C. elegans* postembryonic development. As mentioned in the Introduction, severe defects upon loss of *vrk-1* are observed in the development of the reproductive organs and the following experiments have provided further insight into the mechanisms by which VRK-1 regulates these processes.

3.6.1. VRK-1 dynamics in *C. elegans* developing vulva and uterus

We have shown in the first part of this thesis, that VRK-1 is ubiquitously expressed in *C. elegans*. To characterize VRK-1 dynamics during vulval and uterine development, we used different approaches.

First, we mounted worms using standard 3% agarose pads and 10mM levamisole. Levamisole acts as an acetylcholine receptor agonist which leads to a hypercontracted paralysis of wild-type nematodes and is a commonly used drug to immobilize worms on glass slide for imaging (Rand, 2007). Although worms were paralyzed, we did not register any cell division, which could be caused by the fact, that longer levamisole treatment usually causes death of the worm. Lower levamisole concentrations, which cause only partial paralysis, did not enable live microscopy time-lapse recordings, because worms were escaping from the recording area. We also tried to embed worms in low melting agarose to prevent the escape of the worms and although it slowed down worm's movements, time-lapse recording was still impossible.

Worm sticking to the agarose pads with a tissue adhesive (Histoacryl) (Richmond, 2006) also failed to satisfactorily immobilize worms in our hands.

We next used a "worm sleep" (5mM tricaine methanesulfonate and 0.5mM levamisole mixture) drug solution in order to reduce the toxicity of levamisole.

We tried several concentrations – 0.5x, 0.33x and 0.2x "worm sleep" solution in M9 buffer.

We never managed to record the entire development of the vulva and uterus since P6.p 4-cell stage until the evertion during last molt, nevertheless we succeed in almost six hours live microscopy documentation using 0.33x "worm sleep" solution (i.e. 1.67mM tricaine methanesulfonate and 0.17mM levamisole added 30 minutes prior to the recording (Figure 31). These experiments demonstrated that VRK-1 accumulates at the nuclear periphery in mitotic prophase (Figure 31; see large uterine cell at t=0 min) as previously reported in embryos (Klerkx et al., 2009a). Moreover, VRK-1 levels are similar in all vulval and uterine cells and are constant during development.

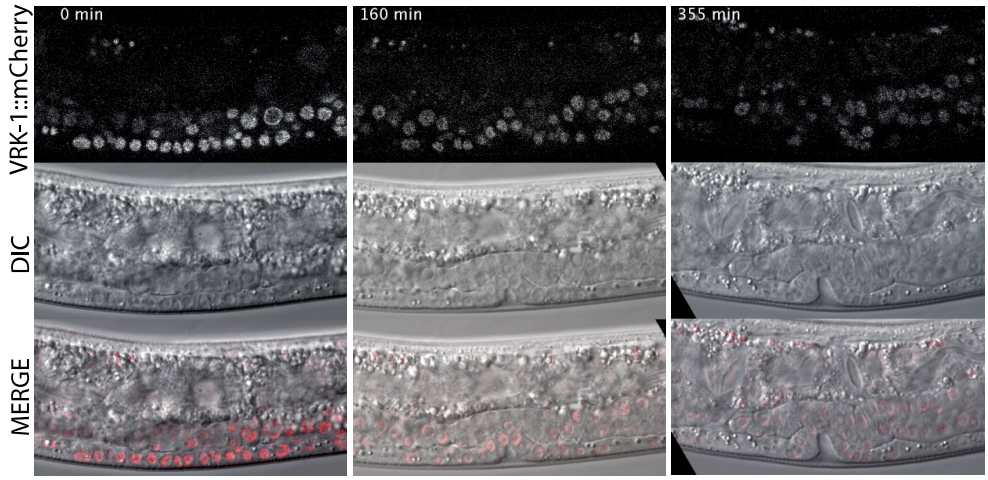

Figure 31. VRK-1::mCherry postembryonic expression in developing *C. elegans* reproductive organs. Expression of VRK-1::mCherry (Strain BN173) in developing vulva and uterus was analyzed by time-lapse live microscopy.

3.6.2. Anchor Cell Morphology and Presumably Contact to Uterine Cells is severely affected in *C. elegans vrk-1* mutants

During vulval development the AC has to be polarized and breach the basement membrane separating vulval and uterine cells. Klerkx and coworkers have

shown that VRK-1 depletion causes delay in AC invasion, which affects 86% of *vrk-1* mutants (Klerkx et al., 2009a). It prompted them to analyze the localization of the actin-binding protein, moeABD, which in wild type animals accumulates at the basal side of the AC, prior to AC invasion through the basement membrane (Ziel et al., 2009). They observed, that in 42% of *vrk-1* mutants, AC polarization was affected, since these mutants had additional apically localized moeABD foci.

In order to decipher if *vrk-1* deletion affects other known markers of AC polarization and invasion, we analyzed the localization of the netrin receptor UNC-40 (DCC) fused to GFP, the phospholipase C-δ *(*PLCδ^{PH}*)* fused to mCherry, the beta-integrin subunit PAT-3 fused to GFP and finally a member of the Rho family of GTP-binding proteins MIG-2 fused to GFP (strains BN120, BN135, BN188, BN191, respectively). To minimize genotypic variability we compared *vrk-1* homozygous mutants with heterozygous siblings (hereafter termed control animals), which develops as wild type animals. We examined the polarity of the AC in the contact with the descendants of the P6.p vulval precursor cell by performing quantitative measurements of the average fluorescence intensity of the basal (invasive) versus apical (noninvasive) membranes of the AC. In control animals UNC-40, MIG-2, PLCδ^{PH}, and PAT-3 are tightly localized to the basal invasive membrane of the AC (Hagedorn et al., 2009; Ziel et al., 2009) (Figure 32A). In *vrk-1* mutants the fusion proteins were also enriched at the invasive membrane of the AC and we did not see any significant differences in the polarity of the AC between control and *vrk-1* mutant animals, except the PAT-3, which was slightly hyperpolarized in *vrk-1* mutants (Figure 32B).

Interestingly, we have observed that in *vrk-1* mutants, the morphology of the AC is severely affected. While in control animals, at the P6.p 4-cell stage, the AC usually had a rounded shape, in *vrk-1* mutants, it was more rectangular, often with long protrusions that were absent in wild type animals (Figure 32A and C).

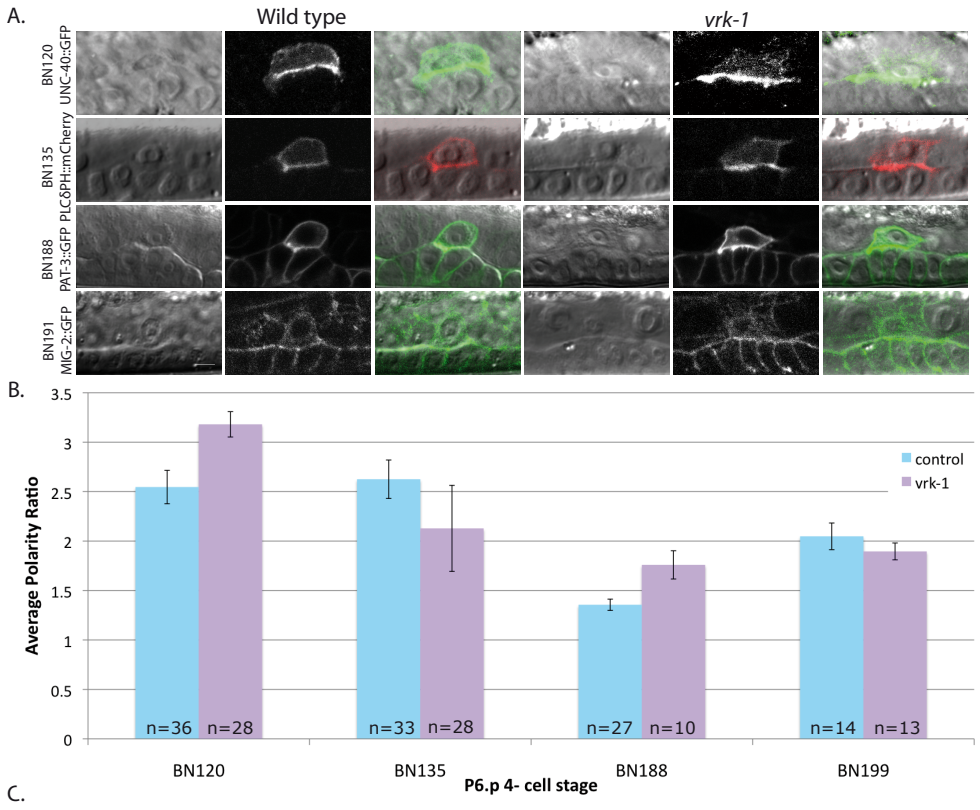

Strain/ Marker	BN120 UNC-40::GFP		BN135 PLC::mCherry		BN188 PAT-3::GFP		BN191 MIG-2::GFP	
	Control (n=36)	*vrk-1* (n=28)	Control (n=33)	*vrk-1* (n=28)	Control (n=27)	*vrk-1* (n=10)	Control (n=14)	*vrk-1* (n=13)
Irregular AC shape (%)	27.7	53.6*	9.1	67.9***	22.2	50	21.4	84.6***
Protrusionsons (%)	13.9	25.0	3.0	17.9	0	0	0	38.5*

Figure 32. Anchor Cell polarization and invasion markers are not affected in *vrk-1* mutants.

A. DIC (left panel), fluorescence (middle panel) and merged images (right panel) of control animals and *vrk-1* mutants show AC expression of UNC-40::GFP, *PLCδ^{PH}*::mCherry**,** PAT-3::GFP and MIG-2::GFP at the P6.p 4-cell stage. Still images taken using the same microscope settings for each

strain. Scale bar 5µm **B.** Quantification of UNC-40, *PLCδ^{PH}*, PAT-3 and MIG-2 polarization in control (blue) and *vrk-1* mutants (violet) at the P6.p 4-cell stage. Polarity of AC invasion and polarization markers in *vrk-1* mutants was not significantly different from control animals (p>0.01, Student's t test), except for PAT-3::GFP (p=0.004, Student's t test). Error bars report the standard error of the mean. **C.** Table illustrating AC morphology defects observed in control animals and *vrk-1* mutants at P6.p 4-cell stage. **P*<0.05, ****P*<0.002 as determined by Fisher's exact test.

3.6.3. Anchor Cell fails to fuse in *C. elegans vrk-1* mutants

It has been demonstrated that proper NE breakdown and reassembly requires VRK-1 phosphorylation and Lem4/PP2A-mediated dephosphorylation of BAF-1, respectively (Asencio et al., 2012). In *C. elegans vrk-1* depleted embryos, cells present dramatic defects in the NE morphology (Gorjanacz et al., 2007) and this phenotype was also described for the uterine tissue (Klerkx et al., 2009a). However, contrary to the uterine cells, the morphology of the vulva cell nuclei is not affected. The observation that in the absence of VRK-1 the morphology of the AC is affected combined with the published data concerning disrupted NE shape in the uterine tissue, prompted us to investigate the AC fusion process in *vrk-1* mutants.

During development of the reproductive organs, the AC fuses with eight of the progeny of the specialized uterine π cells to form the utse, which, as it was mentioned in the introduction, is not formed in *vrk-1* mutants, potentially because of a failure in π cell specification (Klerkx et al., 2009a). However, the implication of VRK-1 in the formation of the utse could also be a result of defective AC fusion. We therefore assayed AC fusion in *vrk-1* mutants. We used a *cdh-3::gfp* reporter as a marker of AC fusion (strain BN26) (Hanna-Rose and Han, 1999; Pettitt et al., 1996). CDH-3 is a member of the cadherin superfamily, which is implicated in cell adhesion, regulation of tissue organization and morphogenesis (Pettitt, 2005). The *cdh-3* reporter expresses soluble GFP in the AC during L3 larval stage and as the AC fuses with descendants of uterine π

cells, GFP spreads from the AC cytoplasm throughout the utse cell (Hanna-Rose and Han, 1999). It is also expressed in VPCs and uterine epithelium closest to the invaginating vulva (Pettitt et al., 1996). Consistently with published data, we observed a strong fluorescence signal of *cdh-3*::GFP in the AC during L3 stage both in control animals and *vrk-1* mutants (Figure 33A). However, when in control animals the fusion of the AC during L3/L4 molt causes a dilution of the GFP signal, in *vrk-1* mutants it remains limited to the area of the AC, suggesting that the AC fails to fuse in *vrk-1* mutants. The summary of these observations is presented in the Figure 33B. In *vrk-1* mutants, we observed some worms with ambiguous phenotype, probably resulting from the fact that CDH-3 is also expressed in the VPCs and, in lower levels, in the uterine tissue and that the morphology of the developing vulva is affected, which made the AC CDH-3 signal unclear.

A.

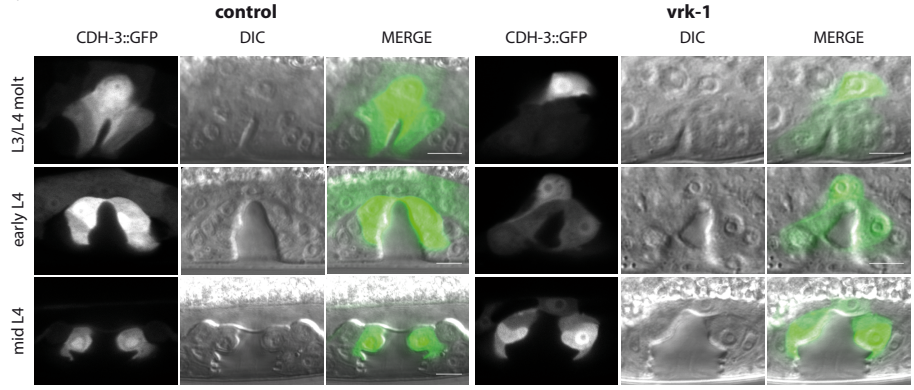

B.

BN26					
control			*vrk-1*		
Fused	**Unfused**	**Ambiguous**	**Fused**	**Unfused**	**Ambiguous**
17	0	0	2	17	5
BN263					
control			*vrk-1;* Pfos-1c::VRK-1::mCherry		
Fused	**Unfused**	**Ambiguous**	**Fused**	**Unfused**	**Ambiguous**
15	0	2	23	8	5

Figure 33. VRK-1 is essential for AC fusion A. AC does not fuse in *vrk-1* mutants. Fluorescence (left panels), DIC (middle panels) and merged images (right panels) of control animals and *vrk-1* mutants show expression of *cdh-3*::GFP (green). At L3/L4 molt stage GFP is expressed in the AC and some of the VPCS both in control animals and *vrk-1* mutants. At the early L4 stage AC fused with uterine π cells to form utse in control animals what is shown by a diffused *cdh-3*::GFP. Expression of *cdh-3*::GFP limited to the area of the AC shows lack of fusion in *vrk-1* mutants. At mid L4 stage in *vrk-1* mutants the fusion protein is still limited to the AC. Arrows – AC, arrowheads – VPCs. Still images taken using different microscope settings. Scale bar 5μm **B.** Table illustrating quantification of AC fusion event observed in control animals and *vrk-1* mutants (strain B26). Lack of AC fusion was partially rescued by the uterine specific expression of VRK-1 under control of *fos-1c* promoter (strain B263) ($P<0.001$ as determined by Fisher's exact test).

To confirm that the observed lack of fusion is a result of the *vrk-1* mutation, we decided to express VRK-1::mCherry specifically in the uterine tissue using *fos-1c* promoter, a sequence that was identified as uterine intermediate precursor enhancer (Oommen and Newman, 2007). FOS-1 is expressed in the AC and uterine tissue where it is required for AC invasion and proper development of the vulva and uterus as well as for fertility and oogenesis (Sherwood et al., 2005). Klerkx and coworkers have previously shown that VRK-1 acts independently from FOS-1 (Klerkx et al., 2009a), however to be sure that the expression of *vrk-1* from the *fos-1c* promoter is not affected in *vrk-1* mutants, we measured the fluorescent intensity of FOS-1A::YFP in the nucleus of the AC at the 1-cell, 2-cell, 4-cell and 6-8-cell stage (strain BN37) (Figure 34A and B). We did not observe any significant differences in the expression of FOS-1A::YFP in control animals and *vrk-1* mutants. These results confirm that VRK-1 acts independently from the FOS-1 pathway.

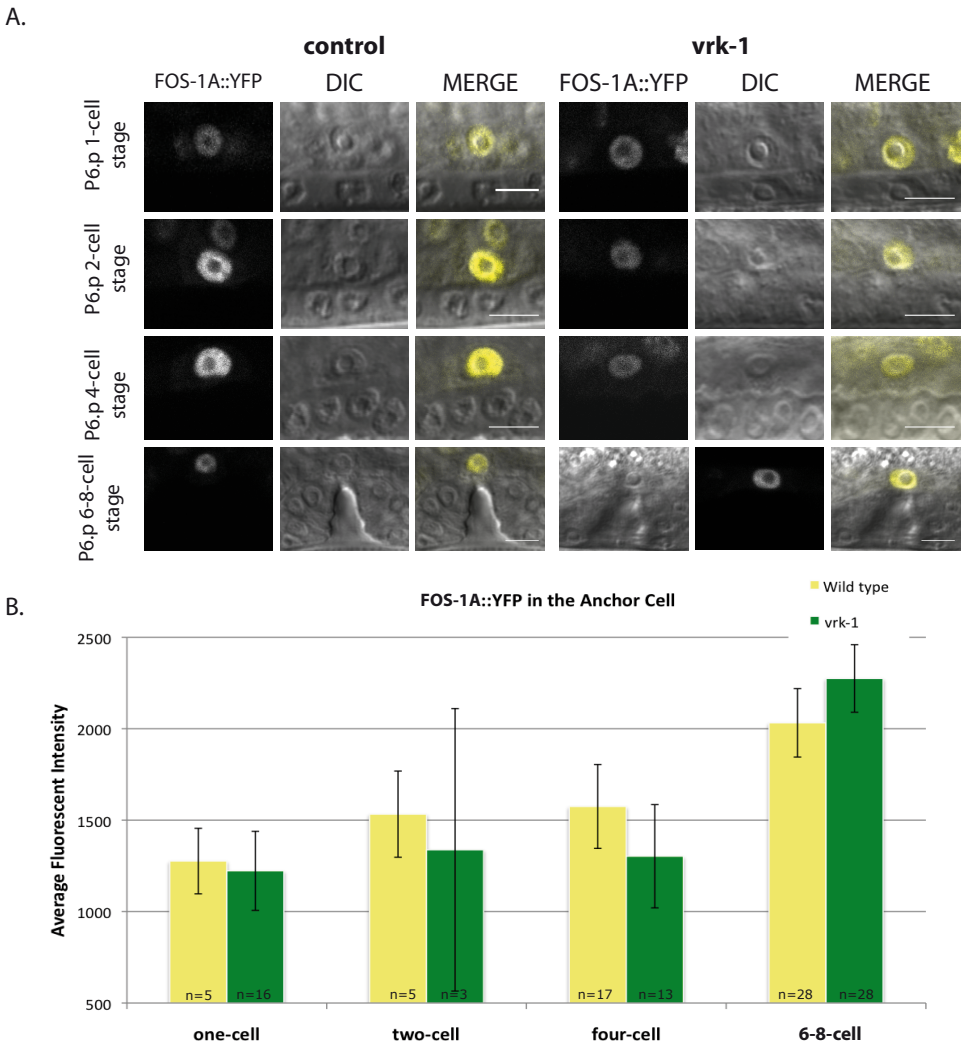

Figure 34. VRK-1 acts independently from FOS-1 pathway A. Expression of FOS-1A::YFP (yellow) in control animals and *vrk-1* mutants during P6.p 1-, 2-, 4-, and 6-8 cell stages. Fluorescence (left panels), DIC (middle panels) and merged images (right panels). Still images taken using the same microscope settings. Scale bar 5µm **B.** Quantification of FOS-1A::YFP intensity in the AC at P6.p 1-, 2-, 4-, and 6-8-cell stages in control (yellow) and *vrk-1* mutants (green). Average fluorescence intensity of FOS-1A::YFP in *vrk-1* mutants was not significantly different from wild type animals. ($p>0.05$, Student's t test). Error bars report the standard error of the mean.

When we expressed VRK-1::mCherry under control of fos-1c promoter (strain BN263), we rescued the lack of AC fusion in *vrk-1* mutants as well as formation of the utse and defects in the uterine lumen (Figure 35; Figure 33B). This data confirms that VRK-1 is necessary for AC and uterine π cells fusion and that VRK-1 expression in the uterine tissue is sufficient for this process.

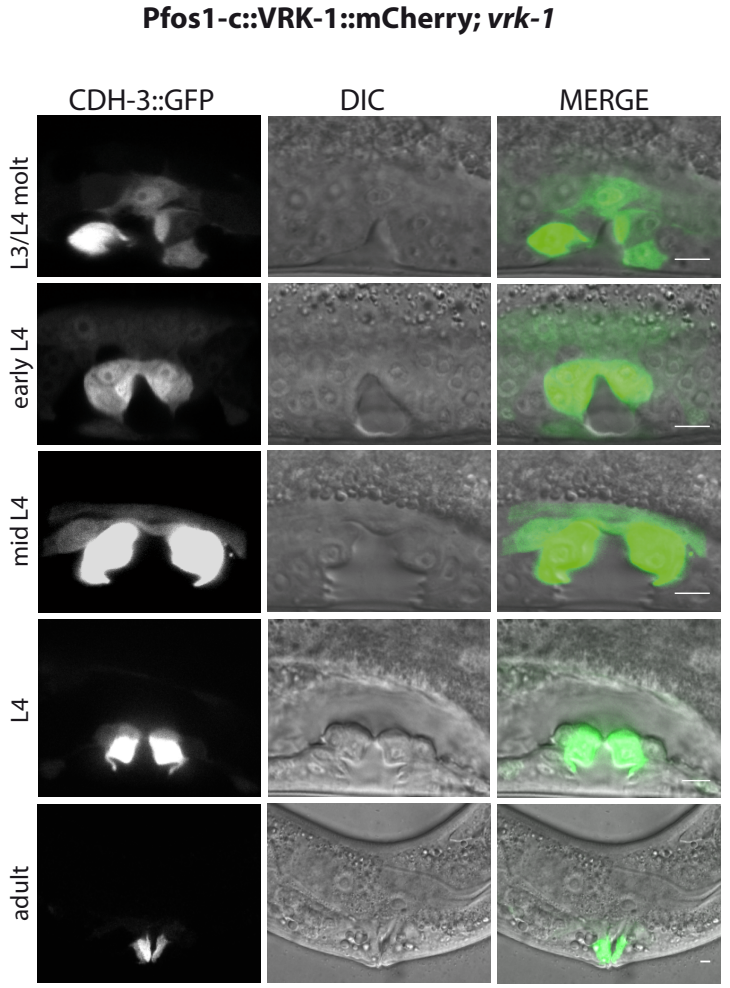

Figure 35. VRK-1 is essential for AC fusion. Fluorescence (left panels), DIC (middle panels) and merged images (right panels) of control animals and *vrk-1* mutants show expression of *cdh-3*::GFP (green). VRK-1::mCherry expression under control of the *fos-1c* promoter in uterine cells and AC rescues the AC fusion phenotype and formation of the utse (arrowhead). Still images taken using different microscope settings. Scale bars, 5µm.

3.6.4. Lack of *vrk-1* causes proliferation and differentiation defects in uterine cells prior to uterine morphogenesis

Our laboratory has previously demonstrated that VRK-1 is necessary for the specification of uterine π cells (Klerkx et al., 2009a). This was based on expression analysis of the LIN-11 transcription factor. To investigate if the effect was specific for LIN-11 or if also other π cell markers are affected, we analyzed the expression of a SOX domain transcription factor fused to GFP, EGL-13::GFP. EGL-13 is controlled dually by FOS-1 and LAG-1 and is required for the maintenance of the uterine π cell fate (Oommen and Newman, 2007). We observed a reduced number of cells expressing EGL-13::GFP upon loss of *vrk-1,* when compared with control animals (Figure 36) confirming abnormal uterine π cell specification in *vrk-1* mutants.

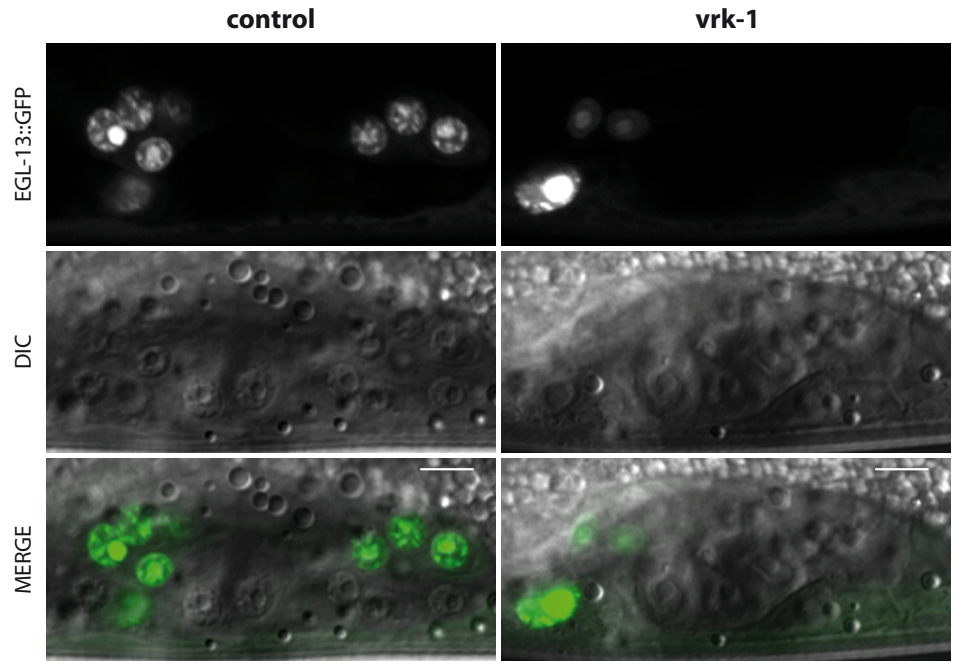

Figure 36. Uterine π cells are not properly specified in *vrk-1* mutants. Fluorescence (top panel), DIC (middle panel) and merged images (bottom panels) of control animals and *vrk-1* mutants show expression of *egl-13*::GFP (green). Still images taken using the same microscope settings. Scale bars, 5μm.

RESULTS

Affected morphology of the uterine tissue was described at the L4 larval stage (Klerkx et al., 2009a). We decided to analyze whether lack of VRK-1 affects, apart from proper specification of uterine π cells, also proliferation, and how early during uterine development we can observe defects in the morphology of the uterine tissue.

In order to decipher if VRK-1 depletion affects proliferation of the uterine cells we decided to use FOS-1A::YFP to mark uterine nuclei in control animals and *vrk-1* mutants (strain BN37). We observed severe malformation in the uterine cells morphology at early L3 larval stage (Figure 36A) what disabled proper quantifications. Nevertheless, comparison of images from several animals clearly suggests that the number of FOS-1A::YFP expressing nuclei is lower in *vrk-1* mutants. Single-copy expression of VRK-1 specifically in the uterine tissue, under control of the *fos-1c* promoter, rescued not only defects in the morphology of uterine cells, but also Pvl phenotype (strain BN263) (Figure 36B-D). We did not observe rescue of the fertility, what agrees with the restricted expression of *vrk-1* in the uterine cells, but not in the germline, from the *fos-1c* promoter. From these observations we conclude that *vrk-1* is necessary for proper proliferation and differentiation of uterine tissue.

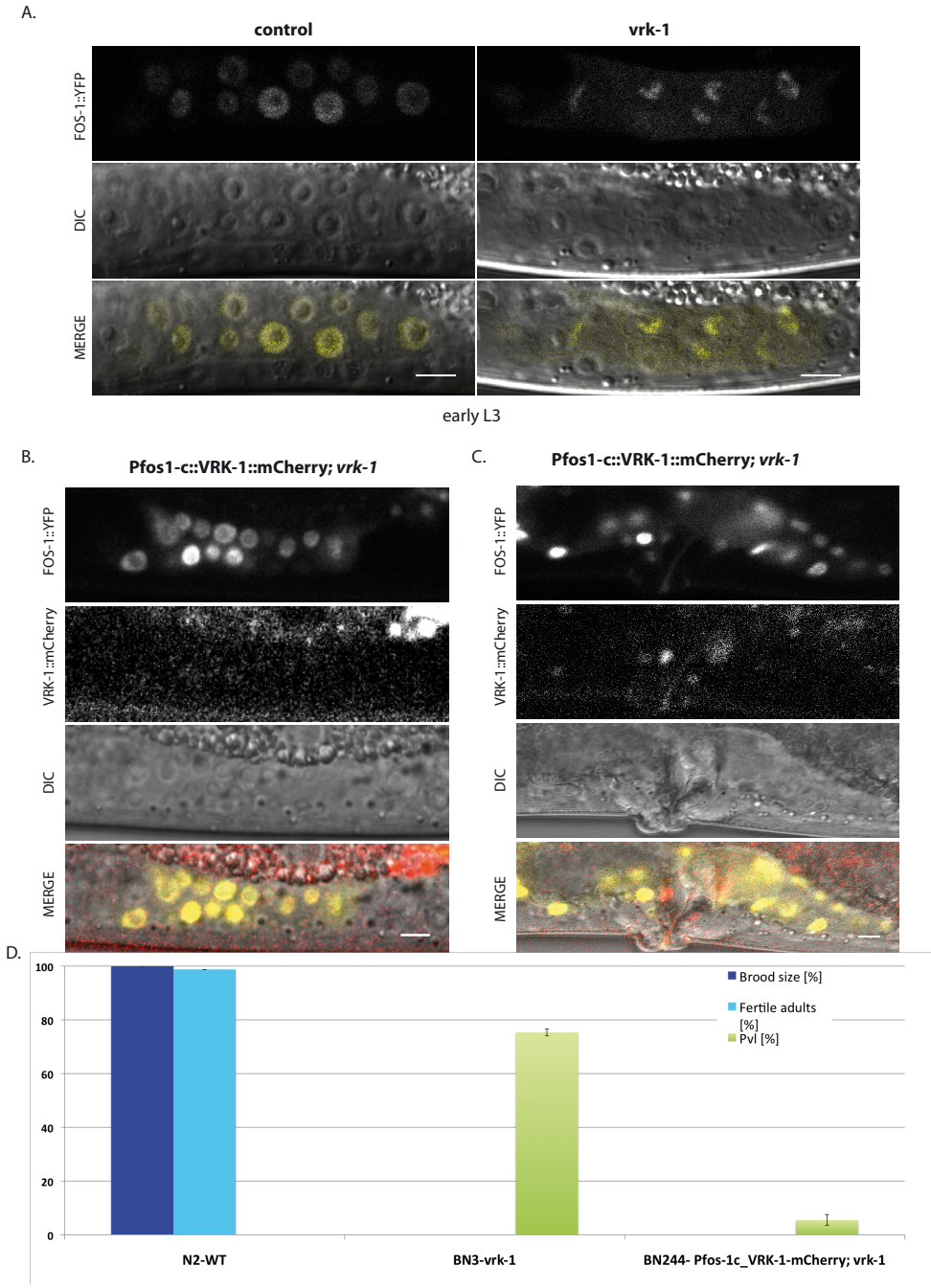

Figure 37. VRK-1 is essential for proliferation and differentiation of uterine tissue. A. Fluorescence (top panels), DIC (middle panels) and merged images (bottom panels) of control animals and *vrk-1* mutants expressing FOS-1A::YFP (yellow). *vrk-1* mutants show severe defects in

the proliferation and differentiation of uterine cells at the early L3 larval stage **B-D.** Uterine VRK-1::mCherry expression under control of the *fos-1c* promoter (red; single-copy transgene producing very low expression) rescues the proliferation and differentiation defects (B) and Pvl phenotype (**C**) Still images taken using different microscope settings. Scale bars, 5μm **D.** The percentage of fertile adults (dark blue), brood size (light blue) and adults with Pvl (green) is shown. Brood size is relative to the value of the wild type animals; fertile adults are relative to the brood size. Error bars report the standard error of the mean.; n>100.

Together, the above experiments suggest that VRK-1 is necessary for the maintenance of AC morphology, proliferation and differentiation of uterine cells and the fusion of the AC with uterine π cells to form the utse syncytium.

3.7. Role of VRK-1 in synaptic transmission

Recent publications have related human VRK1 with a serious neurodegenerative disease with pontocerebellar degeneration and muscular atrophy (Renbaum et al., 2009) and VRK2 with development of several neurological disorders, such as schizophrenia, epilepsy and Huntington's disease (Kim et al., 2014; Li et al., 2012; Steffens et al., 2012; Steinberg et al., 2011). The first part of this thesis reports that *C. elegans* VRK-1 is ubiquitously expressed in most of the neurons in the head and tail of the worm as well as in the VNC (Figure). Moreover, in a large scale yeast two hybrid (Y2H) screen of the *Drosophila melanogaster* proteome (Giot et al., 2003), the fly ortholog of VRK-1, NHK-1, was reported to interact with a phospholipase C (NORPA). The *C. elegans* ortholog of norpA, *egl-8*, encodes a phospholipase C beta (PLCß), which is expressed throughout the nervous system and the intestine (Miller et al., 1999) and *egl-8* mutants have defects in locomotion, egg laying and defecation (Lackner et al., 1999). More specifically, EGL-8 has been implicated in the synaptic transmission by acting with EGL-30 $G_q\alpha$ to facilitate neurotransmitter release (Lackner et al., 1999).

To investigate if the physical interaction of NHK-1/VRK-1 and NORPA/PLCß is conserved in worms, we performed Y2H assays, by co-expressing these proteins in budding yeast. As a positive control we used the VRK-1 interaction partner and substrate BAF-1 (Giot et al., 2003; Gorjanacz et al., 2007). We cloned full-length *C. elegans vrk-1* and *baf-1* cDNA into prey pGADT7 as well as bait pGBKT7 vectors. We observed that VRK-1 interacted with BAF-1 only when it was fused to the Gal4 activation domain and BAF-1 to the Gal4 DNA binding domain (Figure 37A).

C. elegans EGL-8 is a big protein of 1419 amino acids and since large proteins may be inefficiently expressed in yeast, in order to perform Y2H assay, we decided to use two smaller, overlapping fragments in the experiment – a N-terminal fragment of 949 amino acids and a C-terminal fragment of 649 amino acids. However, there is no published information regarding EGL-8 structure so we might disrupt important secondary or tertiary structures in these fragments. We therefore also used the *egl-8* full length cDNA in the Y2H assay. All of the constructs were cloned into the prey pGADT7 vector. As shown in Figure B, we did not observe any interaction between VRK-1 and truncated or full length EGL-8, which may imply that the interaction between VRK-1 and EGL-8 is not conserved between species. However, we do not rule out the possibility that the observed lack of interaction between these two proteins in the Y2H assay is due to problems with the expression or folding of any of the two proteins in yeast.

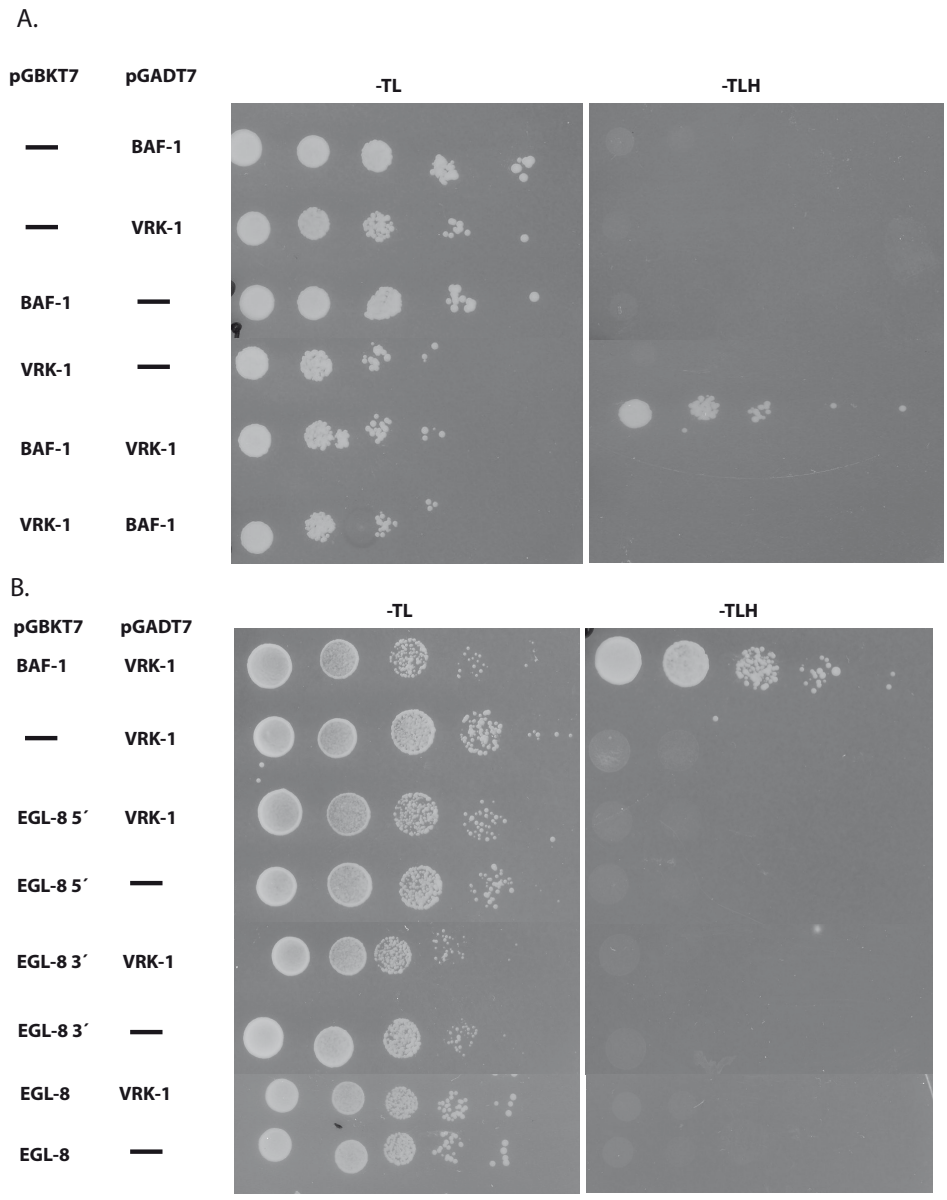

Figure 38. VRK-1 does not physically interact with EGL-8 in the yeast two hybrid assay. Yeast host strain was transformed with GAL4 binding domain (BD) and activation domain (AD) fusion plasmids as indicated and grown on plates lacking tryptophan and leucine (-TL) or lacking tryptophan, leucine and histidine (-TLH) selecting for interactions **A.** Interaction between VRK-1 fused to the GAL4 activation domain and BAF-1 fused to the GAL4 binding domain was observed, but not when VRK-1 was fused to binding domain and BAF-1 to activation domain **B.** No interaction was observed between VRK-1 and EGL-8.

Because of the role of *egl-8* in the nervous system, *egl-8* loss-of-function mutants are resistant to aldicarb (Lackner et al., 1999). The aldicarb sensitivity assay is widely used to investigate synaptic transmission in *C. elegans.* It is a reversible acetylcholinesterase inhibitor and causes the accumulation of the acetylcholine in the synaptic cleft, which leads to muscle hyper-contraction and paralysis. Mutants defective in acetylcholine release are aldicarb resistant and mutants that have enhanced acetylcholine release are aldicarb hypersensitive (Mahoney et al., 2006).

In order to reveal possible role of VRK-1 in the synaptic transmission, we performed the aldicarb sensitivity assay using N2 worms as a control and vrk-1 mutants (homozygous BN3 worms). Although first two experiments clearly suggested that vrk-1 mutants show mild resistance to the aldicarb (Figure 38A), several repetitions were quite variable (Figure 38B) and the average of 7 separate experiments did not show significant differences between wild type N2 worms and vrk-1 mutants. Nevertheless, we are working on the optimization of the aldicarb assay.

A.

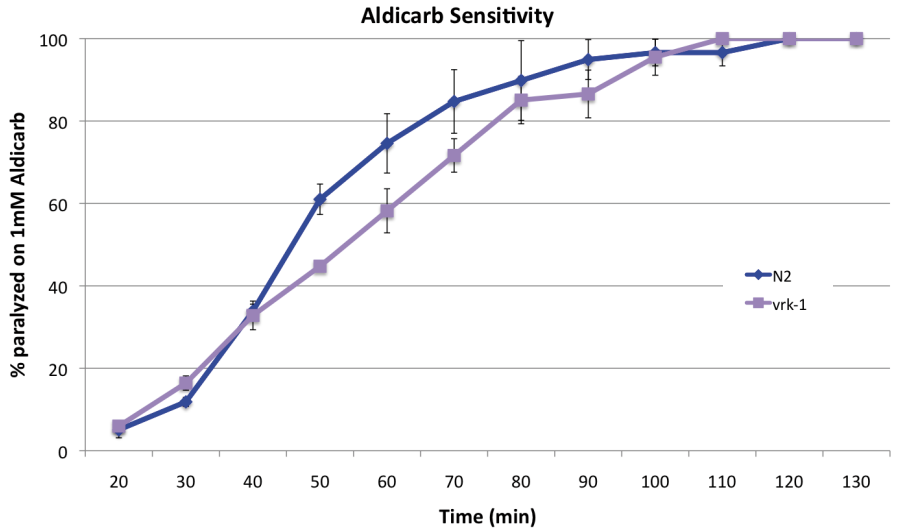

B.

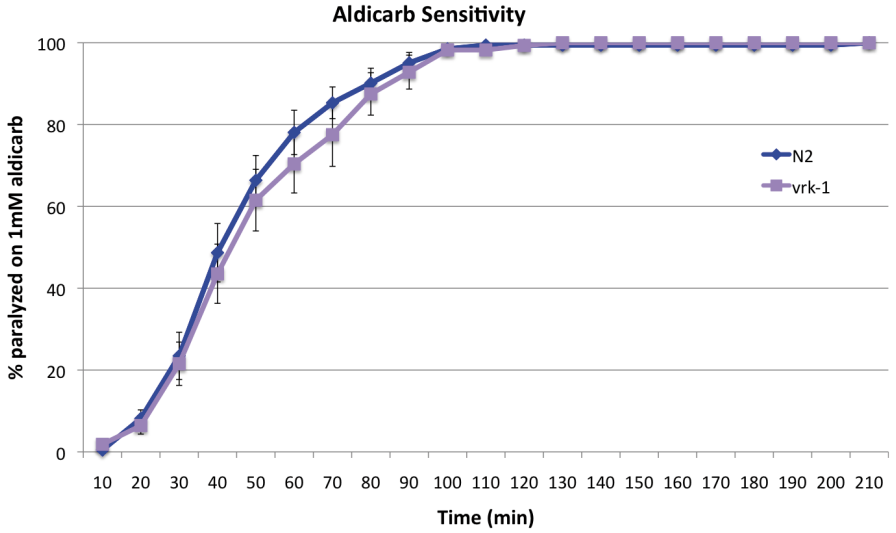

Figure 39. Aldicarb sensitivity assay A. vrk-1 mutants (violet) compared to N2 (blue) worms are mildly resistant to aldicarb (average of two experiments) **B.** vrk-1 mutants (violet) compared to N2 (blue) in aldicarb sensitivity assay (average of seven experiments).

OBJECTIVE 3

3.8. Identification of VRK1 interacting partners

Protein-protein interactions play not only a fundamental role in most biological processes, but also can serve as a tool to predict protein functions. We decided to use co-immunoprecipitation (Co-IP) combined with mass spectrometry (MS) to identify interacting partners of hVRK1.

As shown above, VRK1 is nuclear during interphase and associated with condensed chromosomes during mitosis. Because of the concordance between localization of endogenous VRK1 and hVRK1-mCherry expressed from a single-copy transgene inserted into the genome of U2OS cells, we initially used our hVRK1-mCherry U2OS cell line to pull down VRK1 interacting proteins. To determine the best purification protocol we tested different conditions, including nocodazole synchronized cells in mitosis and asynchronic cells, and lysates with or without a chromosome isolation step: 1) Mitotic cells with chromosome isolation step, 2) Asynchronized cells with chromosome isolation step, 3) Total cell lysate from mitotic cells, 4) Total cell lysate from asynchronized cells. In some experiments, we purified the highest amounts of VRK1 in the soluble fractions without chromosome purification, nevertheless these results were not reproducible.

After several unsuccessful attempts to set up a stable purification protocol for the single-copy hVRK1-mCherry U2OS cell line, we decided to use a HeLa Flp-In T-rex cell line instead which allows for tetracycline regulated expression of the single-copy integrated gene of interest. We inserted hVRK1 cDNA into the pcDNA5/FRT/TO plasmid with a Flag-Venus tag at the N-terminus. The pcDNA5/FRT/TO/Flag-Venus plasmid contains a CMV/2xTet-operator (TetO2) promoter upstream of the multiple cloning site (MCS), where hVRK1 was inserted. Like the pHY12 plasmid, it also contains a hygromycin resistance, so cells with integrated Venus-hVRK1 are hygromycin resistant. The expression of

the integrated gene can be induced by addition of tetracycline or doxycycline. To test that changing the position of the fluorescent tag from the C-terminus to the N-teminus of hVRK1 did not interfere with localization, we performed live microscopy imaging of tetracycline induced HeLa cells. Venus-hVRK1 localized to the nucleus during interphase and was associated with condensed chromosomes during mitosis (Figure 39).

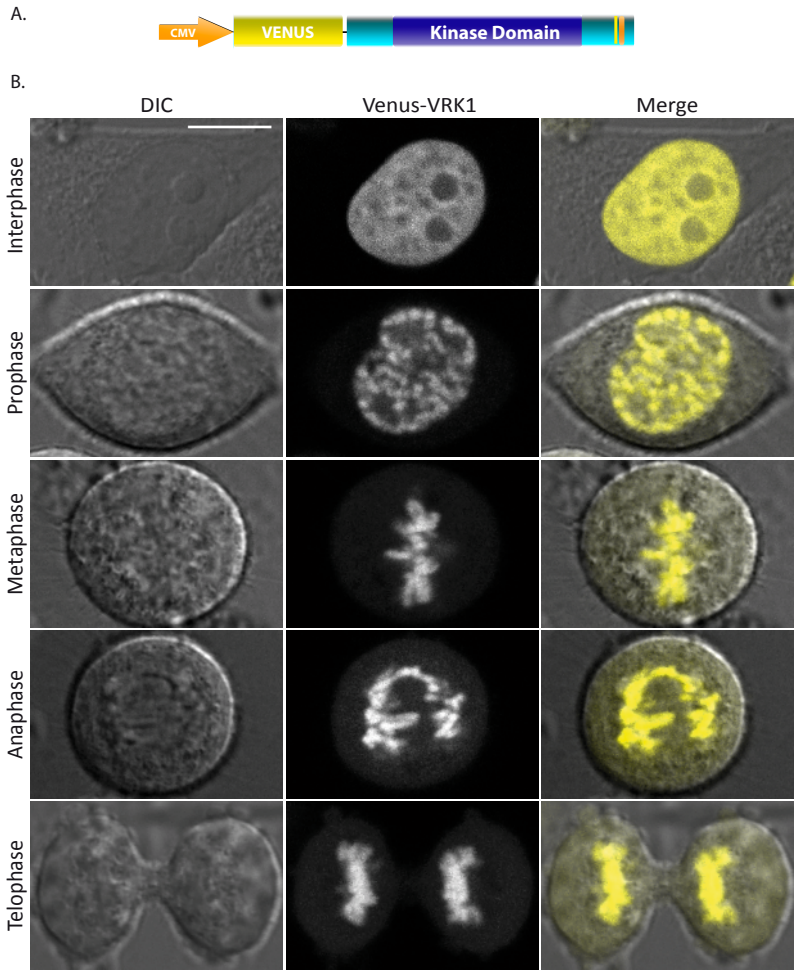

Figure 40. Human Venus-VRK1 expression and dynamics during cell cycle A. Schematic representation of Venus-hVRK-1 expressed under control of CMV promoter **B.** Stable human HeLa/FRT/TO cell line expressing Venus-hVRK1 (yellow in merge), which is nuclear during

interphase and binds chromatin during mitosis. Still images taken using the same microscope settings. Scale bar, 10μm.

We prepared extracts from control and doxycycline induced HeLa/FRT/TO cells expressing Venus-VRK1 using five different washing buffers containing different salts and NP40 concentrations in order to identify the best conditions for purification– 1) 1% NP40 and 125mM NaCl, 2) 1% NP40 and 150mM NaCl, 3) 2% NP40 and 150mM NaCl, 4) 1%NP40 and 300mM KCl, 5) 2%NP40 and 300mM KCl. The best purification was achieved by using washing buffer containing 2% NP40 and 150mM NaCI (data not shown). We undertook a large scale purification using the two different conditions of purification - in duplicate for asynchronous cells (control and doxycyclin induced) and a single experiment for cells arrested in mitosis with nocodazole treatment (control and doxycyclin induced). Soluble cell extracts were prepared and protein complexes were affinity purified using GFP–TRAP columns separated by SDS-PAGE, Coomassie blue stained and analyzed by MS analysis (Figure 40).

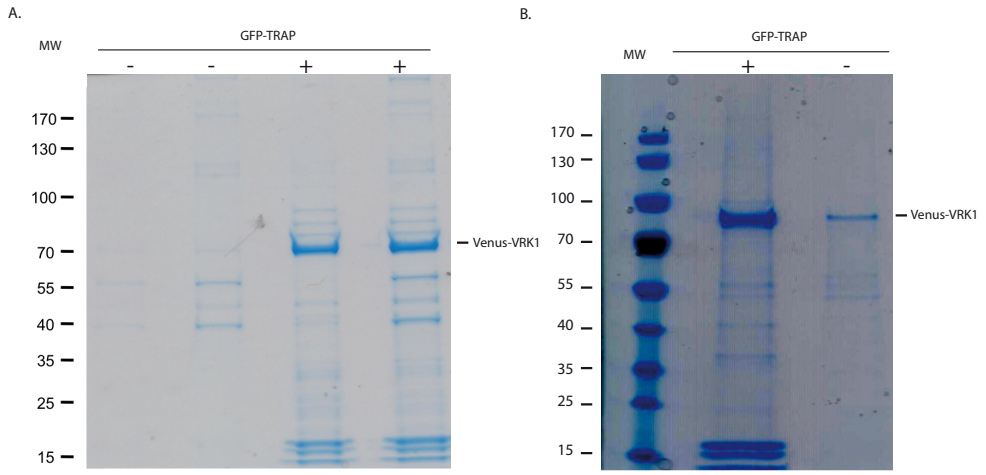

Figure 41. Coomassie blue stained gels of proteins co-immunoprecipitated with GFP-TRAP from asynchronous (A) and mitotic (B) stable HeLa/FRT/TO cell lines expressing Venus-hVRK1 A. Two independent immunoprecipitated samples from non-induced (-) and induced (+) cells were loaded. **B.** One sample from nocodazole synchronized non-induced (-) and induced (+) cells were loaded and Coomassie blue stained. Molecular masses of protein size markers are

indicated (MW). Strong band corresponding to Venus-VRK1 of approximately 74kDa was present in doxycycline induced cells.

We were supplied with a list of over two thousands of protein identified in the purified fractions from two independent experiments from asynchronously growing cells. Among these, 617 proteins were ≥2-fold enriched in the induced samples and represent putative candidates interacting with hVRK1. We selected a list of top candidate proteins with a low posterior error probability (PEP), which interaction with hVRK1 will be investigated with independent methods (Table 4). One of the top candidates was the VRK1 substrate BANF1 (BAF), which serves also as a validation of the experiment.

HGNC NAME	COMMON NAME
BANF1	Barrier-to-autointegration factor
CDCA8	Borealin
AURKB	Aurora kinase B
SUN1	SUN domain-containing protein 1
LMNB1	Lamin-B1
BIRC5	Baculoviral IAP repeat-containing protein 5
EMD	Emerin
TMEM201	Transmembrane protein 201
EMD	Protein ELYS
MECP2	Methyl-CpG-binding protein 2
JUNB	Transcription factor jun-B
JUND	Transcription factor jun-D
HMG20A	High mobility group protein 20A
CETN2	Centrin-2
PARP2	Poly [ADP-ribose] polymerase 2
CEBPB	CCAAT/enhancer-binding protein beta

ZFHX3	Zinc finger homeobox protein 3
MAFK	Transcription factor MafK
LMNB2	Lamin-B2
SUN2	SUN domain-containing protein 2
RUVBL1	RuvB-like 1

Table 2. Protein candidates interacting with hVRK1. Candidate proteins interacting with hVRK identified in a large scale Co-IP assay.

Among 21 top candidate proteins are three out of four members of Chromosomal Passenger Complex (CPC) – Aurora Kinase B (AURKB), Borealin (CDCA8) and BIRC5. CPC is a main regulator of mitotic events and is involved in correction of chromosome-microtubule attachment errors and accurate chromosomes segregation (Carmena et al., 2012). We decided to validate the pull down results by two different approaches – by yeast-two-hybrid and by immunoprecipitation assays.

To confirm the physical interaction between hVRK-1 and members of CPC, we cloned full length AURKB, CDCA8, BIRC5 and, the fourth member of the CPC, INCENP, into prey pGADT7 vectors. As a positive control we used *C. elegans* VRK-1 interaction with BAF-1 (Figure 37). We also cloned full length and truncated fragments of hVRK1 and BANF-1 into bait pGBKT7 and pray GADT7 vectors. Truncated hVRK1 1-321 is insoluble in bacterial cells, hVRK1 1-331 is soluble but inactive, while hVRK1 1-341 and hVRK1 1-351 are soluble with marginal kinase activity (Shin et al., 2011). Based on these data as well as our localization data, we decided to assay physical interaction with candidate proteins using full length hVRK1 (1-396) and three fragments: hVRK1 1-331, hVRK1 1-361 and the C-terminal localization domain containing residues 332-396. Until now we were not able to express AURKB in yeast. As shown in Table 5, we did not observe physical interaction between hVRK1 and BANF1 or candidate proteins, however we do not have a good positive control for the individual candidates.

	hVRK1 1-396	hVRK1 1-331	hVRK1 1-361	hVRK1 332-396	BANF1 - BAF	Ce-vrk-1
AURKB						
BANF1	-	-	-	-	-	
BIRC5	-	-	-	-		
INCENP	-	-	-	-		
CeBAF-1						+
empty	-	-	-	-	-	

Table 3. Analysis of the physical interaction between hVRK1 and members of Chromosomal Passenger Complex.

In order to validate hVRK1 interaction with CPC components by immunoprecipitation, we decided to clone AURKB, BIRC5, INCENP and CDCA8, as well as BANF1 into the pcDNA5/FRT/TO/Flag-Venus plasmid in order to express these proteins in human HeLa/FRT/TO cells and pull down with α-VRK1 mouse monoclonal antibody. We managed to successfully clone and inducing with tetracycline express AURKB, BIRC5 INCENP and BANF-1 in human cells and we are working on the optimization of the purification protocol.

IV. DISCUSSION

IV. DISCUSSION

4.1. VRK-1 is a ubiquitously expressed protein

The first part of my thesis is concentrated on the characterization of the localization and mobility of VRK1 both in *C. elegans* and human cells. In *C. elegans* VRK-1 is reported to be expressed only in certain tissues – hypodermal cells, the ventral nerve cord, vulva precursor cells (VPCs) and germ line (Klerkx et al., 2009a; Waters et al., 2010). The MosSCI method, a novel tool for generating single copy *C. elegans* transgenic strains allowed us to generate transgenic strains expressing VRK-1 fused to three different fluorescent tags – GFP, mCherry and Dendra2, and we have shown that VRK-1 is a ubiquitously distributed protein. Based on the observation that VRK-1 is expressed in the VPCs but not in the anchor cell (AC) and uterine tissue, Klerkx and coworkers suggested that VRK-1 acts cell non-autonomously. However, results presented in this thesis strongly indicate that VRK-1 is expressed not only in previously described cells, but also broadly in the nervous system and uterine tissue, including the AC. Ubiquitous expression of VRK-1 suggests that this kinase may be related not only to the development of the reproductive organs, but also to *C. elegans* development in general.

There are several publications regarding ubiquitous expression of the hVRK1, both in highly proliferative tissues and cancers, and in tissues with lower proliferation rates (Finetti et al., 2008; Nezu et al., 1997; Santos et al., 2006; Valbuena et al., 2007b). We therefore consider likely a role of CeVRK-1 in the worm in both proliferative and postmitotic cells. Although we observed that *vrk-1* mutants are slightly resistant to the acetylcholine esterase inhibitor aldicarb, what suggests a putative role in the synaptic transmission, there is no other phenotype observed in the *vrk-1* mutants that would indicate a role in non-proliferative tissues. On one hand, this can also be supported by the fact, that

the phenotypes upon loss of *vrk-1* are observed since L3 larval stage and affect development of the proliferative tissues related to the reproductive organs (Klerkx et al., 2009a; Waters et al., 2010) and it has been proposed that lack of earlier defects in *vrk-1* mutants is presumably due to the maternal contribution (Klerkx et al., 2009a). On the other hand, ubiquitous expression of VRK-1 in the worm and the fact that VRK1 among species plays a role in many different biological processes, strongly supports the possibility that VRK-1 controls several aspects of the *C. elegans* biology. However further, more detailed studies would be required to reveal VRK-1's role in *C. elegans* development.

Although the more ubiquitous expression pattern in the strains generated by the MosSCI method clearly argues for the advantage of the single-copy integration system in generating transgenic *C. elegans* strains, it is important to emphasize that in single-copy transgenic strain VRK-1::GFP expression was dramatically lower, what can be a disadvantage when analyzing genes with low expression level.

Multiple copy transgenes integrated into the *C. elegans* genome by microparticle bombardment, that were previously used for the characterization of the VRK-1 localization were functional and could partially rescue *vrk-1* depletion phenotypes (Klerkx et al., 2009a). Our new, single copy transgenes however, rescued almost completely *vrk-1* mutant phenotypes. Surprisingly, we could see variable rescue efficiency of these transgenes. In contrast to VRK-1::mCherry and VRK-1::Dendra2, the VRK1::GFP transgene was expressed at lower frequency in the germ line and did not rescue the sterility phenotype. It has been previously described that single copy transgenes inserted at the same chromosomal site are stochastically either expressed or silenced in the germ line (Shirayama et al., 2012) and our observations of variable CeVRK-1::GFP expression agree with that statement. A novel MosSCI method, which allows insertion of the same transgene at several locations in the *C. elegans* genome with a single targeting vector (Frokjaer-Jensen et al., 2014) could be a good and

fast method to generate new single-copy transgenic strains in order to compare the expression pattern and rescue efficiency of the transgenes integrated on different chromosomes.

In *C. elegans* many genes are members of operons and *vrk-1* is the downstream part of the CEOP2747 operon containing two genes. Although VRK-1 in previous studies as well as in this thesis was expressed under control of the putative, directly upstream endogenous promoter, it is possible that it does not fully recapitulate the native expression pattern. To address this, we have initiated experiments based on the recently developed "clustered, regularly interspersed, short palindromic repeats" RNA-guided Cas9 nuclease and homologous recombination (CRISPR- Cas9) method, which enables the insertion of foreign sequences, such as protein tags into endogenous loci (Dickinson et al., 2013). We have designed constructs to insert mCherry into the *vrk-1* locus between the last codon and the stop codon, and we expect thereby to recapitulate expression from both the operon promoter and the immediate upstream promoter.

4.2. Proper nuclear localization of VRK-1 depends on its C-terminus and is independent from kinase activity

VRK1 in humans as well as in *Drosophila* and *C. elegans* is a nuclear protein and members of the VRK family contain a highly conserved protein kinase domain and differ in their C-terminal, potentially regulative fragments (Lopez-Borges and Lazo, 2000; Nichols and Traktman, 2004). In contrast to hVRK1, which has a reported putative nuclear localization signal (NLS) (Lopez-Borges and Lazo, 2000), the sequence targeting *C. elegans* VRK-1 to the nucleus is unknown. In this study we show that proper nuclear localization of VRK-1 depends on its C-terminus and is independent from kinase activity, since the N-terminal half, containing the catalytic domain fails to localize properly to the nucleus, and full length, but inactive protein, localizes correctly. More detailed analysis of further

truncated fragments is required to identify nuclear localization sequence of VRK-1.

4.3. VRK1 is nuclear during interphase and associates to condensed chromosomes during mitosis via its C-terminal domain

Previous studies have described the nuclear distribution of VRK-1 during interphase and its chromosome association during mitosis (Gorjanacz et al., 2007). Published data regarding hVRK1 dynamics during cell division is, on the other hand contrary, since some authors claim that it behaves like its worm ortholog (Kang et al., 2007) and others that it is dispersed during mitosis (Valbuena et al., 2011b). In this study we have demonstrated both, by life imaging of cell lines containing single-copy transgenes and immunofluorescence detection of endogenous protein, that hVRK1 is nuclear during interphase and is associated with condensed chromosomes in mitosis. The similar localization of VRK1 among species suggests that functions observed of *C. elegans, Drosophila* and mammalian VRK1 kinases might also be conserved.

Possible explanations for the differences reported on the localization of the human kinase during mitosis could be because of the usage of different antibodies and fixation protocols. Unfortunately, the protocol used by Valbuena and colleagues is not sufficiently described to perform a detailed comparison of the used methods. Two different fixation methods - ice-cold methanol used in this study, as well as formaldehyde followed by Triton X-100 treatment (Kang et al., 2007) led to detection of chromatin associated hVRK1. In this study we used a monoclonal affinity purified antibody that recognizes a region at the extreme N-terminus of hVRK1 and in the other study showing hVRK1 chromosome association during mitosis hVRK1 antiserum recognizing internal amino acids was used (Kang et al., 2007). It is possible that antibodies that detect other, e.g.,

C-teminal epitopes, do not detect the chromatin associated population of hVRK1 during mitosis.

Interestingly, we have observed that in contrast to VRK-1, which accumulates at the nuclear rim just at the mitotic entry (Gorjanacz et al., 2007), hVRK1 does not localize at the nuclear envelope in prophase. VRK-1 accumulation at the NE at the mitotic entry agrees with VRK-1 phosphorylation of BAF and its release from chromatin. Lack of this accumulation of hVRK1 is surprising and could be due to divergent C-terminal domains of human and *C. elegans* orthologs, which could affect its interaction with NE proteins. These differences could also imply different ratios of VRK1 substrates and interactors. There is approximately 30 times more chromatin in mammalian cells compared to worms, thus strong enrichment of VRK-1 at the nuclear rim in worms could reflect relatively more VRK1 binding sites at the NE compared to chromatin in this species.

Through truncation analysis, we have shown that both VRK-1 and hVRK1 bind chromatin during mitosis via their C-terminal domains. Although the C-terminal fragment of VRK1 is approximately five times bigger in *C. elegans* than in humans, VRK1 association to mitotic chromatin is conserved among species. Using site-directed mutagenesis we uncovered a novel C-terminal motif of which R389, R391 and R393 are essential for hVRK1 chromatin localization during mitosis. This motif is highly conserved among vertebrates, nevertheless when we mutated R432, R434 and K436 of VRK-1, which potentially correspond to the mutated arginines of the human kinase, it did not abrogate chromatin association during *C. elegans* cell division. The ratio between chromatin associated and cytoplasmic signal during mitosis was not significantly changed for the mutated C-terminal VRK-1 fragment, which implies that these residues do not bind DNA, but suggest that there are other C-terminal residues crucial for the chromatin association in worms.

Although the three-dimensional position of R389-R393 identified in this study at the extreme C-terminal end of hVRK1 remains unknown, the published NMR structure of residues 1-361 of VRK1, demonstrates that the C-terminal tail is surface-exposed and orients around the catalytic site (Shin et al., 2011), thus it is quite possible that also the motif critical for chromatin association uncovered in this study is situated in a DNA- accessible position. We have shown in this study that VRK-1 interacts with chromatin via its C-terminal end, however more experiments are necessary to answer if VRK1 can bind DNA directly.

4.4. VRK1 is highly mobile protein

Examining by FRAP analysis the mobility of hVRK1-mCherry in U2OS cells we found that hVRK1 is a highly mobile protein both during interphase and mitosis ($t^1/_2$=3.19sec and $t^1/_2$= 3.36sec, respectively); reported half-life of free GFP is ~0.30sec, GFP-BAF ~1.15sec, GFP-lamin ~90 min (Kruhlak et al., 2000; Molitor and Traktman, 2014). We observed almost identical kinetics in both cell cycle stages, which suggest that several of VRK1's interaction partners are the same during interphase and mitosis and that VRK1 forms short, transient interactions with its binding partners. Recently published data regarding BAF mobility in human MCF-10 cells indicates that although hVRK1 depletion did not affect the velocity of GFP-BAF recovery, it increased the immobile fraction of GFP-BAF during interphase, suggesting that lack of hVRK1 disturbs BAF interaction with binding partners (Molitor and Traktman, 2014). Our observation that VRK1 has a comparable half-life in FRAP assays as its *bona fide* substrate BAF is intriguing. During interphase, BAF could serve as a main interaction partner of VRK1 on chromatin. However, phosphorylation of BAF by VRK1 at mitotic entry abolishes BAF's chromatin association, implying that VRK1 must bind chromatin via other proteins, potentially histones, which are known VRK1 substrates. FRAP analysis

of truncated VRK1 as well as of the *C. elegans* ortholog would be interesting experiments to perform to further characterize VRK1 dynamics.

4.5. VRK-1 is required for AC fusion and proliferation and differentiation of uterine tissue

The second part of my thesis is concentrated on the relation of VRK-1 with signaling pathways involved in development of *C. elegans* reproductive organs. Defects in AC invasion disrupt uterine-vulval attachment and lead to the lack of utse formation, which causes a protruding vulva (Pvl) phenotype. In this study we show that VRK-1 is essential not only for proper specification of uterine π cells (Klerkx et al., 2009a), this study), but also for the AC fusion. Importantly, VRK-1 specific expression in the uterine cells was sufficient to rescue lack of AC fusion and Pvl phenotype.

The interesting observation that lamin (LMN-1), a component of the nuclear envelope, showed unaffected staining in the VPCs in *vrk-1* mutants, but was severely affected in the uterine tissue at the L4 larval stage (Klerkx et al., 2009a) was complemented by our results showing that the morphology of the uterine cells is disrupted very early during development, already at the early L3 larval stage, prior to uterine morphogenesis. The latter observation suggests defects in the proliferation of the uterine cells, however, until now, we were not able to address this issue more thoroughly, because the affected morphology of the uterine tissue in *vrk-1* mutants prevented proper quantifications. VRK-1 is a mitotic kinase clearly related with cell proliferation, thus dramatic defects in the uterine tissue could be due to a general block in the cell cycle progression. However, we also note that divisions of VPCs, which take place later in development than the uterine cell divisions described here, are not affected in *vrk-1* mutants. This might indicate an unknown, specific role of VRK-1 in uterine

cells. Careful analysis of the proliferation of uterine cells early during development of the reproductive organs could clarify that issue (see below).

Accumulation of the actin-binding protein, moeABD, at the apical, noninvasive, membrane of the AC is affected in *vrk-1* mutants (Klerkx et al., 2009a) suggesting a role of VRK-1 in the pathways controlling polarization and invasion of the AC. However, we did not observe significant differences in the distribution, except for the PAT-3::GFP, of other proteins involved in the polarization and invasion of the AC through the basement membrane. In fact, quantification of PAT-3::GFP polarity in *vrk-1* mutants and control animals suggested a mild hyperpolarization of the basal membrane of the AC. PAT-3 is a beta-integrin subunit, and integrins regulates F-actin recruitment at the cell membrane (Hagedorn et al., 2009), so having in mind apically accumulated acin-binding moeABD in *vrk-1* mutants, one would expect reduced amount of PAT-3::GFP at the basal AC membrane. Upon depletion of VRK-1, morphology of the uterine, but not the vulval tissue is affected, and what is more, our analysis of the AC polarization and invasion markers revealed that also the shape of this cell is altered. Severe AC shape changes and the fact that in *vrk-1* mutants, despite the delay in the invasion, AC finally breaches the basement membrane (Klerkx et al., 2009a), combined with the observation that main invasion markers are not affected, suggested abnormal contacts to the neighboring, uterine cells. The apically accumulated actin-binding moeABD, could therefore be not a consequence of AC mis-polarization in *vrk-1* mutants, but of the severe defects in the morphology of the uterine cells that causes abnormal contacts between AC and uterine cells. Aberrant morphology of the uterine cells could affect contacts with the AC, thus its actomyosin cytoskeleton and morphology. AC induces development of the uterus and we have shown in this study, that proper proliferation and differentiation of the uterine cells depends on the *vrk-1*. The AC, as other uterine cells, is derived from cells of the somatic gonad primordium, so we plan to check if *vrk-1* functions already in the AC-VU decision

in the late L2 larval stage. The *C. elegans* ortholog of the *tailless* nuclear receptor (*nhr-67*) functions in AC specification and development of the uterine π cells (Verghese et al., 2011). In the L2 larval stage *nhr-67::gfp* is expressed in the four pre-VU cells, that become the AC and three VU cells, so it would be relevant to analyze its behavior in the *vrk-1* mutants.

In this study we have shown that VRK-1 has a crucial role in the development of the reproductive organs of the *C. elegans* and that tissue specific expression of *vrk-1* rescues defects in the uterine tissue, AC fusion and Pvl phenotype. These observations are contrary to the previous publication from our laboratory, which related development of the uterus, including AC behavior, with a cell non-autonomous role of *vrk-1* (Klerkx et al., 2009a). The hypothesis that *vrk-1* acts cell non-autonomously was based on the fact that strains generated by microparticle bombardment express VRK-1::GFP in the VPCs, but not in the AC and uterine tissue, and on tissue specific knockdown (Klerkx et al., 2009a). We speculate that perhaps low levels of VRK-1::GFP were indeed expressed in the uterine cells, but masked by the bright signal in the VPCs. Tissue-specific knockdown of VRK-1 was made using the *lin-31* promoter, which is annotated as being VPC specific. However, because this annotation is based on expression of lin-3::gfp from multicopy tansgenes, there is a possibility that the *lin-31* promoter is lowly expressed outside the vulval tissue.

4.6. VRK-1 and its role in synaptic transmission

Based on our observation that *vrk-1* is expressed in all or most of *C. elegans* neurons, we also tried to answer the question, if *vrk-1* has a role in the nervous system. To do that, we used two different approaches. On one hand, we checked if the NHK-1 and phospholipase C (NORPA) interaction reported in *Drosophila* using yeast two-hybrid assays (Y2H) (Giot et al., 2003) is conserved in *C. elegans.* However, Y2H assays with *vrk-1* and the NORPA ortholog, *egl-8* did not

show any physical interaction. This may imply that the interaction between these two proteins is not conserved among species. However *C. elegans* egl-8 has three isoforms – isoform a of 1419 aa, isoform b of 1431 aa and isoform c of 592 aa. In the Y2H assay we used isoform a, so analysis of the VRK-1 interaction with the other isoforms that each contain aa residues absent in the a isoform would be relevant. Moreover, interactions between large proteins are often inefficient in the Y2H system compared to shorter cDNA fragments. Unfortunately, the large-scale study that identified the interaction between NHK-1 and NORPA did not report, which fragments scored positive.

On the other hand, we monitored the sensitivity of *vrk-1* mutants to the paralyzing effect of the pesticide aldicarb, which is an acetylcholinesterase inhibitor (Mahoney et al., 2006). Interestingly, we observed a mild resistance of *vrk-1* mutants to that drug, which suggests a possible defect in acetylcholine release. Nevertheless more detailed studies are necessary to characterize *vrk-1* role in the nervous system, especially that publications that associate mutations in hVRK1 with complex axonal motor and sensory neuropathy accompanied by severe non-progressive microcephaly and cerebral dysgenesis and spinal muscular atrophy with pontocerebellar hypoplasia (Gonzaga-Jauregui et al., 2013; Renbaum et al., 2009), support a putative role of VRK-1 in the *C. elegans* nervous system. VRK-1 is a mitotic kinase and this study as well as previous publications proves its role in cell proliferation, so experiments analyzing possible defects in the proliferation of neurons could address this issue.

4.7. Co-IP Identifies Members of a Chromosomal Passenger Complex (CPC) as interaction partners of hVRK1

One of the main goals of this study was to identify VRK1 interaction partners. To approach this issue, we expressed and purified tagged VRK1 from human asynchronous and mitotic cells, followed by high-resolution mass spectrometry.

Among the top candidates of the hVRK1 interacting proteins we identified three members of the chromosomal passenger complex (CPC) – Aurora B, borealin and survivin. CPC is a key regulator of diverse mitotic events and is composed of four subunits – a kinase module formed by Aurora B and a localization module composed of inner centromere protein (INCENP), borealin and survivin (Carmena et al., 2012). INCENP is the largest CPC subunit and would not have been detected in our mass spectrometry analysis because large proteins were omitted. The CPC is essential for proper chromosome segregation, kinetochore-microtubule attachments and cytokinesis. RNAi against VRK-1 and mutation in NHK-1 or overexpression of hVRK1 causes hypercondensation of chromatin (Cullen et al., 2005; Gorjanacz et al., 2007; Ivanovska et al., 2005) and defects in meitotic spindle formation in flies (Cullen et al., 2005), mitotic progression and proliferation (Choi et al., 2010; Gorjanacz et al., 2007; Molitor and Traktman, 2014; Waters et al., 2010; Wiebe et al., 2010), thus similar phenotypes observed upon depletion of CPC complex (Gassmann et al., 2004; Hegarat et al., 2011). Moreover, RNAi against *bir-1*, the *C. elegans* baculoviral inhibitor-of-apoptosis repeat protein gene which encodes a homolog of the human Survivin cause a Pvl phenotype, (Kostrouchova et al., 2003) which could potentially link it to the VRK-1, although the Pvl phenotype is caused by defects in many genes related with several signaling pathways.

In order to validate the hVRK1 interaction with candidate proteins, we expressed members of human CPC in yeast and tested for interactions with hVRK1. Until now, we were not able to see any interaction between hVRK1 and the analyzed proteins, however, we do not have a good positive control of the interaction between human proteins. Although hVRK1-BAF1 does not interact in our Y2H assay, that interaction is biochemically demonstrated (Nichols et al., 2006) and in *C. elegans* we show a robust VRK-1 – BAF-1 interaction in Y2H. The reported survivin and borealin interaction in Y2H (Klein et al., 2006) could be used as a positive control in next experiments.

In our Co-IP assay, we also identified several nuclear envelope proteins as potential VRK-1 interacting proteins (SUN1-2, LMNB1-B2, EMD, TMEM201, ELYS). There are several observations suggesting that VRK-1 interacts with NE proteins. First of all, loss of *vrk-1* causes severe defects in the NE morphology (Gorjanacz et al., 2007; Molitor and Traktman, 2014) and VRK1 mediated phosphorylation of BAF is crucial for its release from chromatin and LEM proteins (Gorjanacz et al., 2007; Margalit et al., 2007; Nichols et al., 2006). Moreover, *C. elegans* embryos, from which *vrk-1* was depleted by RNAi, contain hypercondensed chromatin surrounded by nuclear membranes that lack NPCs (Gorjanacz et al., 2007; Margalit et al., 2007; Nichols et al., 2006). Also the newly described interaction of a member of the LEM domain protein family, Lem4, which is required for BAF dephosphorylation and inhibits VRK1 in *C. elegans* and human cells (Asencio et al., 2012) testifies for VRK1 interactions with other NE proteins. Furthermore, a recent RNAi-based screen identified *vrk-1* as one of the *mel-28* (ELYS) genetic interactors (Fernandez et al., 2014). Because of our positive Y2H results with *C. elegans* VRK-1 and BAF-1, we are now cloning several *C. elegans* homologs of proteomics candidate genes into the Y2H vectors to assay their interaction with *C. elegans* VRK-1.

V. CONCLUSIONS

V. CONCLUSIONS

1. Single copy transgenic *C. elegans vrk-1* strains show ubiquitous expression and are capable to fully rescue *vrk-1(ok1181)* mutant phenotypes.
2. VRK1 in *C. elegans* and human U2OS and HeLa cells is nuclear during interphase and associated with condensed chromatin during mitosis.
3. The carboxyl domain of *C. elegans* VRK-1 (residues 321-610) is necessary and sufficient for proper nuclear localization.
4. The carboxyl domains of human VRK1 (residues 332-396) and *C. elegans* VRK-1 (residues 321-610) bind chromatin during mitosis.
5. Conserved arginines at positions 389, 391 and 393 in human VRK1 are essential for VRK1 association with chromatin during mitosis.
6. Substitution of R432A, R434A and K436A in *C. elegans* VRK-1 did not affect its association with chromatin during mitosis.
7. Human VRK1 is a highly mobile protein both during interphase and mitosis.
8. The Anchor Cell (AC) morphology and presumably contact to uterine cells are severely affected in *C. elegans vrk-1(ok1181)* mutants.
9. Lack of *C. elegans vrk-1* causes proliferation and differentiation defects in uterine tissue prior to uterine morphogenesis.
10. VRK-1 is essential for AC fusion with uterine π cells.
11. *C. elegans* VRK-1 interacts physically with barrier to autointegration factor (BAF-1) in yeast-two-hybrid (Y2H) assay.

CONCLUSIONS

12. Large scale Co-Immunoprecipitation assays from human cells identified 617 putative candidates interacting with human VRK1, including members of the Chromosomal Passenger Complex.

VI. MATERIALS AND METHODS

VI. MATERIALS AND METHODS

6.1. *C. elegans* strains

C. elegans strains were maintained using standard techniques (Brenner, 1974). Strains used in this study are listed below.

Strain name	Description	Genotype	Source
BN3	Balanced *vrk-1* deletion strain	vrk-1(ok1181)/mIn1[mIs14 dpy-10(e128)] II	Klerkx et al 2009
BN26	Balanced *vrk-1* deletion strain expressing CDH-3::GFP. Made by crossing strain PS3352 with BN3	vrk-1(ok1181)/mIn1[mIs14 dpy-10(e128)] II; syIs50[pkEx246 [pMH86 (dpy-20 rescue plasmid) + JP#38 (cdh-3::GFP)]] X	Klerkx et al 2009
BN37	Balanced *vrk-1* deletion strain expressing Ce-fos-L-YFP	vrk-1(ok1181)/mIn1[mIs14 dpy-10(e128)] II; syIs123[unc-119(+)(65ng/ul) + Ce-fos-L-YFP(65ng/ul]; May carry unc-119(ed4) III	Klerkx et al 2009
BN120	Balanced *vrk-1* deletion strain expressing UNC-40::GFP in AC. Marked with YFP in pharynx. Made by crossing strain BN3 with NK389	vrk-1(ok1181)/mIn1[mIs14 dpy-10(e128)] II; qyIs67[Pcdh-3::unc-40::GFP] ? (not II)	This study
BN135	Balanced *vrk-1* deletion strain expressing mCherry::PLCdeltaPH in AC. Low to moderate VD neuron expression. Made by crossing strain BN3 with NK323	vrk-1(ok1181)/mIn1[mIs14 dpy-10(e128)] II; qyIs24(Pcdh-3::mk62-63::membrane cherry) (III, IV or X)	This study
BN156	Expression of VRK-1::GFP. Integrated Pvrk-1::vrk-1::gfp. Made by MosSCI injection of EG5003 with plasmid #962 (+plasmids #889 pJL43.1 + #868 + #879 + #885). Outcrossed twice with N2 strain. Do not carry Mos. May carry unc-119(ed3) III	bqSi156[p962(unc-119(+) Pvrk-1::vrk-1::gfp)] IV	This study
BN171	Expression of VRK-1::mCherry. Integrated Pvrk-1::vrk-1::mCherry. Made by MosSCI injection of EG5003 with plasmid #961 (+plasmids #889 pJL43.1 + #868 + #879 + #885). Outcrossed twice with N2 strain. Do not carry Mos. May carry unc-119(ed3) III	bqSi171[p961(unc-119(+) Pvrk-1::vrk-1::mCherry)] IV	This study
BN172	Balanced *vrk-1* deletion strain expressing VRK-1::GFP. Balanced vrk-1(ok1181) with integrated Pvrk-1::GFP. Made by crossing strain BN3 with BN156	vrk-1(ok1181)/mIn1[mIs14 dpy-10(e128)] II; bqSi156[p962(unc-119(+) Pvrk-1::vrk-1::gfp)] IV	This study
BN173	Balanced *vrk-1* deletion strain expressing VRK-1::mCherry. Balanced vrk-1(ok1181) with integrated Pvrk-1::mCherry. Made by crossing strain BN3 with BN171	vrk-1(ok1181)/mIn1[mIs14 dpy-10(e128)] II; bqSi171[p961(unc-119(+) Pvrk-1::vrk-1::mCherry)] IV	This study
BN174	Balanced *vrk-1* deletion strain expressing EGL-13::GFP. Balanced vrk-1(ok1181) with expression of egl-13::GFP. Made by crossin strain BN3 with MH1317	vrk-1(ok1181)/mIn1[mIs14 dpy-10(e128)] II; kuIs29[unc-119(+) egl-13::GFP(pWH17)] V	This study
BN175	Expression of C-terminus VRK-1::mCherry. Integrated Pvrk-1::C-terminal_vrk-1::mCherry. Made by MosSCI injection of EG5003 w plasmid #1011 (+plasmids #889 pJL43.1 + #973 + #1005 + #1008). Outcrossed twice with N2 strain. Do not carry Mos. May carry unc-119(ed3) III	bqSi175[p1011(unc-119(+) Pvrk-1::C-terminal_vrk-1::mCherry)] IV	This study

BN176	Expression of N-terminus VRK-1-mCherry. Integrated Pvrk-1::N-terminal_vrk-1::mCherry. Made by MosSCI injection of EG5003 with plasmid #1010 (+plasmids #889 pJL43.1 + #973 + #1005 + #1008). Outcrossed twice with N2 strain. Do not carry Mos. May carry unc-119(ed3) III	bqSi176[p1010(unc-119(+) Pvrk-1::N-terminal_vrk-1::mCherry)] IV	This study
BN178	Balanced vrk-1deletion strain expressing C-terminus VRK-1-mCherry. Balanced vrk-1(ok1181) with integrated Pvrk-1_C-terminal::mCherry. Made by crossing strain BN3 with BN175	vrk-1(ok1181)/mIn1[mIs14 dpy-10(e128)] II; bqSi175[p1011(unc-119(+) Pvrk-1::C-terminal_vrk-1::mCherry)] IV	This study
BN179	Balanced vrk-1deletion strain expressing N-terminus VRK-1-mCherry. Balanced vrk-1(ok1181) with integrated Pvrk-1_N-terminal::Mcherry. Made by crossing strain BN3 with BN176	vrk-1(ok1181)/mIn1[mIs14 dpy-10(e128)] II; bqSi176[p1010(unc-119(+) Pvrk-1::N-terminal_vrk-1::mCherry)] IV	This study
BN180	Expresion ofK169E vrk-1-mCherry. Integrated Pvrk-1::vrk-1_K169E::mCherry. Made by MosSCI injection of EG5003 w plasmid #1028(+plasmids #889 pJL43.1 + #973 + #1005 + #1008). Outcrossed twice with N2 strain. Carry Mos. May carry unc-119(ed3) III	bqSi180[p1028(unc-119(+) Pvrk-1::K169E_vrk-1::mCherry)] IV	This study
BN183	Balanced vrk-1deletion strain expressing K169E VRK-1-mCherry. Balanced vrk-1(ok1181) with integrated Pvrk-1_K169E::mCherry. Made by crossing strain BN3 with BN180	vrk-1(ok1181)/mIn1[mIs14 dpy-10(e128)] II; bqSi156[p1028(unc-119(+) Pvrk-1::K169E_vrk-1::mCherry)] IV	This study
BN188	Balanced vrk-1deletion strain expressing PAT-3-GFP and genomic INA	vrk-1(ok1181)/mIn1[mIs14 dpy-10(e128)] II; gyIs43[pat-3::GFP +ina(genomic)+unc-119(+)]	This study
BN191	Balanced vrk-1 deletion strain expressing MIG-2-GFP. Balanced vrk-1(ok1181) with expression of mig-2::GFP. Made by crossing strain BN3 with CF579M	vrk-1(ok1181)/mIn1[mIs14 dpy-10(e128)] II	This study
BN193	Expression of VRK-1::Dendra2. Integrated Pvrk-1::vrk-1::Dendra2. Made by MosSCI injection of EG5003 w plasmid #1047 (+plasmids #889 pJL43.1 + #868 + #879 + #885). Outcrossed twice with N2 strain. Do not carry Mos. May carry unc-119(ed3) III	vrk-1(ok1181)/mIn1[mIs14 dpy-10(e128)] II; bqSi193[p1047(unc-119(+) Pvrk-1::vrk-1::Dendra2)] IV	This study
BN207	Balanced vrk-1deletion strain expressing VRK-1::Dendra2. Made by crossing strain BN3 with BN193	vrk-1(ok1181)/mIn1[mIs14 dpy-10(e128)] II; bqSi193[p1047(unc-119(+) Pvrk-1::Dendra2)] IV	This study
BN223	Expression of VRK-1::mCherry from fos-1c promoter. Integrated Pfos-1c::vrk-1::mCherry. Made by MosSCI injection of EG5003 w plasmid #1101 (+plasmids #889 pJL43.1 + #973 + #1005 + #1008). Outcrossed twice with N2 strain. Do not carry Mos. May carry unc-119(ed3) III	bqSi223[p1101(unc-119(+) Pfos-1c::vrk-1::mCherry)] IV	This study
BN244	Balanced vrk-1deletion strain expressing VRK-1::mCherry from fos-1c promoter. Balanced vrk-1(ok1181) with integrated Pfos-1c::vrk-1::mCherry. Made by crossing strain BN3 with BN223	vrk-1(ok1181)/mIn1[mIs14 dpy-10(e128)] II; bqSi223[p1101(unc-119(+) Pfos-1c::vrk-1::mCherry)] IV	This study
BN253	Balanced vrk-1deletion strain expressing VRK-1::mCherry from fos-1c promoter and translational fos-1a::yfp. Made by crossing strain BN37 with BN244	vrk-1(ok1181)/mIn1[mIs14 dpy-10(e128)] II; syIs123[unc-119(+)(65ng/ul) + Ce-fos-L-YFP(65ng/ul]; May carry unc-119(ed4) III; bqSi223[p1101(unc-119(+) Pfos-1c::vrk-1::mCherry)] IV	This study
BN263	Balanced vrk-1deletion strain expressing CDH-3-GFP and VRK-1::mCherry from fos-1c promoter. CDH-3::gfp in mutant vrk-1 background with integrated Pfos-1c::vrk-	vrk-1(ok1181)/mIn1[mIs14 dpy-10(e128)] II; bqSi223[p1101(unc-119(+) Pfos-1c::vrk-1::mCherry)] IV; syIs50[pkEx246 [pMH86 (dpy-20	This study

	1::mCherryandtranslational fos-1a::yfp. Made by crossing strain BN26 with BN244	rescue plasmid) + JP#38 (cdh-3::GFP)]] X	
BN303	Expresion of GFP-VRK1 under control of the heat-shock promoter. Integrated Phsp-16.41::gfp::vrk-1. Made by MosSCI injection of EG4322 with plasmid #1239 (+ plasmids #1183 + #868 + #879 + #885). Outcrossed twice with N2 strain. May carry Mos and unc-119(ed3) III	bqSi303[pBN156(unc-119(+) Phsp-16.41::gfp::vrk-1)] II	This study
BN304	Expression of GFP::C-term VRK-1 under control of heat-shock Phsp-16.41 promoter. Made by MosSCI injection of EG4322 with plasmid #1240 (+ plasmids #1183 + #868 + #879 + #885). Out crossed twice w N2	Integrated Phsp-16.41::gfp::C-term_vrk-1. Made by MosSCI injection of EG4322 with plasmid #1240 (+ plasmids #1183 + #868 + #879 + #885). Out crossed twice w N2.	This study
Bristol N2	Wild type strain		CGC
PS3352	Expression of CDH-3::GFP. Integrated line from Pettitt et al. Dev 122: 4149.	pkEx246 [pMH86 (dpy-20 rescue plasmid) + JP#38 (cdh-3::GFP)]	CGC
YL255	Expression of VRK-1-GFP regulated by its own promoter and 3'UTR	unc-119(ed3) III; vrIs13[Pvrk-1::VRK-1:GFP:VRK3UTR; unc-119(+)]	Klerkx et al 2009
NK358	Expression of integrin-beta subunit PAT-3::GFP	gyls43[pat-3::GFP +ina(genomic)+unc-119(+)]	
NK389	Expression of UNC-40::GFP in AC. Marked with YFP in pharynx.	qyls67[Pcdh-3::unc-40::GFP] ? (not II); unc-119(ed4) III	Joshua Ziel/David Sherwood
NK323	Not backcrossed. Beautiful AC expression of mCherry::PLCdeltaPH. Low to moderate VD neuron expression. Publication and information sent with strains do not agree on where transgene is inserted.	unc-119(ed4) III; qyls24(Pcdh-3::mk62-63::membrane cherry) (III, IV or X)	Joshua Ziel/David Sherwood
MH1317	Expression of EGL-13::GFP	kuIs29[unc-119(+) egl-13::GFP(pWH17)] V.	CGC
CF579M	Expression of MIG-2::GFP. GFP is membrane enriched and expressed in many cells throughout development. Not known to which LG muls 27 is integrated; integrated with gamma rays; outcrossed once	dpy-20(e1282) IV; him-5(e1490)V; muls27	CGC
EG4322	For MosSCI single copy insertion on chromosome II. Unc. Not caused by ttTi5605. Mos1 allele generated by NemaGENETAG consortium.	ttTi5605 II; unc-119(ed3) III.	
EG5003	For MosSCI single copy insertion on chromosome IV. Unc. Not caused by cxTi10882. Mos1 allele generated by NemaGENETAG consortium.	unc-119(ed3) III; cxTi10882 IV.	

Table 4 *C. elegans* strains used in this study.

6.2. Cell lines

Human cell lines used in this study are listed below.

Cell line	Origin	Description	Culture conditions	Source
U2OS FRT/TO	Human osteosarcoma	Modified U2OS cell line containing integration site for FRT constructs	DMEM, 10% FBS, 1x Penicilin/Streptomycin, 100µg/ml Zeocin, 5mg/ml Blasticidin	Nilsson J.
HeLa FRT/TO	Human cervical carcinoma	Modified HeLa cell line containing integration site for FRT constructs	DMEM, 10% FBS, 1x Penicilin/Streptomycin, 100µg/ml Zeocin, 5mg/ml Blasticidin	Nilsson J.
U2OS FRT/TO/VRK1-mCherry	Human osteosarcoma	U2OS cell line stably expressing human VRK1-mCherry. Made by transfection with plasmid #1094	DMEM, 10% FBS, 1x Penicilin/Streptomycin, 200µg/ml Hygomycin, 5mg/ml Blasticidin	This study
U2OS FRT/TO/C-terminus VRK1-mCherry	Human osteosarcoma	U2OS cell line stably expressing human 321-396 VRK1-mCherry. Made by transfection with plasmid #1129	DMEM, 10% FBS, 1x Penicilin/Streptomycin, 200µg/ml Hygomycin, 5mg/ml Blasticidin	This study
U2OS FRT/TO/C-terminus 30a.a VRK1-mCherry	Human osteosarcoma	U2OS cell line stably expressing human 332-361 VRK1-mCherry. Made by transfection with plasmid #1129	DMEM, 10% FBS, 1x Penicilin/Streptomycin, 200µg/ml Hygomycin, 5mg/ml Blasticidin	This study
U2OS FRT/TO/C-terminus 42 a.a VRK1-mCherry	Human osteosarcoma	U2OS cell line stably expressing human 355-396 VRK1-mCherry. Made by transfection with plasmid #1129	DMEM, 10% FBS, 1x Penicilin/Streptomycin, 200µg/ml Hygomycin, 5mg/ml Blasticidin	This study
HeLa FRT/TO/FLAG Venus-VRK1	Human cervical carcinoma	HeLa cell line stably expressing human Venus-VRK1. Made by transfection with plasmid #1248	DMEM, 10% FBS, 1x Penicilin/Streptomycin, 200µg/ml Hygomycin, 5mg/ml Blasticidin	This study
U2OS FRT/TO/C-terminus RG VRK1-mCherry	Human osteosarcoma	U2OS cell line stably expressing human 321-396 R389G, R391G and R393G VRK1-mCherry. Made by transfection with plasmid #1208	DMEM, 10% FBS, 1x Penicilin/Streptomycin, 200µg/ml Hygomycin, 5mg/ml Blasticidin	This study
U2OS FRT/TO/C-terminus STA VRK1-mCherry	Human osteosarcoma	U2OS cell line stably expressing human 321-396 S388A, T390A VRK1-mCherry. Made by transfection with plasmid #1209	DMEM, 10% FBS, 1x Penicilin/Streptomycin, 200µg/ml Hygomycin, 5mg/ml Blasticidin	This study
U2OS FRT/TO/C-terminus DA VRK1-mCherry	Human osteosarcoma	U2OS cell line stably expressing human 321-396 D340A, D335A and D336A VRK1-mCherry. Made by transfection with plasmid #1207	DMEM, 10% FBS, 1x Penicilin/Streptomycin, 200µg/ml Hygomycin, 5mg/ml Blasticidin	This study
U2OS FRT/TO/RG VRK1-mCherry	Human osteosarcoma	U2OS cell line stably expressing human R389G, R391G and R393G VRK1-mCherry. Made by transfection with plasmid #1242	DMEM, 10% FBS, 1x Penicilin/Streptomycin, 200µg/ml Hygomycin, 5mg/ml Blasticidin	This study

Table 5. Cell lines used in this study.

6.3. Plasmids

Plasmids used in this study are listed below.

Plasmid	Vector	Insert	Description
301	L4440		Feeding vector
803	F28B12	VRK-1	
908		Pnpp-2_Cherry_STOP_npp2	
911	L4440	GFP	
936	pCRII	Pvrk-1_vrk-1	PCR fragment from plasmid #803 amplified with primers B259 and B261
937	pCRII	vrk-1 3'UTR	vrk-1 3'UTR amplified with primers B260 and from plasmid #803
938	L4440	Pvrk-1_vrk-1_UTR	vrk-1 promoter and ORF cut with SpeI and BsrGI from plasmid #936, and vrk-1 3'UTR cut with BsrGI and NotI from plasmid #937; fragments were ligated and cut with SpeI and NotI, then inserted into vector #301
942	L4440	Pvrk-1_vrk-1_mCherry_UTR	vrk-1 gene with mCherry before stop codon. BsrGI mCherry fragment from #908 inserted into BsrGI of #938.
941	L4440	Pvrk-1_vrk-1_GFP_UTR	GFP fragment from #911 was inserted into BsrGIof plasmid #938
957	L4440	Pvrk-1_vrk-1_mCherry_UTR, Left Recombination arm for MOSSCI chr IV.	PvuII/SpeI fragment (LR) from pBN9 inserted into SmaI/SpeI of #942.
941	L4440	Pvrk-1_vrk-1_GFP_UTR	vrk-1 gene with GFP before stop codon. Acc65I GFP fragment from #911 inserted into BsrGI of #938.
942	L4440	Pvrk-1_vrk-1_mCherry_UTR	mCherry fragment from #908 inserted into BsrGI of #938
958	L4440	Pvrk-1_vrk-1_GFP_UTR, Left Recombination arm for MOSSCI chr IV.	PvuII/SpeI fragment from pBN9 inserted into SmaI/SpeI of #941.
959	L4440	Pvrk-1_vrk-1_mCherry_UTR, Left Recombination arm for MOSSCI chr IV.	Plasmid #957 cut SmaI/SpeI, fill-in w Klenow, religate.
960	L4440	Pvrk-1_vrk-1_GFP_UTR, Left Recombination arm for MOSSCI chr IV.	Plasmid #958 cut SmaI/SpeI, fill-in w Klenow, religate.
961	L4440	Pvrk-1_vrk-1_mCherry_UTR, Left + Right Recombination arm for MOSSCI chr IV.	Right Recombination arm amplified w B292+B293, cut EagI, inserted into EagI of #959.
962	L4440	Pvrk-1_vrk-1_GFP_unc-119_RR_LR	Right Recombination arm from #961 inserted into EagI of #960.
1010	L4440	L4440_Pvrk-1_N-term_vrk-1_mCherry_MSCI_IV	N-terminal vrk-1 fragment amplified w B007+B221, inserted into pCRII, cut

			MluI/SgrAI, inserted into MluI/SgrAI of #961
1011	L4440	Pvrk-1_C-term_vrk-1_mCherry_MSCI_IV	C-terminal vrk-1 amplified w B008+B221,cutNruI/MluI, inserted into NruI/MluI of #961
1029	L4440	Pvrk-1_vrk-1_Dendra2_UTR	vrk-1 gene with Dendra2 before stop codon. Acc65I Dendra2 fragment from #975 inserted into BsrGI of #938.
1028	L4440	_Pvrk-1_vrk-1_K169E_mCherry_MSCI_IV	K169E point mutation, primers 307 and 308
1037	pGADT7		npp-15 3'end BamHI fragments from #1033 and #1034 pooled and inserted into BamHI of pGADT7 #989.
1039	pGBKT7		baf-1 cDNA amplified from #428 w B356+B357, inserted into pCRII Blunt, cut EcoRI/BamHI, inserted into EcoRI/BamHI of #969.
1047	L4440	Pvrk-1_vrk-1_Dendra2_ for MOSSCI chr IV	Right Recombination arm from #961 inserted into EagI of #1046.
1060		pCEFL-GST-VRK1	Pedro Lazo
1066	pGBKT7	egl-8 3' cDNA	egl-8 3'end cDNA EcoRI/PstI fragment from #1051 inserted into EcoRI/PstI of pGBKT7 NcoI #1039.
1070	pGBKT7	egl-8 5' cDNA	egl-8 5'end cDNA EcoRI/BamHI fragment from #1049 inserted into EcoRI/BamHI of pGBKT7 #969.
1077	pGBKT7	egl-8 cDNA	egl-8 3'end cDNA BamHI/PstI fragment from #1066 inserted into BamHI/PstI of pGBKT7 egl-8 5'end #1070.
1094		pHY12_mCherry_HsVRK1	
1101	pBN90 MSC_IV	Pfos-1c_vrk-1_mCherry_emr-1_3UTR	vrk-1 fragment amplified w B413+B078 from #942, cut NotI/MluI, inserted into NotI/MluI #1100
1129	pHY12	C-term_HsVRK1_mCherry	BamHI/NotI fragment from #1131 insertet into BamHI/NotI pHY12
1129	pHY12	pHY12_C-term_HsVRK1_mCherry	
1204	pHY12	pHY12_C-term_NLS_HsVRK1_mCherry	
1205	pHY12	pHY12_NLS_C-term_HsVRK1_mCherry	
1207	pHY12	pHY12_C-term_HsVRK1_mCherry_Asp-Ala	
1208	pHY12	pHY12_C-term_HsVRK1_mCherry_Arg-Gly	
1209	pHY12	pHY12_C-term_HsVRK1_mCherry_Ser-Thr	
1239	pBN155_Mos SCI_II	Phsp16.41::gfp::vrk-1	PCR w B555 + B554from #961;cut NheI/NgoMIV, inserted into #938 NheI/NgoMIV
1240	pBN156-MosSCI_II	Phsp16.41::gfp::C-term_vrk-1	PCR w B556 + B554 from #961, cut NheI/NgoMIV, inserted into #938 NheI/NgoMIV
1241		vrk-1_RG::mCherry_MosSCI_IV	

1242	pHY12	human vrk1_RG_mCherry	
1243	pcDNA5	Venus-AURKB	pcDNA5/FRT/TO 3X FLAG/Venus_AURKB
1244	pcDNA5	Venus-INCENP	pcDNA5/FRT/TO 3X FLAG/Venus_INCENP
1245	pcDNA5	Venus-BIRC5	pcDNA5/FRT/TO 3X FLAG/Venus_BIRC5
1246	pcDNA5	Venus-BANF1	pcDNA5/FRT/TO 3X FLAG/Venus_BANF1
1247	pcDNA5	Venus_C-term-VRK1	pcDNA5/FRT/TO 3X FLAG/Venus_C-termVRK1
1248	pcDNA5	Venus_VRK1	pcDNA5/FRT/TO 3X FLAG/Venus_VRK1

Table 6. Plasmids used in this study.

6.4. Primers

Primers used in this study are listed below.

Primer	Description	Sequence
B007	vrk-1(ok1181)	ggtagaatgccaccgaaaaa
B008	vrk-1(ok1181)	accaccaggatgattttcca
B214	Detection of Mos1 transposon	caaccttgactgtcgaaccaccatag
B215	Detection of Mos1 transposon	tctgcgagttgtttttgcgtttgag
B221	3'Cherry-BsrGI	agtgtacaCTTATACAATTCATCCATGCC
B259	vrk-1 promoter	ACTAGTCGACATACTCAGTTTTGTGTTTC
B260	vrk-1 3´UTR	GCGGCCGCTGGGAAAAGGCGGAAATGT
B261	vrk-1 rev	TGTACACACTTCCGACGAGCAGCTC
B262	vrk-1 UTRf	TGTACATAAACCATTGGAATCTTCAATCG
B307	Site-directed mutagenesis of K169	CTCACGCAGATGTAgAGGCTGCCAACATTC
B308	Site-directed mutagenesis of K169	GAATGTTGGCAGCCTcTACATCTGCGTGAG
309	Cloning of VRK-1 N-term fused to mCherry	TGAGACtgtacaCGTTGGCGTCTTTTTACCATCAC
310	Cloning of VRK-1 N-term fused to mCherry	AAGACGCCAACGtgtacaGTCTCAAAGGGTGAAGA
313	vrk-1 C-term rev	caggtagaATGTCAAGTGATGGTAAAAAGACGCCA
314	vrk-1 C-term forw	CCATCACTTGACATtctacctgaaaatgaaatgt
356	baf-1-Y2Hf	tgaattcATGTCGACTTCTGTTAAGCA
357	baf-1-Y2Hr	aggatccTTACATGAACTGATCTGCCCACT
B389	HsVRK1_f	caggatccGCCACCATGCCTCGTGTAAAAGCAGCT
B390	HsVRK1_r	gagcggccgcCTTCTGGACTCTCTTTCTGG
B397	mCherry_f	gagcggccgcGGTGAGCAAGGGCGAGGAGG
B404	mCherry_r	ctgcggccgcgccaggaaacagctat
B461	fwd_HsVRK1_C-term	caGGATCCGCCACCATGGGAAGTAAGGATGATGGC
B481	C_term_VRK1_Kozak_AUG_NLS, BamHI	caGGATCCGCCACCATGACAAAGAAGCGAAAGAAAG
B482	C_term_VRK1_NLS, NotI	ctGCGGCCGCTTCTTTCTTTCGCTTCTT
B543	HsVRK1_C-term fwd, 3 Asp->Ala substitutions, BamHI w Kozak sequence w AUG	caGGATCCGCCACCATGGGAAGTAAGGcTGcTGGCAAATTGGcCCTCAGT
B544	rev primer human VRK1 w/o stop, similar to B390 but EagI/NotI destroyed; for PCR stitch	gcggctgcCTTCTGGACTCTCTTTCTGG
B545	mCherry forward, PCR stitch primer to use w B544; destroy NotI	GAGAGTCCAGAAGgcagccgcGGT
B546	HsVRK1_C-term rev, 3 Arg->Gly	gcggctgcCTTCTGGACTCcCTTTCcGGTTCcTGAACG

	substitutions, for PCR stitch	GGTCTG
B547	HsVRK1_C-term rev, 2 Ser/Thr->Ala substitutions, for PCR stitch	gcggctgcCTTCTGGACTCTCTTTCTGGcTCTTGcACG GGTCTG
B556	Forward primer to amplify C-term vrk-1, NgoMIV, with AUG,	ctGCCGGCTCAAGTGATGGTA
B557	B557 Rev vrk-1 RG	GATAATTGTACTccACTTCcAGATCcTGACGACTTC
B568	B558 Fwd vrk-1 RG	gGAAGTggAGTACAATTATCTG
B574	Forward primer for human CDCA8/Borealin, BamHI (internal BamHI also present)	ctggatccATGGCTCCTAGGAAGGGCA
B575	Reverse primer for human CDCA8/Borealin, NotI	tagcggccgCTATTTGTGGGTCCGTATGC
B576	Forward primer for human BIRC5/Survivin, BamHI	ctggatccATGGGTGCCCCGACGTT
B577	Reverse primer for human BIRC5/Survivin, NotI	tagcggccgCTAATCCATGGCAGCCAGC
B578	B578AURKB_F	ctggatccATGGCCCAGAAGGAGAAC
B579	Reverse primer for human AuroraB, NotI	tagcggccgCTAGGCGACAGATTGAAG
B580	Forward primer for human BANF1, BamHI	ctggatccATGACAACCTCCCAAAAGCACC
B581	Reverse primer for human BANF1, NotI	tagcggccgcTCACAAGAAGGCGTCGCACCA
B582	B582INCENP_F	ctggatccATGGGGACGACGGCCCCA
B583	Reverse primer for human INCENP, NotI	tagcggccgcTCAGTGCTTCTTCAGGCTGT

Table 7. Primers used in this study.

6.5. Mos1 mediated Single Copy gene Insertion (MosSCI)

Single copy integration transgenic strains were made by microinjection into EG4322 (chromosome II) or EG5003 (chromosome IV) *unc-119* worms. Injection mixes contained 50ng/µl of transgene in targeting vector (containing a rescuing *unc-119* gene), 50ng/µl Mos1 transposase (P_{glh-2}::transposase or P_{eft-3}::transposase), 10ng/µl pBN1 (P_{lmn-1}::mCherry::his-58), 5ng/µl pCFJ104 (P_{myo-3}::mCherry) and 1.25 ng/µl pCFJ90 (P_{myo-2}::mCherry). *unc-19* worms are severely paralyzed and egg-laying defective, so L1-L2 worms were manually distributed across a lawn of OP50, and very young adults were selected for injection. Injected worms were individually transferred to standard NGM plates and placed at 16˚C for a few hours to recover followed by incubation at 25˚C. Plates were scored for the number of phenotypically rescued F1 worms 3 days after injection.

Individual injected worms were allowed to exhaust the food source. Once starved, plates containing transgenic lines were screened for insertion events on a fluorescence dissection microscope based on a wild-type movement, but complete lack of fluorescent coinjection markers. Plates containing insertion events typically had a large proportion of non-fluorescent moving worms, although some plates only had a few. Integrated strains were outcrossed to wild type N2 twice. Presence or absence of Mos1 transposon was confirmed by PCR with primers B214 and B215.

6.6. Rescue experiments

Worms at L4 stage were placed on NGM plates containing OP50 bacteria and removed 24 hours later, when number of laid embryos was scored. 24 hours later dead embryos were counted. Fertile adults and Pvl phenotype were scored 72 hours after placing L4 on NGM plates. Experiment was performed at 20˚C.

6.7. Aldicarb sensitivity assay

Plates were prepared 24-48 hours before use. Aldicarb (Sigma-Aldrich, 33386) was added directly to drug-free plates from 100mM stock of aldicarb in 70% ethanol. Drug sensitivity was assayed by placing in each experiment 20-25 L4 worms on NGM plates containing 1mM aldicarb and the effect on animal movement was observed every 10 minutes by gentle poking each worm. Animals were defined as paralyzed, when they did not respond with movement when prodded on the head and tail.

6.8. Yeast two-hybrid assay

Yeast strain AH109 (Clontech, MATa, trp1-901, leu2-3, 112, ura3-52, his3-200, gal4Δ, gal80Δ, LYS2::GAL1$_{UAS}$-GAL1$_{TATA}$-HIS3, GAL2$_{UAS}$-GAL2$_{TATA}$-ADE2, URA3::MEL1$_{TATA}$-lacZ) was transformed using LiAc method and selected in the appropriate synthetic (SC) minimal medium. Transformants containing pGADT7-vrk-1 and either pGBKT7-baf-1 or pGBKT7-egl-8 were grown at 30˚C to OD_{600}0.5 in SC-Leu-Trp medium and spotted as 10-fold serial dilutions to detect the ability to grow on minimal-medium plates lacking histidine or lacking adenine and histidine. Growth was assayed after 3 days at 30˚C. Combination of empty pGADT7 and GBKT7 vectors were also transformed into AH109 with each construct to assess self-activation.

6.9. Live imaging

Live animals imaging:

Animals were mounted in a 5 µl drop of 10 mM levamisole on a 3% agarose pad, covered with a 24 mm × 24 mm coverslip. Images were taken using Nikon A1R confocal microscope and Leica confocal SP2 microscope and processed with Fiji.

Live embryos imaging:

Embryos were mounted in M9 buffer between a cover slip and a 2% agarose pad. Epifluorescence and transmitted light were recorded with a NIKON-A1R confocal microscope through a 60x/1.4 objective, captured using integral Nikon software and processed with Fiji. The laser intensity was adjusted so that no effect on development was observed.

Time-lapse imaging:

Cells were plated in 35mm MatTek Glass Bottom Culture Dishes in growth media. 24-48 hours after seeding, cells were washed three times with PBS and

for imaging the medium was changed to L-15 (Leibovitz) medium (Sigma) supplemented with 10% fetal bovine serum (Sigma).

Time-lapse images were taken using Nikon A1R confocal microscope with 63x or 40x oil objective at 37°C in a heated environmental chamber set. Videos were cropped and contrast and brightness was adjusted using Fiji.

6.10. Cell culture and transfections

Cells (Table XX) were cultured in appropriate medium and were maintained at 37˚C with 5% CO_2.

For transfection cells (U2OS FRT/TO) were plated in 6-well plates (~30% confluence), cultured 24 hours in media without antibiotics and transfected with FuGENE® 6 according to the manufacture's instructions. 24 hours after transfection cells were split into three wells with medium with Penicillin and Streptomycin. Selection with Hygromycin started 48 hours after transfection and media was changed every fifth day.

Stable cell line expressing Venus-VRK1 was made using HeLa FRT/TO cells, which were plated in 10cm dishes (~45% confluence) and transfected 24 hours later using Lipofectamine® 2000 according to the manufacture's instructions. 24 hours after transfecton cells were split into three 15cm dishes with medium without antibiotics. Selection with Hygromycin started when cells were approximately 30% confluent and media was changed every fifth day.

Transient transfection was made using stable U2OS FRT/TO cell line expressing hVRK1-mCherry. Cells were plated in 35mm MatTek Glass Bottom Culture Dishes in media without antibiotics and transfected with FugeneFuGENE® 6 according to the manufacture's instructions. Live images were taken 24 hours after transfection.

6.11. Cells Synchronization

Cells were plated in 35mm MatTek Glass Bottom Culture Dishes in antibiotic free media. Thymidine (Sigma cat no) was added to a 2.5mM final concentration and cells were incubated for 16 hours. After incubation cells were washed three times with PBS and fresh media without antibiotics was added. After 8-9 hours incubation, thymidine was added to a 2.5mM final concentration and cells were incubated again for 16 hours. After incubation, cells were washed three times with PBS and fresh culture media was added.

6.12. Fluorescence Recovery After Photobleaching (FRAP)

Cells were plated in 35mm MatTek Glass Bottom Culture Dishes in growth media. 24-48 hours after seeding, cells were washed three times with PBS and incubated in colorless, CO_2-insensitive L-15 (Leibovitz) medium (Sigma-Aldrich, L1518) supplemented with 10% fetal bovine serum (Sigma- Aldrich).

Fluorescence photobleaching was performed with a high intensity laser light on a small region of interest (ROI) of the nucleus (interphase cells) or metaphase plate (mitotic cells). Two to ten images were taken before the bleach pulse and 50–200 images after bleaching. FRAP experiments were performed using a NIKON-A1R confocal microscope through a 60x objective. A single iteration was used for a bleach pulse at 4,03 seconds/frame using the Resonant scanner and 402 nm laser at 100% , and images were acquired using the Galvano scanner. Images were processed using Fiji. FRAP data were corrected for background signals and scan bleaching signal decay. The recovery equations were programmed in Matlab.

6.13. Western blot

U2OS cells for Western blot analysis were grown in 6-well plates in growth media. When they were ~80% confluent they were trypsinized, collected in 15ml falcons and washed twice with PBS. Then they were disrupted by boiling three minutes at 95˚C in 10% ß-mercaptoethanol in 1xSDS buffer and sonicated, followed by 10% SDS-PAGE separation. Proteins were transferred to Immobilon-P membranes (Milipore) which were blocked with PBS containing 0,05% Tween and 3% milk (PBST-M) and probed for 2 hours at room temperature with primary α-VRK1 mouse monoclonal antibody (gift from T. Haraguchi, Kobe Advanced ICT Research Institute, Japan) diluted 1:100 in PBST-M. Next, membranes were washed with PBST for one hour, incubated with anti-mouse peroxidase-conjugated secondary antibody (Sigma-Aldrich, 1:5000) for 2 hours at room temperature, washed one hour with PBST and developed with ECL Plus (GE Amersham).

6.14. Immunofluorescence

U2OS cells were seeded on coverslips in the bottom of 6-well plates 24-48 hours before experiment. Cells were rinsed in PBS and fixed with ice-cold methanol for 10 minutes. Then, they were permeabilized with PBS with 0.5% Triton X-100 for 5 min at room temperature. Cells were blocked with PBS containing 0,05% Tween and 3% milk (PBST-M) and probed for 2 hours at room temperature with primary α-VRK1 mouse monoclonal antibody (gift from T. Haraguchi, Kobe Advanced ICT Research Institute, Japan) diluted 1:100 in PBST-M. Next, membranes were washed with PBST for one hour, incubated with anti-mouse Alexa546-conjugated secondary antibody (Invitrogen cat no, 1:1000) for 2 hours at room temperature, washed one hour with PBST. Finally cells were stained with Mowiol containing 5mg/ml Hoechst 33258. Confocal images were obtained with a Leica confocal SPE microscope and processed with Fiji.

6.15. Co-immunoprecipitation

Stable HeLa/FRT/TRex cell lines expressing FLAG-Venus-VRK1 grown on 25cm dishes were scrapped off in growth medium, centrifuged for 3 minutes at 1300rpm and washed twice with ice cold PBS. Cellular pellets were incubated for 30 minutes in lysis buffer on ice (50mM TRIS pH 7.5, 125mM NaCl, 1mM EDTA, 1% NP40, 1x protease inhibitor cocktail (Roche), 1x phosphatases inhibitor cocktail (Roche), 1mM DTT) with extensive pipeting every 10 min. Samples were sonicated using a Bioruptor (five sonication cycles 30sec ON, 30 sec OFF). Extracts were clarified by centrifugation at 14000rpm at 4˚C for 15 minutes and protein concentration was measured by a Bradford assay. 10mg of extracts were immunoprecipitated using 50µl GFP-Trap® A beads (ChromoTek) and incubated with agitation (1350rpm) at 4°C for 1 hour. Samples were washed four times for 5 minutes with ice cold lysis buffer, resuspended in 2xSDS sample buffer and boiled for 10minutes at 95˚C to dissociate complexes from the beads, which was followed by reduction (10 minutes at 70˚C in darkness with 1mM DTT solution in 2x LDS sample buffer) and alkylation (30 minutes at room temperature in darkness with 5mM chloroacetamide) of samples prior loading samples onto a SDS-PAGE gel. The gel was visualized with Coomasie blue using a Colloidal Blue staining kit (Sigma) and analyzed by mass spectrometry (The Novo Nordisk Foundation Center for Protein Research, Copenhagen, Denmark).

VII. REFERENCES

REFERENCES

VII. REFERENCES

Aihara, H., Nakagawa, T., Yasui, K., Ohta, T., Hirose, S., Dhomae, N., Takio, K., Kaneko, M., Takeshima, Y., Muramatsu, M*., et al.* (2004). Nucleosomal histone kinase-1 phosphorylates H2A Thr 119 during mitosis in the early Drosophila embryo. Genes Dev *18*, 877-888.

Angelov, D., Molla, A., Perche, P.Y., Hans, F., Cote, J., Khochbin, S., Bouvet, P., and Dimitrov, S. (2003). The histone variant macroH2A interferes with transcription factor binding and SWI/SNF nucleosome remodeling. Mol Cell *11*, 1033-1041.

Asencio, C., Davidson, I.F., Santarella-Mellwig, R., Ly-Hartig, T.B., Mall, M., Wallenfang, M.R., Mattaj, I.W., and Gorjanacz, M. (2012). Coordination of kinase and phosphatase activities by Lem4 enables nuclear envelope reassembly during mitosis. Cell *150*, 122-135.

Bannister, A.J., and Kouzarides, T. (2011). Regulation of chromatin by histone modifications. Cell research *21*, 381-395.

Barcia, R., Lopez-Borges, S., Vega, F.M., and Lazo, P.A. (2002). Kinetic properties of p53 phosphorylation by the human vaccinia-related kinase 1. Arch Biochem Biophys *399*, 1-5.

Blanco, S., Klimcakova, L., Vega, F.M., and Lazo, P.A. (2006). The subcellular localization of vaccinia-related kinase-2 (VRK2) isoforms determines their different effect on p53 stability in tumour cell lines. The FEBS journal *273*, 2487-2504.

Brenner, S. (1974). The genetics of Caenorhabditis elegans. Genetics *77*, 71-94.

Brittle, A.L., Nanba, Y., Ito, T., and Ohkura, H. (2007). Concerted action of Aurora B, Polo and NHK-1 kinases in centromere-specific histone 2A phosphorylation. Exp Cell Res *313*, 2780-2785.

Carmena, M., Wheelock, M., Funabiki, H., and Earnshaw, W.C. (2012). The chromosomal passenger complex (CPC): from easy rider to the godfather of mitosis. Nat Rev Mol Cell Biol *13*, 789-803.

Choi, Y.H., Park, C.H., Kim, W., Ling, H., Kang, A., Chang, M.W., Im, S.K., Jeong, H.W., Kong, Y.Y., and Kim, K.T. (2010). Vaccinia-related kinase 1 is required for the maintenance of undifferentiated spermatogonia in mouse male germ cells. PLoS ONE *5*, e15254.

Chudakov, D.M., Lukyanov, S., and Lukyanov, K.A. (2007). Using photoactivatable fluorescent protein Dendra2 to track protein movement. BioTechniques *42*, 553, 555, 557 passim.

Cohen, P. (2000). The regulation of protein function by multisite phosphorylation--a 25 year update. Trends in biochemical sciences *25*, 596-601.

Costanzi, C., and Pehrson, J.R. (1998). Histone macroH2A1 is concentrated in the inactive X chromosome of female mammals. Nature *393*, 599-601.

Cullen, C.F., Brittle, A.L., Ito, T., and Ohkura, H. (2005). The conserved kinase NHK-1 is essential for mitotic progression and unifying acentrosomal meiotic spindles in Drosophila melanogaster. J Cell Biol *171*, 593-602.

Dickinson, D.J., Ward, J.D., Reiner, D.J., and Goldstein, B. (2013). Engineering the Caenorhabditis elegans genome using Cas9-triggered homologous recombination. Nat Methods *10*, 1028-1034.

Fernandez, A.G., Mis, E.K., Lai, A., Mauro, M., Quental, A., Bock, C., and Piano, F. (2014). Uncovering buffered pleiotropy: a genome-scale screen for mel-28 genetic interactors in Caenorhabditis elegans. G3 (Bethesda) *4*, 185-196.

Fernandez, I.F., Blanco, S., Lozano, J., and Lazo, P.A. (2010). VRK2 inhibits mitogen-activated protein kinase signaling and inversely correlates with ErbB2 in human breast cancer. Mol Cell Biol *30*, 4687-4697.

Fernandez, I.F., Perez-Rivas, L.G., Blanco, S., Castillo-Dominguez, A.A., Lozano, J., and Lazo, P.A. (2012). VRK2 anchors KSR1-MEK1 to endoplasmic reticulum forming a macromolecular complex that compartmentalizes MAPK signaling. Cell Mol Life Sci *69*, 3881-3893.

Finetti, P., Cervera, N., Charafe-Jauffret, E., Chabannon, C., Charpin, C., Chaffanet, M., Jacquemier, J., Viens, P., Birnbaum, D., and Bertucci, F. (2008). Sixteen-kinase gene expression identifies luminal breast cancers with poor prognosis. Cancer research *68*, 767-776.

Gassmann, R., Carvalho, A., Henzing, A.J., Ruchaud, S., Hudson, D.F., Honda, R., Nigg, E.A., Gerloff, D.L., and Earnshaw, W.C. (2004). Borealin: a novel chromosomal passenger required for stability of the bipolar mitotic spindle. J Cell Biol *166*, 179-191.

Giot, L., Bader, J.S., Brouwer, C., Chaudhuri, A., Kuang, B., Li, Y., Hao, Y.L., Ooi, C.E., Godwin, B., Vitols, E.*, et al.* (2003). A protein interaction map of Drosophila melanogaster. Science *302*, 1727-1736.

Gonzaga-Jauregui, C., Lotze, T., Jamal, L., Penney, S., Campbell, I.M., Pehlivan, D., Hunter, J.V., Woodbury, S.L., Raymond, G., Adesina, A.M.*, et al.* (2013). Mutations in VRK1 associated with complex motor and sensory axonal neuropathy plus microcephaly. JAMA neurology *70*, 1491-1498.

Gorjanacz, M., Klerkx, E.P., Galy, V., Santarella, R., Lopez-Iglesias, C., Askjaer, P., and Mattaj, I.W. (2007). Caenorhabditis elegans BAF-1 and its kinase VRK-1 participate directly in post-mitotic nuclear envelope assembly. EMBO J *26*, 132-143.

Gupta, B.P., Hanna-Rose, W., and Sternberg, P.W. (2012). Morphogenesis of the vulva and the vulval-uterine connection. WormBook, 1-20.

Hagedorn, E.J., Yashiro, H., Ziel, J.W., Ihara, S., Wang, Z., and Sherwood, D.R. (2009). Integrin acts upstream of netrin signaling to regulate formation of the anchor cell's invasive membrane in C. elegans. Dev Cell *17*, 187-198.

Hagedorn, E.J., Ziel, J.W., Morrissey, M.A., Linden, L.M., Wang, Z., Chi, Q., Johnson, S.A., and Sherwood, D.R. (2013). The netrin receptor DCC focuses invadopodia-driven basement membrane transmigration in vivo. J Cell Biol *201*, 903-913.

Hanks, S.K., and Hunter, T. (1995). Protein kinases 6. The eukaryotic protein kinase superfamily: kinase (catalytic) domain structure and classification. FASEB J *9*, 576-596.

Hanna-Rose, W., and Han, M. (1999). COG-2, a sox domain protein necessary for establishing a functional vulval-uterine connection in Caenorhabditis elegans. Development *126*, 169-179.

Haraguchi, T., Koujin, T., Segura-Totten, M., Lee, K.K., Matsuoka, Y., Yoneda, Y., Wilson, K.L., and Hiraoka, Y. (2001). BAF is required for emerin assembly into the reforming nuclear envelope. J Cell Sci *114*, 4575-4585.

Hegarat, N., Smith, E., Nayak, G., Takeda, S., Eyers, P.A., and Hochegger, H. (2011). Aurora A and Aurora B jointly coordinate chromosome segregation and anaphase microtubule dynamics. J Cell Biol *195*, 1103-1113.

Hennig, E.E., Mikula, M., Rubel, T., Dadlez, M., and Ostrowski, J. (2012). Comparative kinome analysis to identify putative colon tumor biomarkers. J Mol Med (Berl) *90*, 447-456.

Hill, R.J., and Sternberg, P.W. (1992). The gene lin-3 encodes an inductive signal for vulval development in C. elegans. Nature *358*, 470-476.

Ivanovska, I., Khandan, T., Ito, T., and Orr-Weaver, T.L. (2005). A histone code in meiosis: the histone kinase, NHK-1, is required for proper chromosomal architecture in Drosophila oocytes. Genes Dev *19*, 2571-2582.

Jeong, M.W., Kang, T.H., Kim, W., Choi, Y.H., and Kim, K.T. (2013). Mitogen-activated protein kinase phosphatase 2 regulates histone H3

phosphorylation via interaction with vaccinia-related kinase 1. Mol Biol Cell *24*, 373-384.

Kang, T.H., and Kim, K.T. (2006). Negative regulation of ERK activity by VRK3-mediated activation of VHR phosphatase. Nat Cell Biol *8*, 863-869.

Kang, T.H., and Kim, K.T. (2008). VRK3-mediated inactivation of ERK signaling in adult and embryonic rodent tissues. Biochim Biophys Acta *1783*, 49-58.

Kang, T.H., Park, D.Y., Choi, Y.H., Kim, K.J., Yoon, H.S., and Kim, K.T. (2007). Mitotic histone H3 phosphorylation by vaccinia-related kinase 1 in mammalian cells. Mol Cell Biol *27*, 8533-8546.

Kang, T.H., Park, D.Y., Kim, W., and Kim, K.T. (2008). VRK1 phosphorylates CREB and mediates CCND1 expression. J Cell Sci *121*, 3035-3041.

Kim, S., Park, D.Y., Lee, D., Kim, W., Jeong, Y.H., Lee, J., Chung, S.K., Ha, H., Choi, B.H., and Kim, K.T. (2014). Vaccinia-related kinase 2 mediates accumulation of polyglutamine aggregates via negative regulation of the chaperonin TRiC. Mol Cell Biol *34*, 643-652.

Kim, W., Chakraborty, G., Kim, S., Shin, J., Park, C.H., Jeong, M.W., Bharatham, N., Yoon, H.S., and Kim, K.T. (2012). Macro histone H2A1.2 (macroH2A1) protein suppresses mitotic kinase VRK1 during interphase. J Biol Chem *287*, 5278-5289.

Klein, U.R., Nigg, E.A., and Gruneberg, U. (2006). Centromere targeting of the chromosomal passenger complex requires a ternary subcomplex of Borealin, Survivin, and the N-terminal domain of INCENP. Mol Biol Cell *17*, 2547-2558.

Klerkx, E.P., Alarcon, P., Waters, K., Reinke, V., Sternberg, P.W., and Askjaer, P. (2009a). Protein kinase VRK-1 regulates cell invasion and EGL-17/FGF signaling in Caenorhabditis elegans. Dev Biol *335*, 12-21.

Klerkx, E.P., Lazo, P.A., and Askjaer, P. (2009b). Emerging biological functions of the vaccinia-related kinase (VRK) family. Histol Histopathol *24*, 749-759.

Kostrouchova, M., Kostrouch, Z., Saudek, V., Piatigorsky, J., and Rall, J.E. (2003). BIR-1, a Caenorhabditis elegans homologue of Survivin, regulates transcription and development. Proc Natl Acad Sci U S A *100*, 5240-5245.

Kruhlak, M.J., Lever, M.A., Fischle, W., Verdin, E., Bazett-Jones, D.P., and Hendzel, M.J. (2000). Reduced mobility of the alternate splicing factor (ASF) through the nucleoplasm and steady state speckle compartments. J Cell Biol *150*, 41-51.

Lackner, M.R., Nurrish, S.J., and Kaplan, J.M. (1999). Facilitation of synaptic transmission by EGL-30 Gqalpha and EGL-8 PLCbeta: DAG

binding to UNC-13 is required to stimulate acetylcholine release. Neuron *24*, 335-346.

Lancaster, O.M., Cullen, C.F., and Ohkura, H. (2007). NHK-1 phosphorylates BAF to allow karyosome formation in the Drosophila oocyte nucleus. J Cell Biol *179*, 817-824.

Lee, K.K., Haraguchi, T., Lee, R.S., Koujin, T., Hiraoka, Y., and Wilson, K.L. (2001). Distinct functional domains in emerin bind lamin A and DNA-bridging protein BAF. J Cell Sci *114*, 4567-4573.

Li, L.Y., Liu, M.Y., Shih, H.M., Tsai, C.H., and Chen, J.Y. (2006). Human cellular protein VRK2 interacts specifically with Epstein-Barr virus BHRF1, a homologue of Bcl-2, and enhances cell survival. The Journal of general virology *87*, 2869-2878.

Li, M., Wang, Y., Zheng, X.B., Ikeda, M., Iwata, N., Luo, X.J., Chong, S.A., Lee, J., Rietschel, M., Zhang, F.*, et al.* (2012). Meta-analysis and brain imaging data support the involvement of VRK2 (rs2312147) in schizophrenia susceptibility. Schizophrenia research *142*, 200-205.

Lopez-Borges, S., and Lazo, P.A. (2000). The human vaccinia-related kinase 1 (VRK1) phosphorylates threonine-18 within the mdm-2 binding site of the p53 tumour suppressor protein. Oncogene *19*, 3656-3664.

Lopez-Sanchez, I., Sanz-Garcia, M., and Lazo, P.A. (2009). Plk3 interacts with and specifically phosphorylates VRK1 in Ser342, a downstream target in a pathway that induces Golgi fragmentation. Mol Cell Biol *29*, 1189-1201.

Lopez-Sanchez, I., Valbuena, A., Vazquez-Cedeira, M., Khadake, J., Sanz-Garcia, M., Carrillo-Jimenez, A., and Lazo, P.A. (2014). VRK1 interacts with p53 forming a basal complex that is activated by UV-induced DNA damage. FEBS Lett *588*, 692-700.

Mahoney, T.R., Luo, S., and Nonet, M.L. (2006). Analysis of synaptic transmission in Caenorhabditis elegans using an aldicarb-sensitivity assay. Nat Protoc *1*, 1772-1777.

Manning, G., Plowman, G.D., Hunter, T., and Sudarsanam, S. (2002a). Evolution of protein kinase signaling from yeast to man. Trends in biochemical sciences *27*, 514-520.

Manning, G., Whyte, D.B., Martinez, R., Hunter, T., and Sudarsanam, S. (2002b). The protein kinase complement of the human genome. Science *298*, 1912-1934.

Margalit, A., Brachner, A., Gotzmann, J., Foisner, R., and Gruenbaum, Y. (2007). Barrier-to-autointegration factor--a BAFfling little protein. Trends Cell Biol *17*, 202-208.

Miller, K.G., Emerson, M.D., and Rand, J.B. (1999). Goalpha and diacylglycerol kinase negatively regulate the Gqalpha pathway in C. elegans. Neuron *24*, 323-333.

Minasaki, R., Puoti, A., and Streit, A. (2009). The DEAD-box protein MEL-46 is required in the germ line of the nematode Caenorhabditis elegans. BMC developmental biology *9*, 35.

Molitor, T.P., and Traktman, P. (2014). Depletion of the protein kinase VRK1 disrupts nuclear envelope morphology and leads to BAF retention on mitotic chromosomes. Mol Biol Cell *25*, 891-903.

Nezu, J., Oku, A., Jones, M.H., and Shimane, M. (1997). Identification of two novel human putative serine/threonine kinases, VRK1 and VRK2, with structural similarity to vaccinia virus B1R kinase. Genomics *45*, 327-331.

Nichols, R.J., and Traktman, P. (2004). Characterization of three paralogous members of the Mammalian vaccinia related kinase family. J Biol Chem *279*, 7934-7946.

Nichols, R.J., Wiebe, M.S., and Traktman, P. (2006). The Vaccinia-related Kinases Phosphorylate the N' Terminus of BAF, Regulating Its Interaction with DNA and Its Retention in the Nucleus. Mol Biol Cell *17*, 2451-2464.

Oommen, K.S., and Newman, A.P. (2007). Co-regulation by Notch and Fos is required for cell fate specification of intermediate precursors during C. elegans uterine development. Development *134*, 3999-4009.

Persengiev, S.P., and Green, M.R. (2003). The role of ATF/CREB family members in cell growth, survival and apoptosis. Apoptosis : an international journal on programmed cell death *8*, 225-228.

Pettitt, J. (2005). The cadherin superfamily. WormBook, 1-9.

Pettitt, J., Wood, W.B., and Plasterk, R.H. (1996). cdh-3, a gene encoding a member of the cadherin superfamily, functions in epithelial cell morphogenesis in Caenorhabditis elegans. Development *122*, 4149-4157.

Praitis, V. (2006). Creation of transgenic lines using microparticle bombardment methods. Methods Mol Biol *351*, 93-107.

Rand, J.B. (2007). Acetylcholine. WormBook, 1-21.

Rempel, R.E., and Traktman, P. (1992). Vaccinia virus B1 kinase: phenotypic analysis of temperature-sensitive mutants and enzymatic characterization of recombinant proteins. J Virol *66*, 4413-4426.

R**enbaum, P., Kellerman, E., Jaron, R., Geiger, D., Segel, R., Lee, M., King, M.C., and Levy-Lahad, E.** (2009). Spinal muscular atrophy with pontocerebellar hypoplasia is caused by a mutation in the VRK1 gene. American journal of human genetics *85*, 281-289.

Richmond, J.E. (2006). Electrophysiological recordings from the neuromuscular junction of C. elegans. WormBook, 1-8.

Rodriguez-Hernandez, I., Vazquez-Cedeira, M., Santos-Briz, A., Garcia, J.L., Fernandez, I.F., Gomez-Moreta, J.A., Martin-Vallejo, J., Gonzalez-Sarmiento, R., and Lazo, P.A. (2013). VRK2 identifies a subgroup of primary high-grade astrocytomas with a better prognosis. BMC clinical pathology *13*, 23.

Santos, C.R., Rodriguez-Pinilla, M., Vega, F.M., Rodriguez-Peralto, J.L., Blanco, S., Sevilla, A., Valbuena, A., Hernandez, T., van Wijnen, A.J., Li, F.*, et al.* (2006). VRK1 signaling pathway in the context of the proliferation phenotype in head and neck squamous cell carcinoma. Mol Cancer Res *4*, 177-185.

Sanz-Garcia, M., Lopez-Sanchez, I., and Lazo, P.A. (2008). Proteomics identification of nuclear Ran GTPase as an inhibitor of human VRK1 and VRK2 (vaccinia-related kinase) activities. Mol Cell Proteomics *7*, 2199-2214.

Scheeff, E.D., Eswaran, J., Bunkoczi, G., Knapp, S., and Manning, G. (2009). Structure of the pseudokinase VRK3 reveals a degraded catalytic site, a highly conserved kinase fold, and a putative regulatory binding site. Structure *17*, 128-138.

Sevilla, A., Santos, C.R., Barcia, R., Vega, F.M., and Lazo, P.A. (2004a). c-Jun phosphorylation by the human vaccinia-related kinase 1 (VRK1) and its cooperation with the N-terminal kinase of c-Jun (JNK). Oncogene *23*, 8950-8958.

Sevilla, A., Santos, C.R., Vega, F.M., and Lazo, P.A. (2004b). Human vaccinia-related kinase 1 (VRK1) activates the ATF2 transcriptional activity by novel phosphorylation on Thr-73 and Ser-62 and cooperates with JNK. J Biol Chem *279*, 27458-27465.

Shaulian, E., and Karin, M. (2002). AP-1 as a regulator of cell life and death. Nat Cell Biol *4*, E131-136.

Sherwood, D.R., Butler, J.A., Kramer, J.M., and Sternberg, P.W. (2005). FOS-1 promotes basement-membrane removal during anchor-cell invasion in C. elegans. Cell *121*, 951-962.

Shin, J., Chakraborty, G., Bharatham, N., Kang, C., Tochio, N., Koshiba, S., Kigawa, T., Kim, W., Kim, K.T., and Yoon, H.S. (2011). NMR solution structure of human vaccinia-related kinase 1 (VRK1) reveals the C-terminal tail essential for its structural stability and autocatalytic activity. J Biol Chem *286*, 22131-22138.

Shirayama, M., Seth, M., Lee, H.C., Gu, W., Ishidate, T., Conte, D., Jr., and Mello, C.C. (2012). piRNAs initiate an epigenetic memory of nonself RNA in the C. elegans germline. Cell *150*, 65-77.

Steffens, M., Leu, C., Ruppert, A.K., Zara, F., Striano, P., Robbiano, A., Capovilla, G., Tinuper, P., Gambardella, A., Bianchi, A.*, et al.* (2012). Genome-wide association analysis of genetic generalized epilepsies implicates susceptibility loci at 1q43, 2p16.1, 2q22.3 and 17q21.32. Human molecular genetics *21*, 5359-5372.

Steinberg, S., de Jong, S., Andreassen, O.A., Werge, T., Borglum, A.D., Mors, O., Mortensen, P.B., Gustafsson, O., Costas, J., Pietilainen, O.P.*, et al.* **(**2011). Common variants at VRK2 and TCF4 conferring risk of schizophrenia. Human molecular genetics *20*, 4076-4081.

Sternberg, P.W. (1988). Lateral inhibition during vulval induction in Caenorhabditis elegans. Nature *335*, 551-554.

Sternberg, P.W. (2005). Vulval development. WormBook, 1-28.

Valbuena, A., Blanco, S., Vega, F.M., and Lazo, P.A. (2008). The C/H3 domain of p300 is required to protect VRK1 and VRK2 from their downregulation induced by p53. PLoS ONE *3*, e2649.

Valbuena, A., Castro-Obregon, S., and Lazo, P.A. (2011a). Downregulation of VRK1 by p53 in response to DNA damage is mediated by the autophagic pathway. PLoS ONE *6*, e17320.

Valbuena, A., Lopez-Sanchez, I., Vega, F.M., Sevilla, A., Sanz-Garcia, M., Blanco, S., and Lazo, P.A. (2007a). Identification of a dominant epitope in human vaccinia-related kinase 1 (VRK1) and detection of different intracellular subpopulations. Arch Biochem Biophys *465*, 219-226.

Valbuena, A., Sanz-Garcia, M., Lopez-Sanchez, I., Vega, F.M., and Lazo, P.A. (2011b). Roles of VRK1 as a new player in the control of biological processes required for cell division. Cellular signalling *23*, 1267-1272.

Valbuena, A., Suarez-Gauthier, A., Lopez-Rios, F., Lopez-Encuentra, A., Blanco, S., Fernandez, P.L., Sanchez-Cespedes, M., and Lazo, P.A. (2007b). Alteration of the VRK1-p53 autoregulatory loop in human lung carcinomas. Lung Cancer *58*, 303-309.

Valbuena, A., Vega, F.M., Blanco, S., and Lazo, P.A. (2006). p53 downregulates its activating vaccinia-related kinase 1, forming a new autoregulatory loop. Mol Cell Biol *26*, 4782-4793.

Vega, F.M., Sevilla, A., and Lazo, P.A. (2004). p53 Stabilization and accumulation induced by human vaccinia-related kinase 1. Mol Cell Biol *24*, 10366-10380.

Verghese, E., Schocken, J., Jacob, S., Wimer, A.M., Royce, R., Nesmith, J.E., Baer, G.M., Clever, S., McCain, E., Lakowski, B.*, et al.* (2011). The tailless ortholog nhr-67 functions in the development of the C. elegans ventral uterus. Dev Biol *356*, 516-528.

Wang, Z., Chi, Q., and Sherwood, D.R. (2014). MIG-10 (lamellipodin) has netrin-independent functions and is a FOS-1A transcriptional target during anchor cell invasion in C. elegans. Development *141*, 1342-1353.

Waters, K., Yang, A.Z., and Reinke, V. (2010). Genome-wide analysis of germ cell proliferation in C.elegans identifies VRK-1 as a key regulator of CEP-1/p53. Dev Biol *344*, 1011-1025.

Wiebe, M.S., Nichols, R.J., Molitor, T.P., Lindgren, J.K., and Traktman, P. (2010). Mice deficient in the serine/threonine protein kinase VRK1 are infertile due to a progressive loss of spermatogonia. Biology of reproduction *82*, 182-193.

Wiebe, M.S., and Traktman, P. (2007). Poxviral B1 kinase overcomes barrier to autointegration factor, a host defense against virus replication. Cell host & microbe *1*, 187-197.

Ziel, J.W., Hagedorn, E.J., Audhya, A., and Sherwood, D.R. (2009). UNC-6 (netrin) orients the invasive membrane of the anchor cell in C. elegans. Nat Cell Biol *11*, 183-189.

REFERENCES

ACKNOWLEDGEMENTS

ACKNOWLEDGEMENTS

My PhD is almost finished and, even though the last part of this journey was kind of a marathon, quite painful and exhausting, these four years and a half were also full of the happiest and fulfilling moments.

First of all, I would like to thank Peter, who gave me this opportunity and without whom I would not have been able to complete this thesis. His patience, understanding, motivation and encouragement made him the best boss one can imagine. I will always be grateful not only for the scientific support, but also for creating an incredible, friendly atmosphere during these last few years.

I would also like to thank all the members, current and former, of Peter's group, who became my best friends. To Cristina G. for her priceless help and whose knowledge always an example to me. To Machupi for her energy and for defending her own thesis so well. It was a great motivation! To Cristina A. for her organizational skills and help with so many experiments. To Gina, for her positivie attitude and all the amazing Mexican specialties she prepared. To Adela for always being there, for me whenever I needed support. Finally, to Eduardo for being such a good colleague.

I am also very grateful to everyone from the Worm Corner. To Antonio, Manolo and Marta for all the help and constructive discussions during our worm meetings. Thank to Maria G., Maria J., Fran, Nando, Briseida, Mer, AnaMaria, Roxani, Ann and Artur for all the help and for so many great moment over these years.

I would also like to thank to Angeles for all her kindness and for introducing me to the world of cells. For all the hints thanks to which I have never got contamination. To Monica Navarro for taking care of the cells at the beginning.

I would also like to thank to Jakob Nilsson and his group for letting me visit their laboratory and helping with the purifications.

Thank to Tokuko Haraguchi for the monoclonal α-VRK1 antibody.

I am very grateful for reagents and materials to Melpi Platini, Pedro Lazo, Michael Glotzer, David Sherwood, Juan Ramon Martínez Morales and Claudio Asencio.

Oczywiście nie może tu zabraknąć podziękowań dla moich Rodziców Sióstr. Dziękuję Wam kochani za nieustanne wsparcie i pomoc przez te wszystkie lata. Bez Was napisanie tej pracy nie byloby możliwe.

Gracias tambien a MariCarmen y JoseMaria por su apoyo continuo y por cuidarme y por estar siempre tan cerca.

Finally, I would like to thank, Guillermo, for his permanent support, patience and understanding, especially during the last six months. I think he and our Little Terrorist are the only ones who really know how difficult and stressful it was to finish this thesis.

Thank you.